MULTI-SENSOR SIGNAL PROCESSING METHODS FOR HOME MONITORING OF CARDIOVASCULAR AND RESPIRATORY DISEASES

A Thesis
Presented to
The Academic Faculty

by

Abdul Q. Javaid

In Partial Fulfillment
of the Requirements for the Degree
Doctor of Philosophy in the
School of Electrical and Computer Engineering

Georgia Institute of Technology
August 2016

MULTI-SENSOR SIGNAL PROCESSING METHODS FOR HOME MONITORING OF CARDIOVASCULAR AND RESPIRATORY DISEASES

Approved by:

Dr. Mary A. Weitnauer, Advisor
School of Electrical and Computer Engineering
Georgia Institute of Technology

Dr. David V. Anderson
School of Electrical and Computer Engineering
Georgia Institute of Technology

Dr. Omer T. Inan, Co-Advisor
School of Electrical and Computer Engineering
Georgia Institute of Technology

Dr. Srini Tridandapani
Radiology and Biomedical Engineering
Emory University School of Medicine

Dr. Pamela T. Bhatti
School of Electrical and Computer Engineering
Georgia Institute of Technology

Dr. Mozziyar Etemadi
Feinberg School of Medicine
Northwestern University

Date Approved: July 6, 2016

Dedicated to,

my parents, my wife and my son - your love makes my life.

ACKNOWLEDGEMENTS

During the course of my PhD, which spanned the last 5 years of my life, many people inspired me, contributed technically towards my work and helped me emotionally to stay focused in pursuit of my goals.

The most important names on this list are those of both my PhD advisors. I would like to thank Dr. Mary Ann Weitnauer for patiently listening to every crazy idea I proposed to her during my research. I joined Dr. Weitnauer's Smart Antenna Research Laboratory (SARL) in Spring 2012 when I signed up for a special problem with her. Her attention to details and hard work has inspired me throughout the course of my PhD. She is one of the most humble person I have ever come across in my life.

I would like to express my heartfelt gratitude to Dr. Omer Inan, my co-advisor, for the guidance and encouragement he provided during my research. I joined Dr. Inan's group in Fall 2014, at a time when Dr. Weitnauer and I were facing extremely complicated problems in data collection for our project. I will always be indebted to Omer for the role he has played in my PhD, career and life. He has allowed me to be creative in using new approaches, supported my ideas and even taught me the simplest things related to making diagrams in research papers. I feel extremely lucky that I had a chance to work with him and can call him a friend.

I would also like to thank my dissertation committee members: Dr. Pamela T. Bhatti, Dr. David V. Anderson, Dr. Srini Tridandapani and Dr. Mozziyar Etemadi. They provided me with extremely valuable feedback after my dissertation proposal for completion of my PhD. I would like to thank Dr. Justin Romberg who permitted me to sit in his classes and also gave me time whenever I requested him to discuss

signal processing problems I faced in my research.

Since I worked in two laboratories, I have been blessed to have really helping and friendly lab-mates in both of them. I would like to thank Van Nguyen, who let me work on her projects when I joined Dr. Weitnauer's lab. Qjongie Lin, who inspires me to work hard, I have never seen any student who works harder than her. She is always the first person to open the door of the SARL in the morning. I would also like to thank all my lab-mates in Inan Research Laboratory (IRL) who helped me during all my projects. Especially, Hazar Ashouri, who is extremely hard working and is always ready to contribute towards any project, has been with me in almost all my projects. I would also like to thank Hakan Toreyin, Andrew Wiens and Andrew Carrick for collaborating with me in different studies.

Hussain, Muneeb and Minhaj, my three roommates during the first year of my PhD at Georgia Institute of Technology, I had some unforgettable times with them. I will never forget the support and encouragement they provided me during my time at Georgia Tech. Especially, Hussain, who has always pushed me to work harder and faster and complete my degree as soon as possible. I would also like to thanks Muhammad Umair Bin Altaf for helping me in the acoustic signal processing part of my PhD work. Umer Tariq, thank you so much for your support during the 5 years I have stayed in Atlanta.

Lastly, I am left with the task of thanking my family. I shall start with my parents, Javaid Majeed and Gul-I-Nasreen, who deep down never wanted me to go away from them to pursue a PhD degree. I owe everything to them for their prayers, love and sacrifices they made for me. My sister, Sadia, who is one year younger than me, talking to her has always brought a smile on my face. She has always been by my side in every situation.

During the third year of my PhD, my wife and I had our first baby, a little boy named Musa. He is good-natured and loves cars and football. He has given a new

meaning to my life and has inspired me to work harder since his birth. He is always curious when I am working on my laptop and wants to press the keys like me. Every day, when I returned home after work, a look at his lovely face made all the day's exhaustion go away.

Finally, to my wife Risham, I don't know how to thank her for the love and support she has provided me ever since she came into my life. She has always picked me up when I am down and has guided me like the North star (Polaris) during the darkest hours of my PhD voyage. I am blessed to have her in my life.

TABLE OF CONTENTS

ACKNOWLEDGEMENTS . . . . . **iv**

LIST OF TABLES . . . . . **xi**

LIST OF FIGURES . . . . . **xii**

SUMMARY . . . . . **xvi**

I INTRODUCTION **1**

1.1 Major Contributions of the Study 5

1.2 Thesis Organization 7

II BACKGROUND **9**

2.1 Sleep Apnea 9

2.1.1 Heart Rate Variability (HRV) 10

2.1.2 Nocturnal Sound Analysis 10

2.1.3 Respiratory Signals 11

2.2 Ballistocardiogram 12

2.2.1 Cardiogenic Vibrations from Different Sensors 12

2.2.2 BCG based Cardiovascular Health Assessment 13

2.2.3 Processing of BCG 16

III SLEEP APNEA DETECTION WITH NON-CONTACT SENSORS 17

3.1 Introduction 17

3.1.1 Measurement Setup & Protocol 17

3.1.2 Pre-processing of Data and Motion Detection 18

3.1.3 Extraction of Normal & Apnea Epochs 20

3.1.4 Features Extracted from Radar Epochs 20

3.1.5 Features Extracted from the Microphone 23

3.2 IR-UWB based Sleep Apnea Detection 24

3.2.1 Training & Testing 25

3.2.2 Results & Discussion 25

3.3 Combined IR-UWB radar and Microphone based Sleep Apnea Detection 26
3.3.1 Training and Testing of the Combined Classifier 27
3.3.2 Results & Discussion 28
3.4 Limitations of the Work 29
IV HEMODYNAMIC ORIGINS OF BALLISTOCARDIOGRAM SIGNALS 30
4.1 Introduction 30
4.2 Protocol 32
4.3 Hardware & Data Processing 33
4.4 Extraction of Features from the BCG, ICG & ABP 35
4.4.1 Features derived from the BCG 35
4.4.2 Features derived from the ICG 36
4.4.3 Features derived from the ABP 36
4.5 Mapping the BCG to Other Modalities 36
4.6 Single-Subject Multi-Day Hemodynamic Assessment 40
4.7 Results 40
4.7.1 Correlation Results from Waveform Features 40
4.7.2 BCG Mapping Results 42
4.7.3 Single-Subject Results 42
4.8 Discussion 43
4.9 Conclusion 44
V POSTURE INDUCED DISTORTION IN BALLISTOCARDIOGRAM SIGNALS 46
5.1 Introduction 46
5.2 Effect of Posture on Weighing Scale BCG 47
5.2.1 Protocol for Data Collection 47
5.2.2 Hardware Design & Data Processing 49
5.2.3 Time Domain Posture-Induced Differences 50
5.2.4 Frequency Domain Posture-Induced Differences 51

5.2.5 Parameter Extraction 51
5.2.6 Improved Feature Estimation from Seated BCG 52
5.2.7 Statistical Analysis of Estimated Parameters 53
5.2.8 Results 54
5.3 Discussion & Limitations 55
5.4 Effect of Posture on Wearable BCG 56
5.4.1 Protocol & Experimental Setup 57
5.4.2 Hardware Design & Data Processing 58
5.4.3 Feature Extraction from ICG & SCG 59
5.4.4 Results 61
5.4.5 Discussion & Limitations 63

VI QUANTIFICATION AND REDUCTION OF MOTION ARTIFACTS FROM BALLISTOCARDIOGRAM SIGNALS MEASURED DURING WALKING 65

6.1 Introduction 65
6.2 Motion Noise Reduction using Multiple Accelerometers 66
6.2.1 Protocol 67
6.2.2 Hardware Design & Data Processing 67
6.2.3 BCG Feature Extraction & DTW based Algorithm 69
6.2.4 Data Fusion from Multiple Accelerometers 71
6.3 Results & Discussion 72
6.3.1 Discussion & Limitations 72
6.4 Removal of Walking Noise 73
6.4.1 Protocol 74
6.4.2 Hardware & Data Processing 75
6.4.3 Signal De-Noising using EMD 76
6.4.4 Dorso-Ventral Feature Detection and Tracking 78
6.4.5 Comparison of ICG and Accelerometer Data 81
6.4.6 Quantitative Determination of Ensemble Size 81

6.4.7 Results 84
6.4.8 ICG vs Accelerometer 84
6.4.9 Discussion & Limitations 87

VII WEARABLE MONITORING OF LEFT VENTRICULAR FUNCTION FOR HEART FAILURE SUBJECTS 91

7.1 Introduction 91
7.2 Protocol 92
7.3 Hardware & Data Processing 93
7.4 Algorithm for Selective Heartbeat Ensemble Averaging 93
7.5 Pre- and Post-Walk PEP Comparison 95
7.5.1 PEP Estimation 95
7.5.2 Percentage Predicted Walking Distance 95
7.5.3 Analysis & Discussion 96
7.6 Future Work 97

VIII CONCLUSION & FUTURE DIRECTIONS 98

8.1 Conclusions 98
8.2 Future Directions 99
8.3 Final Remarks 100

REFERENCES 101

LIST OF TABLES

1 The first- and second-order features extracted from the IR-UWB epochs. 21

2 Classification results for apnea (OA & OH) and normal epochs. . . . 25

3 Results For Minimum Number of Heartbeats N_e in an Ensemble for PEP and LVET. 86

LIST OF FIGURES

1 The organization of research work presented in this thesis. 4

2 Cardiac cycle showing different systolic time intervals. 14

3 Important features and points on the ECG and BCG signals. The R-peaks in the ECG signal are used to segment the signals from the BCG sensors. The BCG signal shown in the figure is from a modified weighing scale sensor. The W-BCG signal shown is from the dorso-ventral axis of an accelerometer placed on the chest. The highest peak in the BCG signal is called the J-peak. Similarly, the features on the dorso-ventral acceleration signal are the AO- and AC-points. The portions of the BCG signals between two ECG R-peaks are extracted and averaged to assist in feature extraction and noise reduction. . . . 15

4 (a) Block diagram of the setup. (b) The IR-UWB radar signal in one epoch of 60-sec duration. (c) The microphone signal in 60-sec epoch. The snores in the signal are shown with a black dash on the top. . . . 18

5 Algorithm for extraction of f_{15}. 21

6 (a) The principal components extracted from the training data. (b) Formation of peak pairs $\zeta_u(\eta_u, \tau_u)$ (u is the pair number, η_u is the peak value while τ_u represents peak position) from the correlation results: for a peak p_g in γ_s, a pair was formed with peak p_h in γ_e, if p_e was the first peak in γ_e for which $\tau_h > \tau_g$. $f_{15} = \{\eta_g + \eta_h : \eta_g \in \zeta_g, \eta_h \in \zeta_h, max|\tau_g - \tau_h|\}$. 22

7 Division of data during the training and testing phases. 24

8 Three 60-sec epochs corresponding to normal sleep, containing a hypopnea event and an obstructive apnea event. 27

9 Flowchart for data division in training ans testing phases. The red boxes indicate that features from snores were also included in classification. 28

10 Physiological phenomena associated with the action of heart. The forced ejection of blood into the aorta (represented by the force vector $\vec{F}_H$) is characterized by blood pressure (derived from ABP, waveforms), blood flow (derived from ICG waveforms) and whole body movement (derived from BCG waveforms). Analyzing the relationship between BCG and ABP or ICG waveforms can provide insight into the hemodynamic origin of the BCG and thereby improve the ability to derive cardiovascular health parameters from this signal. 31

11 (a) Experimental setup and processing steps for the measured signals. (b) Different phases of the data protocol used for collection of data from each subject. The mean and standard deviation for change in PP and SV are shown for different phases in the protocol. The values shown are for post-Valsalva recovery, handgrip and post-handgrip recovery phases. 32

12 (a) Extraction of features from the heartbeats of three measurement modalities. (b) Block diagram from system identification based mapping of the BCG heartbeats to the ICG and ABP heartbeats. The system was trained for data in the resting phase of each subject and then tested on the data from the perturbation phases. 35

13 (a) Correlation results for SV values obtained from the BCG mapped waveforms and the ICG waveforms. The relationship is statistically significant ($p < 0.05$) (b) Correlation results for change in PP from the BCG mapped and original ABP waveforms. N represents the total number of data points while n denotes the number of data points considered in the analysis after outlier rejection. 41

14 Single subject multi-day trial results. The system was trained on the 1st day and tested on the remaining 4 days for estimation of SV from the BCG signals. 42

15 (a) Experimental setup. Three standing postures: upright ($\theta_S \approx 0°$), slightly slouched ($\theta_S = 20 - 40°$) and heavily slouched ($\theta_S = 40 - 60°$). Two seated postures: upright($\theta_k = 90°$) and bent knee upright($\theta_K = 60 - 80°$). (b) The BCG heartbeats in standing postures. 48

16 Modified R-J interval estimation method from the weighing scale BCG in sitting postures. 53

17 Average power spectra with standard deviations for all subjects. (a) Upright standing. (b) Slightly slouched standing. (c) Heavily slouched standing. 54

18 Correlation results. (a) Upright standing. (b) Slightly slouched standing. (c) Heavily slouched standing. (d) Upright sitting (e) Bent knees sitting. N is the total number of data points while n is the number of data points used in linear regression after removing the outliers. . . . 55

19 Experimental setup and processing steps. 57

20 (a) The division of heartbeats into three bins based on mean and standard deviation of PEP values from individual ICG heartbeats. (b) Extraction of features from the ICG heartbeats and different components of sternal acceleration. 60

21 Correlation results: (a) $\text{LVET}_{\text{D-V}}$ vs LVET_{ICG} for P_1 (b) $\text{PEP}_{\text{D-V}}$ vs PEP_{ICG} for P_1 (c) $\text{R-J}_{\text{H-F}}$ vs PEP_{ICG} for P_1 (d) $\text{LVET}_{\text{D-V}}$ vs LVET_{ICG} for P_2 and P_3 (e) $\text{PEP}_{\text{D-V}}$ vs PEP_{ICG} for P_2 and P_3 (f) $\text{R-J}_{\text{H-F}}$ vs PEP_{ICG} for P_2 and P_3. 62

22 Bland-Altman plot for comparison of LVET estimated from $\text{SCG}_{\text{D-V}}$ and ICG in different postures. 63

23 (a) Block diagram of the setup. Data were collected in resting and walking states. (b) Position of accelerometers on the body. 68

24 (a) Extraction of template ψ_h from the resting H-F heartbeat and detection of the feature f_{ψ_h} ($\tau_h = \tau_h' = 250ms$). ψ_h is matched to the H-F heartbeat during walking and the correct J-peak is detected. (b) Extraction of ψ_o and ψ_c from the D-V heartbeat in the resting state and detection of features f_{ψ_o} and f_{ψ_c}. ($\tau_o = \tau_o' = 125ms$, $\tau_c = 100ms, \tau_c' = 2\tau_c$) 69

25 (a) Correlation plot between RJ-intervals from arm combined with sternum and the PEP from the ICG. (b) Correlation plot between RJ-intervals from ear combined with clavicle and the PEP from the ICG. (c) Correlation between LVET from sternum combined with neck and the LVET from the ICG. The red data points indicate the outliers and were not used in correlation analysis. n is the number of data points used in correlation. $\alpha = \beta = \frac{1}{2}$. 72

26 (a) The wearable patch that houses ECG and accelerometer sensors. Three adhesive electrodes are used with the device. (b) The inside assembly of the wearable patch houses a Micro-SD card on which the data is recorded. (c) The wearable patch attached to the sternum with three adhesive electrodes. (d) Block diagram of the setup. Two sets of data, which comprised of walking at normal speed (the speed at which each subject usually walked) and walking at 1.34 m/s on the treadmill, were collected from each subject. 75

27 (a) De-noising of the D-V heartbeat during walking using EMD algorithm. Four intrinsic mode functions were generated after the application of EMD. The first intrinsic mode function (I_1) was chosen as the de-noised D-V heartbeat for feature extraction. (b) Extraction of features from the resting state D-V heartbeat. The features were tracked during the heartbeats measured while the subjects were walking. The values of w_a and w_c were chosen as 60ms and 100ms for user-specific walking and 100ms and 120ms for 1.34m/s walking. 80

28 (a) The PEP estimates from the wearable patch and the Biopac ICG sensor for one subject during different phases of the 6 minute walk test. The data was divided into 15-s ensembles for both types of sensors. (b) The mean and standard deviation of PEP estimated from the accelerometer and ICG sensor for all subjects. The accelerometer estimates PEP with better accuracy for both types of walking tests and these are significantly different ($p << 0.05$) from the ICG estimates. 83

29 Determination of minimum ensemble size using the polynomial fitting approach for one subject. (a) 64 heartbeats. (b) 32 heartbeats. (c) 16 heartbeats. (d) 4 heartbeats. The data points in blue are outliers. In order to have same y-axis scale for each plot, the outliers for some plots are not shown in the above figures but are explained as follows: 2 data points were detected as outliers in (a), 1 data point as outlier in (b), 2 data points as outliers in (c) but are not shown, and, 5 data points as outliers in (d) which are not shown. An outlier was detected by removing the data point which was more than 1.75 standard deviation away from the mean of all data points. 85

30 Comparison of minimum ensemble size for the PEP during walking at a self-determined pace and at 1.34 m/s on treadmill and track for one subject. The dotted grey line shows a threshold of 2ms RMSE for the PEP estimates. The minimum number of heartbeats required for the self-determined pace is greater than 8 while walking at 1.34 m/s in an uncontrolled environment such as a jogging track requires more than 16 heartbeats in the ensemble. 89

31 New method of ensemble averaging that involves rejection of extremely distorted or noisy heartbeats. The heartbeats which have more than γ_n % of total data points beyond one standard deviation above or below the mean trace are rejected. $\gamma_n = 40\%$ was chosen for the data set. The cleaner ensemble averaged trace is then calculated using the remaining heartbeats. 94

32 Δ PEP vs % Predicted Distance for HF subjects. The class IV subjects are concentrated in the lower right corner of the figure with mean and standard deviation of -0.11 ± 0.06 for Δ PEP and 0.35 ± 0.11 for the % Predicted Distance. Similarly, the class I-II subjects are concentrated in the upper left corner of the figure with mean and standard deviation of -0.26 ± 0.15 for Δ PEP and 0.78 ± 0.25 for the % Predicted Distance. 96

SUMMARY

Cardiovascular disease (CVD) is the leading cause of death across the globe claiming 17.3 million lives every year. According to the most recent report from the American Heart Association (AHA), heart disease strikes a person every 42 seconds in the United States and the direct and indirect costs of heart disease total more than $316.6 billion. Hence, it is of no surprise that AHA recommends home monitoring of patients with heart failure (HF) and other heart disorders. Recently, many devices have been proposed for monitoring hemodynamics at home. However, most if not all of these are obtrusive and require trained experts to operate them. Moreover, for a thorough assessment of cardiovascular function, it is important to monitor respiratory parameters as well since both systems are functionally interconnected with each other and cardiac diseases affect the respiratory system and vice versa.

This research focused on a variety of sensors to estimate mechanical parameters related to respiration and cardiovascular health. Specifically, the work explored the use of non-contact sensors for detection of sleep apnea, a pause in breathing during sleep, and wearable and unobtrusive sensors for measuring body vibrations caused by flow of blood into the vasculature.

Despite the presence of different types of sensors for sleep apnea monitoring, there are still stringent requirements on position and placement of the sensors for the whole night recording. Some of the sensors are a source of discomfort to the patients as they require contact with the skin and also are a cause of concern for hygiene. Sensors which do not require direct skin contact—such as radar based measurement of chest wall movement, and microphones to record snoring and breathing sounds—would be preferable, but require advanced processing methods to extract actionable information

regarding sleep quality. In this work, such processing methods including feature extraction and machine learning algorithms were developed and verified.

In parallel to the efforts focused on non-contact chest wall movement analysis for sleep apnea detection, this work investigated the analysis and interpretation of cardiogenic body vibrations caused by flow of blood into the vasculature. These minute body vibrations are called ballistocardiogram (BCG) signals and the phenomenon is termed as ballistocardiography (BCG). Specifically, this work delved deep into the hemodynamic origins of these vibrations and used feature based methods and system identification techniques to associate the BCG vibrations to more known phenomenon related to flow and pressure of blood. A novel system was presented to estimate stroke volume changes from the BCG signals. Further, the effect of posture on these vibrations from wearable and / or unobtrusive sensors and how these affect the accuracy of measured parameters was also investigated. Features of the signal specific to non-ideal posture were identified, such that changes due to underlying patho-physiology could be separated in future studies from changes related to posture.

The body vibrations are sensitive to motion artifacts and any movement on the part of the subject can compromise the signal-to-noise ratio (SNR) of the measured signal from any type of sensor. Novel algorithms were presented in this work to remove walking related motion artifacts from the BCG signals measured using accelerometers. These methods open the door for robust estimation of systolic time intervals from the BCG during walking and can help in understanding the changes in cardiovascular physiology in response to stressors caused by exercise or simple activities.

The algorithms and methods presented in this work for respiratory and cardiogenic vibrations can be used to monitor cardiovascular patients at home using inexpensive and compact sensors. This would decrease the number of re-hospitalizations each year and also increase the quality of living.

CHAPTER I

INTRODUCTION

Cardiovascular and respiratory diseases are leading contributors of health problems in the world. Cardiovascular disease (CVD) alone accounted for 25% of the total deaths in the United States last year and heart-related healthcare expenditures totaled more than $300B annually [64]. These numbers are expected to rise in the coming decades and by 2030, 40% of the US population is predicted to be afflicted by some form of CVD. This will lead to a further increase in the sky-rocketing costs of healthcare and other health-related expenditures. At the same time there is an expected shortage of healthcare providers per patient in the coming ten years [17]. This imminent problem of mismatch between the number of patients and healthcare resources available per patient can be addressed by inexpensive devices that enable assessment of patient health in home settings and can be operated without the supervision of trained clinicians. However, most of the devices that exist today lack the capabilities to measure a wide variety of physiological parameters required for assessment of respiratory and cardiac function.

The recent advances in semiconductor fabrication processes and increase in the number of computing tools has resulted in the advent of low-cost miniature sensors that can be embedded into novel and unobtrusive wearable technologies or used with existing devices that can be easily integrated into the infrastructure of a patient's home. These novel technologies, which include radars, miniature acoustic sensors, accelerometers, pressure mats and other electro-mechanical sensors, can increase the span of physiological parameters that can be measured via home monitoring without causing any significant change or hindrance in a patient's daily routine or activities.

Home monitoring of CVD requires the sensing of both cardiovascualr and respiratory health parameters, as these two systems are intertwined with each other. The human cardiovascular system receives oxygenated blood from the lungs in the left atrium while simultaneously receiving de-oxygenated blood in the right atrium from the vessels [72]. The oxygenated blood is then pumped into the aorta through left ventricle while the de-oxygenated blood is sent to the lungs through right ventricle [72]. Hence, both the cardiovascular and respiratory system work in conjunction with each other. Any issue that affects the respiratory system can also impact the cardiovascular system and, conversely, early symptoms of many cardiovascular health issues also manifest in the respiratory system.

One such respiratory disorder that affects heart health is sleep apnea [92], which is caused by involuntary cessation of breathing during sleep [8]. Approximately 92% of women and 83% of men with sleep apnea remain undiagnosed imposing a burden of $3.4B on the annual medical costs [77]. If left untreated, sleep apnea is linked to a growing number of cardiovascular health problems that include high blood pressure, diabetes, irregular heart rate and depression [63]. Moreover, recent studies have shown that people with sleep apnea are at higher risk of developing coronary heart disease and heart failure (HF) [38]. Accordingly, there is a growing need to have monitoring systems which utilize minimally invasive and unobtrusive sensors for early detection of sleep apnea.

Such early detection of sleep apnea can potentially reduce the incidence of downstream cardiovascular disorders including HF—a progressive condition in which the heart cannot supply sufficient blood to meet the demand of the tissues and organs [53]. In the early stages of HF, the contracting muscles of the heart get bigger and the blood is pumped more strongly to meet the demand of the body. The body also tries to compensate by diverting blood away from less important tissues. However, as the HF condition worsens, there comes a time when the body and heart cannot keep up

with each other. The compensatory methods of the body are the reasons people do not notice their condition until the decline of the heart reaches its later stages. HF is an archetypal example of a cardiovascular disorder that requires improved continuous monitoring [19].

For both sleep apnea detection and HF monitoring, the major technological obstacle is the inability to monitor the mechanical parameters of physiological function outside of clinical settings. Home monitoring systems for both sleep apnea and CVD include sensing modalities such as electrocardiography (ECG), nasal air flow sensors, impedance cardiography (ICG), respiratory plethysmography and pulse-oximetry. Although these sensors can provide accurate information regarding respiratory and cardiovascular function, they are far from unobtrusive and require trained personnel for operation. For example, ICG requires placement of eight electrodes on the neck and thorax by a trained professional [43]. Patient discomfort and thus low acceptance of the sensing modalities can also pose challenges: for example, wearing the nasal air flow and respiratory plethysmography sensors can certainly cause discomfort and possibly even vary the sleeping behavior of the subject.

The aim of this research is to not only explore signals from existing measuring modalities, but also look for new sensors for measuring physiological parameters for monitoring of sleep apnea and cardiovascular health. In this context, we aim to combine the respiratory effort signals from a non-contact impulse-radio ultra-wide band (IR-UWB) radar and acoustic signals from a microphone for screening and detection of sleep apnea. Similarly, for HF we aim to investigate ballistocardiogram (BCG), the measurement of reactionary forces of the body caused by ejection of blood into the vasculature [43]. BCG is not a new methodology. In fact, it was first discovered in the late 19th century by J. W. Gordon who observed fluctuation in the weighing scale needle while a person stood on it [37]. Later in the mid 20th century, Starr and

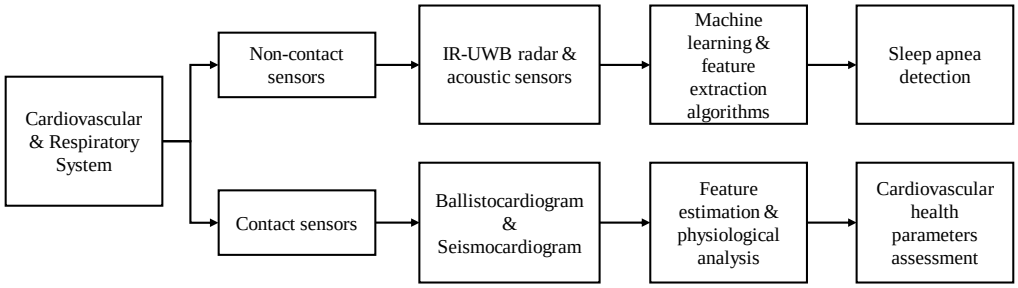

Figure 1: The organization of research work presented in this thesis.

his colleagues showed that BCG can be used for detection of cardiovascular anomalies [95]. However, at that time, BCG measurement required heavy and cumbersome instrumentation; on the other hand, there were rapid improvements in other cardiovascular measurement instruments such as ECG and imaging technologies. Hence, the interest in BCG slowly waned as these other devices became commonplace. Recent advances in sensing technologies have allowed for unobtrusive and even wearable BCG measurement instrumentation to be developed over the past decade, and this has in turn revived the interest in BCG as a tool for physiological monitoring. These instrumentation advances are also bolstered by the fact that research in both the engineering and clinical communities has demonstrated the potential clinical relevance of BCG signal features.

Thus, the objectives of proposed research are two-fold: (1) to design signal processing techniques and algorithms for detection of sleep apnea using a combination of non-contact under-the-mattress IR-UWB radar and a microphone placed on the side-table, and (2) to develop methods for accurate estimation of various cardiac parameters from the BCG signal obtained from variety of sensors and investigate the physiological origins of the BCG. The step-by-step flow of research work in this thesis is presented in Fig. 1.

1.1 Major Contributions of the Study

There has been a considerable amount of work done on the use of non-contact sensors and BCG for measuring mechanical parameters of physiological function. However, there are important gaps in the existing framework of these methodologies that need to be bridged in order to use them for continuous home monitoring of respiratory and cardiovascular health.

The existing research has already explored the use of IR-UWB radars and microphone based snore analysis for the detection of sleep apnea. However, a major limitation in this field has been the stringent constraints on the placement of sensors during the recording process. Moreover, a combined system composed of both IR-UWB radar and microphone has also not been investigated. *Can a radar alone provide excellent accuracy in detection of sleep apnea? Will adding other non-contact sensors such as a microphone cause an improvement in the overall performance of the system? Can multiple sensors provide relaxation in strict requirements placed on the position of a single sensor?* In this work we try to address these important questions.

Similarly, BCG has shown to be able to provide features that can be used for cardiovascular assessment. But whilst the BCG provides parameters based on body vibrations, clinicians and physicians are more interested in existing hemodynamic parameters describing the cardiovascular function in terms of flow and pressure of blood. Moreover, these body vibrations are affected by change in posture and movement. This work focuses on expanding the number of parameters estimated from the BCG for cardiovascular monitoring while exploring the relationship of BCG with existing hemodynamic phenomenon and also on expressing these estimated BCG parameters in terms familiar to clinicians and cardiac experts. Moreover, methods are presented to overcome the changes in the BCG signal induced by posture related changes and walking to improve the accuracy of BCG-derived parameters in these phases.

Thus, the major contributions of this work, and their potential impact in the field of research and more broadly to society, are given below:

1. Designed algorithms for extraction of novel features from respiratory signal measured using an IR-UWB radar. Combining these with features from non-contact microphone sensors can lead to the design of a user-friendly and robust system for automated detection of sleep apnea in home settings.

2. Demonstrated using system identification techniques that a linear relationship in mapping BCG signals to ICG-based blood flow signals was preserved during physiological perturbations, and significantly better than the corresponding relationship between BCG and arterial blood pressure (ABP) signals. Converting BCG signals to corresponding ICG signals can broaden the range of hemodynamic features estimated from the BCG and also provide clinically relevant insight into the BCG signal's origin.

3. Designed and validated robust data driven algorithms for estimating systolic time intervals (STIs) from BCG signals during walking at light to moderate speeds and in non-ideal postural conditions. Specifically, the BCG data during walking is either completely ignored due to very low signal-to-noise ratio (SNR) or limited to heart rate estimation only. These algorithms can, for the first time, capture changes in cardiovascular physiology during exercise or movement intervals using BCG signals.

4. Demonstrated that wearable ECG / BCG based measures of pre-ejection period (PEP) changes in response to the six minute walk test were significantly ($p < 0.05$) lower for patients with decompensated heart failure (New York Heart Association (NYHA) Class IV) as compared to compensated heart failure (NYHA Class I-II). Knowing that PEP changes in response to exercise captured by a wearable patch can separate compensated from decompensated

HF patients and lead to an automated wearable system to potentially predict decompensation beforehand, allowing physicians to intervene accordingly.

1.2 Thesis Organization

The rest of the thesis is organized as follows: The previous work in both sleep apnea detection and BCG based cardiovascular monitoring are reviewed in Chapter II. The chapter also discusses important nomenclature for the BCG signals measured with different sensors and from different locations on the body. Chapter III discusses the detection of sleep apnea disorder with non-contact sensors. Novel algorithms are presented for extraction of features from the IR-UWB radar signal along with the effect of adding a microphone sensor on the overall performance of the system.

The hemodynamic origins of BCG are investigated in Chapter IV by exploring the feature based relationship of BCG with pressure and flow of blood. Moreover, the chapter also outlines a system identification approach for converting the BCG waveforms to equivalent ICG waveforms which leads to estimation of stroke volume. The method presented in Chapter IV can be extended for monitoring stroke volume changes at home.

The effect of posture on BCG signals is analyzed in Chapter V. Two different types of sensors are considered in this work. The first half of the Chapter focuses on the BCG signals from a modified-weighing scale sensor while the later later half analyzes the BCG signals from a wearable sensor. A novel method is presented for estimation of cardiovascular parameters in sitting postures using the modified-weighing scale. Similarly, novel features are extracted from the wearable BCG to improve the accuracy of cardiovascular parameters during different standing postures.

Algorithms are presented to estimate cardiac parameters from the BCG during walking in Chapter VI. As briefly mentioned earlier, the body vibrations measured using any BCG sensor are extremely sensitive to motion. Almost all of the current

research on the BCG based physiological monitoring focuses on the signals measured during the resting state while ignoring the signals in the movement related periods. Thus, data during these periods which has low SNR but contains extremely useful information about changes in cardiovascular changes in response to simple activities such as walking is discarded. In Chapter VI, we focus on removal of walking induced noise by implementing empirical mode decomposition (EMD) algorithm from the BCG signals measured with a wearable patch. The chapter lays the foundation for future work on walking BCG signals and identifies how walking speed contributes towards a decrease in time resolution of the estimates obtained from the de-noised BCG signals.

Chapter VII discusses the work on monitoring of HF patients using BCG. The work involves data from a pool of HF subjects at different stages of the disorder. A novel method is presented that estimates PEP from wearable BCG signals before and after a 6-minute walk test, commonly used in clinics for evaluation of an HF patient, and quantifies the change in PEP that occurs due to the walking exercise. Initial results show that wearable BCG can be used for assessing the condition of HF patients and also indicate that features from the BCG can be used for prognosis of the disease. Finally, conclusion and future work is briefly discussed in Chapter VIII.

CHAPTER II

BACKGROUND

2.1 Sleep Apnea

Apnea is a Greek word that means 'without breath'. Sleep apnea involves cessation of breathing for 10 or more seconds [8]. There are three main types of apneas: (1) obstructive sleep apnea (2) central sleep apnea, and (3) mixed sleep apnea. The obstructive sleep apneas, with an estimated prevalence of 5-15% among adults [77], are the most common occurrence of sleep related breathing disorders (SBD) in which muscles such as soft palate and tongue relax and block the upper airway during sleep. This causes a temporary pause in breathing. A 90% or greater drop in breathing amplitude is termed as obstructive apnea (OA) while a 30% or greater decrease is referred to as an obstructive hypopnea (OH) event [8]. Thus, obstructive apneas are caused by complete obstruction of upper airway while hypopneas are due to partial obstruction. In central apneas, the brain fails to send signals to breathing muscles and an interruption in breathing occurs without narrowing of upper airway. The metrics to quantify the severity of the disorder includes Apnea-Hypopnea Index (AHI), which is the number of apnea and hypopnea events in one hour [8]. The standard approach of diagnosing sleep apnea is polysomnography (PSG), which monitors sleep and respiration by measuring a number of physiological parameters including ECG, blood oxygen saturation (SpO_2), chest effort signals and nasal pressure. However, PSG is an expensive procedure and requires sleeping in well equipped and technician attended laboratories. However a large number of sensors are attached to body at various locations that may cause discomfort and also vary the sleeping behavior for that particular night.

Research on monitoring and detection of sleep apnea at home can be divided into three main categories based on physiological signals under consideration:

2.1.1 Heart Rate Variability (HRV)

The onset of sleep apneas are accompanied by decrease in heart rate (bradycardia) and the culmination involves elevated heart rate (tachycardia). HRV is the most common and highly used feature in automated detection of sleep apnea outside clinical settings. It involves calculation of R-R time intervals from ECG signal [20, 106]. Statistical features are then derived from time and frequency domain representation of the R-R intervals [20] followed by application of classification algorithms. Research has shown that HRV based features can accurately detect sleep apena events. Along with ECG derived features, authors in [20] have also used features from respiration signals estimated from the raw ECG data. The ECG signal, obtained from electrodes attached to chest, contain the respiratory component which can be filtered out and features can be derived from it to assist in HRV based sleep apnea detection.

2.1.2 Nocturnal Sound Analysis

Loud snoring has long been associated with monitoring of sleep apnea [74]. Vibrations of soft-palate and uvula produce snoring sounds. Since obstructive sleep apnea is caused by blocking of the upper airway due to tongue and soft palate, this narrowing of the upper airway causes a change in the properties of the snores. Many researchers have analyzed snoring sounds to differentiate between normal and apneic subjects. The snores from apnea patients exhibit different acoustic attributes than those from healthy subjects. The most prominent of these features include pitch of the snoring sound [1, 2, 7], spectral features [69, 87, 91], mel cepstral coefficients (MFCCs) [2, 7] and formant frequencies [68, 89, 90].

In order to record snores, a contact microphone, placed on neck, has been used in [91] while a non-contact microphone has been utilized in [69]. The non-contact

microphone needs to be placed at an optimal position to avoid loss in efficiency of the system [74].

2.1.3 Respiratory Signals

Respiratory signals, more commonly known as 'Respiratory Effort' signals, derived from chest abdominal straps and nasal sensors, have been used in [67, 101] to successfully detect apnea events. Any change in the air volume in the lungs is measured by the change in cross-sectional area of ribs and abdomen. Microwave radars (doppler and IR-UWB) have gained a lot of popularity in measuring vital signs [56, 70, 94]. The radar signal, if directed towards a human torso, is reflected from the skin interface and contains information about respiration [70]. Thus any change in chest displacement, caused by apnea or any other respiratory disorder, will manifest itself in the reflected signal. The main differences between the doppler and the IR-UWB radars are the bandwidth, power, and the band of operation. The IR-UWB radar signal can be spread throughout the 3 to 10 gigahertz band [15], which spans many other licensed and unlicensed bands. The doppler radar must be used in either a licensed band or an ISM (industrial, scientific and medical) band, and makes more interference on other devices because of its more narrow bandwidth and also it is more vulnerable to the interference from these other devices. Because of its extremely wide bandwidth, the IR-UWB radar can be operated at a much lower average power than the doppler radar, for the same SNR in the radar receiver, and it has higher time resolution which translates to more sensitivity to small periodic movements of the reflecting surfaces. A doppler radar has been used in [57] to detect different types of breathing disorders that include apneas. Similarly two microwave radars are used in [49] to detect sleep apneas. Doppler radar is used in [21, 107], in a device placed on the bedside table named 'Sleepminder', developed by Biancamed for detection of sleep and wake patterns along with apnea events.

As discussed earlier, even though there are many portable devices for home monitoring of the sleep apnea disorder, most of these still require contact with the skin and thus may cause discomfort and skin irritation. On the other hand, the devices like microphone and radars do not cause any skin contact but they still impose strict constraints on placement of the sensors. The work in Chapter IV will try to address these constraints by exploring combination of more than one measurement modality.

2.2 Ballistocardiogram

BCG is the measure of the whole body motion caused by the ejection of blood into the vessels [37]. It was first discovered by J. W. Gordon in 1877 who observed a fluctuation in the weighing scale needle due to heart beat [37] and proposed that change in the weighing scale measurement is caused by ejection of blood. In 1940, I. Starr [95] showed that BCG can be used to assess cardiac anomalies. However, due to presence and advent of electrical and electromagnetic heart monitoring and imaging techniques, the interest in BCG related sensors vanished. As the 20th century approached its conclusion, the rapid growth in population and a resultant mismatch in health resources triggered the need for home based unsupervised patient monitoring. The concurrent developments in semiconductor and fabrication technologies ushered an era of extremely small and low-cost sensors which can be integrated into existing devices. In the last few decades, researchers have measured BCG using instrumented chairs and beds [5, 11, 24, 60], weighing scales [36, 45], accelerometers [102], pressure sensors [83] and force plates [98].

2.2.1 Cardiogenic Vibrations from Different Sensors

The choice and type of sensor and its placement on the human body dictates the type of vibrations picked by it. The signals from a weighing scale, which can be modeled as a second order mechanical system governed by Hook's law [74], are directly proportional to displacement [43]. On the other hand, the signals from a wearable

accelerometer sensor [43], when placed anywhere, are acceleration measurements of the surface of the skin. The position of the wearable sensor on the body such as an accelerometer also affects the range of signals captured by it. For instance, if a tri-axial accelerometer is placed on the sternum or anywhere in the chest region, the vibrations in the head-to-foot direction (along the body) are low frequency signals and contain information about hemodynamics. However, the vibrations in the dorso-ventral direction (axis of the accelerometer perpendicular to the surface of the body) not only contain vibrations due to flow of blood but these also have high frequency components which are caused by opening and closure of the heart valves [13]. These high frequency vibrations from the chest are given a specific name in literature and are called *seismocardiogram* (SCG). It has been shown in [13] that a tri-axis accelerometer can detect the first and the second heart sounds from the dorso-ventral axis signal if placed on the sternum. It is important to mention here that the term SCG is only used for dorso-ventral vibrations from the chest region. If the accelerometer sensor is placed on any other location in the body, these vibrations will not be termed as SCG. In fact, vibrations from other body locations will not contain heart sound components. Hence, *wearable ballistocardiography* (W-BCG), a more generic term, is used in this thesis for all types of signals measured from a wearable tri-axial accelerometer sensor placed any where on the body including the sternum.

2.2.2 BCG based Cardiovascular Health Assessment

Since the BCG measurements are due to the flow of blood, these can provide reliable estimates for hemodynamic assessment and can yield insight into the mechanical health of the heart. The mechanical health refers to amount of time a human heart spends during different phases of a cardiac cycle as shown in Fig. 2. The cardiac cycle is composed of four distinct phases—isovolumic contraction, rapid ejection, isovolumic relaxation, and passive filling. Measuring the time spent by the heart in each of

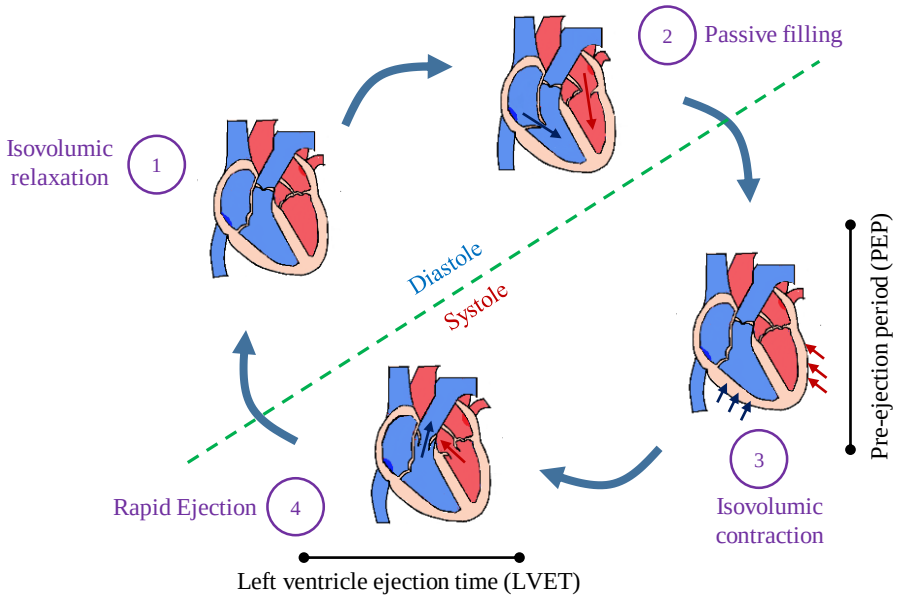

Figure 2: Cardiac cycle showing different systolic time intervals.

these phases can provide great insight into the health and function of a person's cardiovascular and autonomic nervous systems [59]. The period of the isovolumic contraction, also known as PEP, is the time between the electrical excitation of the ventricular cardiomyocytes and the ensuing opening of the aortic valve. PEP is a surrogate non-invasive measure of myocardial contractility [58]. The period of the systolic ejection, also know as left ventricular ejection time (LVET), is the time taken for the blood to be ejected from the ventricles, started by the aortic valve opening and ended by its closing. PEP and LVET are called STIs. The sum of PEP and LVET is the total time the heart spends in systole (ejection) as compared to diastole (filling) and is an important parameter for monitoring of patients with heart disorders [19].

In the coming decades, the number of patients with heart disorders is expected to increase dramatically [64] as is the corresponding cost of healthcare; accordingly, there is an impending need for creating new, inexpensive and ubiquitous technologies for continuously monitoring cardiovascular health parameters, such as STIs. Unfortunately, STIs cannot be readily estimated from existing wearable cardiovascular sensing

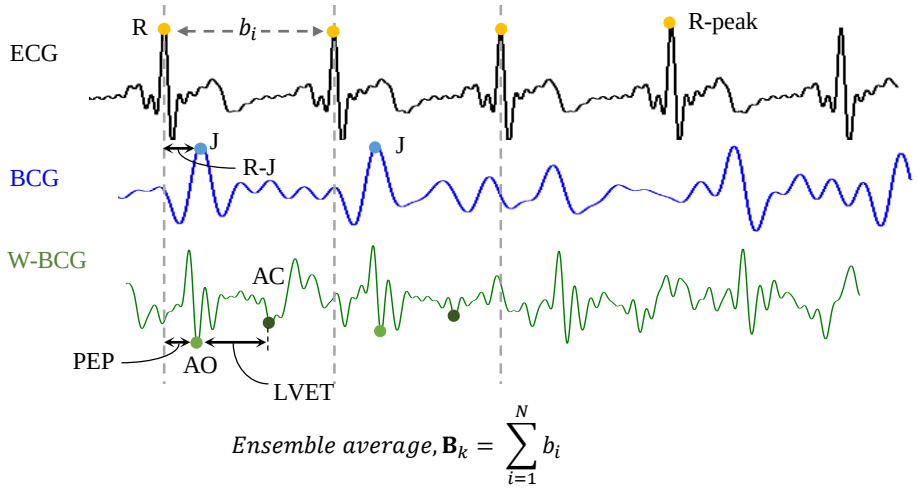

Figure 3: Important features and points on the ECG and BCG signals. The R-peaks in the ECG signal are used to segment the signals from the BCG sensors. The BCG signal shown in the figure is from a modified weighing scale sensor. The W-BCG signal shown is from the dorso-ventral axis of an accelerometer placed on the chest. The highest peak in the BCG signal is called the J-peak. Similarly, the features on the dorso-ventral acceleration signal are the AO- and AC-points. The portions of the BCG signals between two ECG R-peaks are extracted and averaged to assist in feature extraction and noise reduction.

devices which typically focus on *electrical* measurements only (e.g. ECG based Holter monitors or patches [30]). Recent research has demonstrated that BCG derived features contain important information regarding myocardial contractility [29]. Authors in [28] showed that the R-J interval (shown in Fig. 3)—defined as the time interval between the ECG R-peak and the maximum peak of BCG signal, the J peak—is highly correlated with PEP, and thus a surrogate measure of cardiac contractility [72]. Similarly, the accelerometer signal along the dorso-ventral axis, as shown in Fig. 3, contains features corresponding to opening and closure of aortic valves, i.e., the AO- and AC-points labeled in Fig. 3. The time difference between the ECG R-peak and the AO-point on the signal gives an estimate of the PEP and the time interval between the AO- and AC-points gives LVET. The choice of AO- and AC-points varies in existing literature. Some authors prefer the global maximas in the first and second half of the trace as AC- and AO-points while some choose minimas as features. In

Fig. 3, the AO- and AC-points are illustrated as the minimas in the first and second half of the dorso-ventral signal between two ECG R-peaks.

2.2.3 Processing of BCG

The common processing of BCG signals from all types of sensors usually involve simultaneous measurement of the ECG which helps in the segmentation of the BCG signals as shown in Fig. 3. The BCG signal between two ECG R-peaks is extracted and the BCG traces within some time interval or a specific number of BCG traces are averaged to reduce noise and get an averaged trace called ensemble average and the whole process is called ensemble averaging [93]. The length of this BCG trace is equal to the R-R interval duration obtained from the ECG. If other reference signals, such as ICG or ABP are measured along with the ECG and BCG in a project, then those undergo similar segmentation.

Most of the current research on the BCG focuses on features in the form of timing intervals for cardiovascular monitoring. There is a compelling need to analyze how different postures and simple activities such as walking affect these features. Moreover, clinicians are more concerned with parameters related to pressure and flow of blood as compared to simple timing based measurements from vibrations. Hence, it is important to deeply investigate the BCG relationship with pressure and flow of blood and also to assess if there is a potential to estimate stroke volume from the BCG.

CHAPTER III

SLEEP APNEA DETECTION WITH NON-CONTACT SENSORS

3.1 Introduction

Sleep apnea, as discussed earlier, is a respiratory disorder that can cause different health and behavioral problems and also effects activities of daily living. It's diagnosis requires overnight monitoring in well equipped laboratories under the supervision of sleep specialists or technicians. The home monitoring of this disorder can be done with different devices most of which utilize contact sensors which may be a source of nuisance for the patient.

The objective of this study was to use non-contact sensors such as a radar and a microphone, placed at sub-optimal locations, and analyze if the features from both the modalities can be combined to give a better performance in classification between epochs belonging to normal sleep and those that contain an apnea or hypopnea event in them. The following sections explain the experimental setup, data processing steps and feature extraction methods used for both the IR-UWB radar and microphone data. Later we discuss the classification results from radar only features and whether including microphone based features can provide an improvement in classification accuracy.

3.1.1 Measurement Setup & Protocol

The data for the project was collected at a sleep research laboratory (Neurotrials Research Inc.) under a protocol approved by the Georgia Institute of Technology Institutional Review Board (IRB). A shotgun microphone (Audio-Technica) was placed

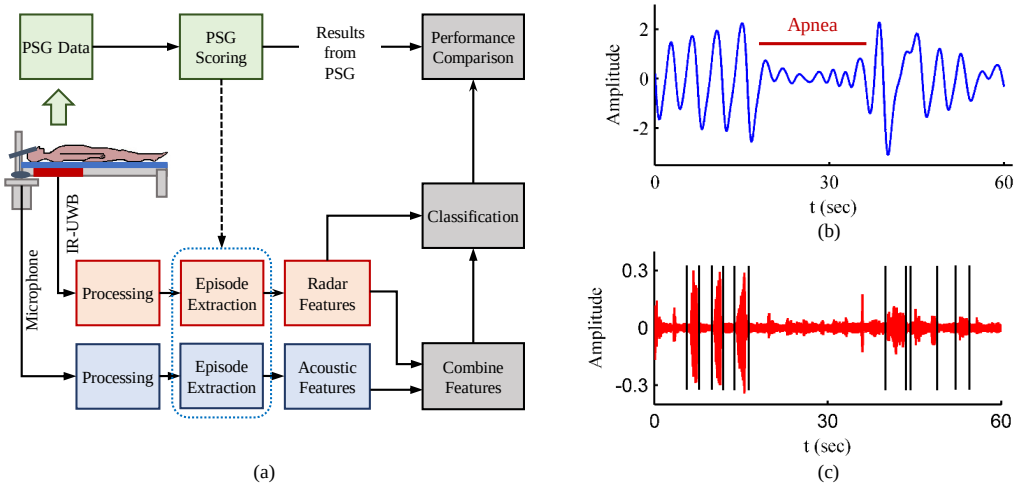

Figure 4: (a) Block diagram of the setup. (b) The IR-UWB radar signal in one epoch of 60-sec duration. (c) The microphone signal in 60-sec epoch. The snores in the signal are shown with a black dash on the top.

on the side-table adjacent to bed while an IR-UWB radar system, developed by Sensiotec Inc. [32] was placed under the mattress. The radar transmitted pulses were 13 ns long, centered at 4.2 GHz. At the receiver, the reflected signal was time-gated and down-converted to baseband and then hardware-filtered into a respiration band (low pass, cut-off frequency 0.7 Hz) and heart band (cut-off frequencies: 0.5 - 6 Hz), respectively. Only the respiration band was considered in this research. Next, the outputs of each filter band were sampled at 128 Hz and quantized for subsequent digital signal processing. The microphone signal was sampled at 44.1 kHz, band-pass filtered (cut-off frequencies: 70 - 2000Hz) and downsampled by a factor of 4 to provide ease in processing and feature extraction. The PSG data was also collected simultaneously. The data from the IR-UWB radar and the PSG data were both time stamped. A specialist from Neurotrials scored the PSG and marked all the normal and apnea epochs. A block diagram of the setup is shown in Fig. 4 (a).

3.1.2 Pre-processing of Data and Motion Detection

In order to facilitate the extraction of features, the quantization noise in time domain respiratory signal was removed by filtering twice with a 20 tap triangular filter. To

avoid changing the amplitude and shape of the signal, only the central tap was assigned a weight of two while the remaining taps had unity weights. An example of the respiration signal produced by the IR-UWB radar after the application of triangular filter is the blue oscillating waveform shown in Fig. 4 (b). The radar signal was very sensitive to motion and showed clipping to the ADC maximum and minimum levels whenever the subject made large muscle movements. The part of the IR-UWB data that contained motion artifacts was detected and removed. All the maximas and minimas in the input time domain signal were compared against pre-defined thresholds. If a maxima was above the upper threshold, then the portion of the signal containing that maxima along with one previous and one next maxima were labeled as motion corrupted. A similar approach was used for a minima that was found below the lower threshold. The reason for including one previous and one next maxima or minima was to make sure that the complete portion encompassing motion was removed. The clean signal that fell between the two motion corrupted parts was standardized by calculating the z-score of each data point in that portion. The z-score was calculated by subtracting the mean and dividing by standard deviation of the signal. The reason for separate standardization of data that were separated by motion corrupted regions was to avoid error in feature extraction stage as the radar signal's amplitude was different for different postures and varied across population, especially across genders.

The microphone signal was manually analyzed to label snoring events. The features from the microphone data were later extracted from these manually detected snores. It is important to mention here that since the data set included only 4 subjects, an automated snore detector was not developed for this study.

3.1.3 Extraction of Normal & Apnea Epochs

Epochs of 60 second duration, that included the marked apnea event, were extracted from the IR-UWB radar data and microphone data. More specifically, the 60 seconds in each epoch were composed of $t_s - 20$s to $t_s + 40$s, where t_s represented the apnea start time which was obtained from the PSG. Also the 60 second duration epochs corresponding to time intervals of normal sleep were extracted from both radar and microphone sensors using information from the scored PSG. All the epochs corresponding to both OA and OH were combined into one class, labeled as *Apnea*, and the normal epochs were assigned class label $Normal$, thus making our task one of binary classification.

3.1.4 Features Extracted from Radar Epochs

The features were extracted from both the time and frequency domains for each epoch. A total number of 15 features were extracted from the epochs obtained from the radar data. We defined f_k to be the k-th feature (k = 1,2,...,15). The first eight features were directly extracted from each epoch. The $f_9 - f_{13}$ were extracted by first dividing each epoch into small parts of t_d duration ($t_d = 10sec$ was chosen as minimum duration of an apnea event must be $10sec$). Let E_i denote a complete epoch of 60 seconds (i is the epoch number) while e_m represent a small division of it (m is the part number, $m = 1, 2, ..., 6$). Let the variance of time domain respiratory signal in each e_m be denoted by $\sigma^2_{e_m}$. Also let d_m be the difference in the upper and lower envelopes of the small epochs e_m and $\sigma^2_{d_m}$ be its variance. The envelopes were obtained by cubic interpolation of maximas and minimas. The features f_1 to f_{13} are explained in Table 1.

In order to extract the features f_{14} and f_{15}, the average energy of all epochs in the training set corresponding to normal periods of sleep was calculated and used as a normalization constant for all the apnea and normal epochs. The apnea epochs were

Table 1: The first- and second-order features extracted from the IR-UWB epochs

Feature f_k	Description
f_1	Mean Absolute Deviation (MAD) of respiratory signal.
f_2	MAD of peaks values of respiratory signal.
f_3	Number of times the signal crosses the mean.
f_4	Variance of samples between mean crossings.
f_5	Variance of maxima-minima intervals.
f_6	Variance of maxima-minima amplitude values.
f_7	The difference between 75th and 25th percentile of f_3.
f_8	The sum of power spectral density values between $0 - 0.5$ Hz.
f_9	Variance of $[\sigma^2_{e_1}, ..., \sigma^2_{e_6}]$.
f_{10}	Variance of $[\lvert\sigma^2_{e_1} - \sigma^2_{e_2}\rvert, ..., \lvert\sigma^2_{e_5} - \sigma^2_{e_6}\rvert]$.
f_{11}	Variance of frequency of the highest peak in spectrum of e_m.
f_{12}	Variance of $[\sigma^2_{d_1}, ..., \sigma^2_{d_6}]$.
f_{13}	Variance of $[\lvert\sigma^2_{d_1} - \sigma^2_{d_2}\rvert, ..., \lvert\sigma^2_{d_5} - \sigma^2_{d_6}\rvert]$.

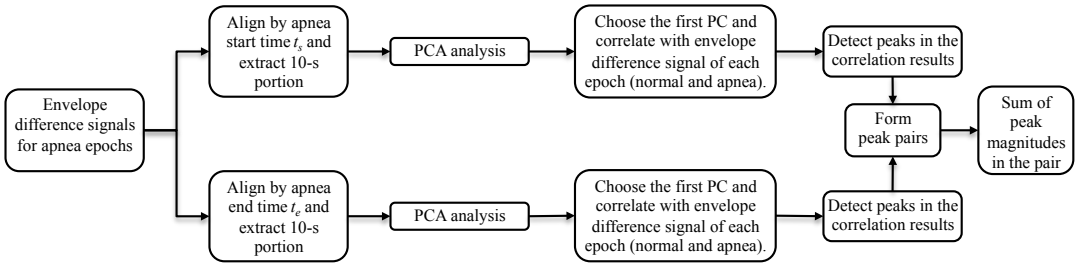

Figure 5: Algorithm for extraction of f_{15}.

not considered in calculation of the normalization constant. The envelope difference D_i was estimated for each epoch E_i and the average envelope difference B_{avg} was calculated for the normal epochs. The feature f_{14} was then calculated as $|D_i - B_{avg}|_2^2$.

The last feature f_{15} was extracted to capture the step-like changes in the envelope at the beginning and ends of the apnea periods. Hence, only apnea epochs in the training set were used for its extraction. In the processing stage, all the envelope difference signals corresponding to apnea epochs in the training set were aligned by apnea start times t_s and a 10-second portion (t_{s-5sec} to t_{s+5sec}) was extracted from each envelope difference signal. Principal component analysis (PCA) was performed on these 10-second extracted signals. PCA reduces the number of dimensions in the data set by transforming it into a new set of variables called principal components

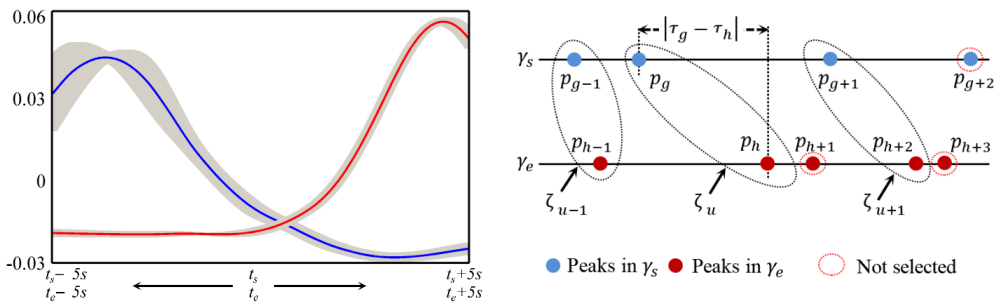

Figure 6: (a) The principal components extracted from the training data. (b) Formation of peak pairs $\zeta_u(\eta_u, \tau_u)$ (u is the pair number, η_u is the peak value while τ_u represents peak position) from the correlation results: for a peak p_g in γ_s, a pair was formed with peak p_h in γ_e, if p_e was the first peak in γ_e for which $\tau_h > \tau_g$. $f_{15} = \{\eta_g + \eta_h : \eta_g \in \zeta_g, \eta_h \in \zeta_h, max|\tau_g - \tau_h|\}$.

(PCs), which are statistically orthogonal to each other [48]. Let the principal component loading vectors obtained from the 10-second extracted signal, aligned by start times, be represented by v_s^m, where m is the column or vector number. The envelope difference signals for apnea epochs were then aligned by apnea end times t_e and principal component analysis was performed on the extracted signals (t_{e-5sec} to t_{e+5sec}). Let the loading vectors from PCA on the end signals be represented by v_e^m. The first PCs from both the start and end sets, i.e., v_s^1 and v_e^1, were selected as these captured the maximum variation in the data sets. After extracting these loading vectors, in the feature extraction phase, the D_i signal for each epoch was correlated with both v_s^1 and v_e^1. In general, the correlation of a signal x with y is given as $\gamma[\tau] = \sum_{j=-\infty}^{\infty} x[j-\tau]y[j]$, where τ indicates the correlation lag. Let the correlation of D_i with v_s^1 be denoted by γ_s and that with v_e^1 by γ_e for the i-th signal. These results contained peaks characterized by magnitude and a position or lag value τ as shown in Fig. 6 (b). In this next step, peak pairs were formed by choosing one peak from γ_s and one from γ_e. In the process of pair formation, for a peak p_g chosen from γ_s, the peak p_h selected from γ_e was the one that was located immediately after p_g as shown in Fig. 6 (b). Hence, some peaks were not selected in any of the resultant pairs

evident from Fig. 6 (b). Finally the *best* peak pair was chosen as the one that had maximum separation between its constituent peaks as shown in Fig. 6 (b). The sum of the peak values was chosen as the last feature f_{15}. It is important to mention here that other features, such as the separation between constituent peaks and product of peak magnitudes and separation between them in the pair were also considered in the study. However, none of these were found useful and the best feature was the one based on sum of the peak values.

3.1.5 Features Extracted from the Microphone

The 7 features extracted from the snores present in each 60-second microphone epoch included:

3.1.5.1 Features Related to the Pitch of Snores

Each snore was divided into 100ms sliding windows / frames (25% overlap between consecutive frames). The pitch of the signal in each frame was calculated by the *Autocorrelation Method* [34]. First the signal was center-clipped, leaving only the parts of the signal above the 70% of the maximum amplitude value present in the signal [34]. The highest peak in the autocorrelation after the main peak was detected and the position of the peak gave an estimate of the time period. The inverse of this value was calculated as the pitch 'P'. The mean (μP) of the pitch values across all frames in a snore was calculated and the mean and standard deviation of μP values across all snores in an epoch were used features.

3.1.5.2 Features related to Formant Frequencies

Existing research has shown that formant frequencies of snores can be used as a distinguishing feature between benign and apneic snores. In this context, the first three formant frequencies were estimated for each of the 100ms frames in the extracted snores using linear predictive coding (LPC) [85]. The signal in each frame was first

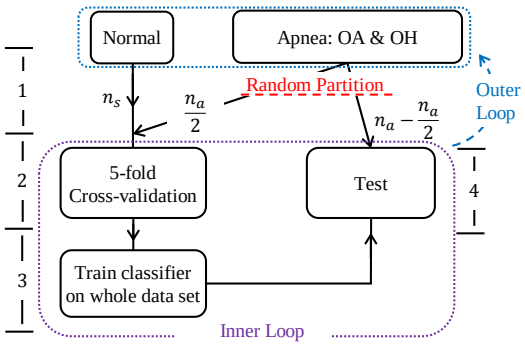

Figure 7: Division of data during the training and testing phases.

pre-processed by multiplying it with a Hamming window and then using a high-pass all-pole filter. The linear prediction coefficients were then estimated for the resulting signal in each frame. The angular frequencies from the roots of the prediction polynomial were estimated. In this work, the first three formants, f_1, f_2 and f_3, were selected from each frame and the mean of these values ($\mu f_1, \mu f_2$, and μf_3) were obtained for each snore. The feature, thus derived from the snores present in each 60-second epoch were the means of the $\mu f_1, \mu f_2$, and μf_3 values estimated from all the snores present in it.

3.1.5.3 Ratio of Energies in the Power Spectral Density Estimate

The power spectral density (PSD) estimate for each snore was calculated using the Welch's periodogram method (100ms frame with 25% overlap) similar to the approach in [88]. The ratio between the sum of PSD values in the 0 - 300 Hz band and the sum of PSD values over the entire frequency range was calculated and denoted by r_l. Similarly, r_h was calculated as the ratio between the sum of PSD values in the 300 - 800 Hz band and the sum of all PSD values. The mean values of r_l and r_h for all snores in an epoch were calculated as a feature.

3.2 IR-UWB based Sleep Apnea Detection

For this section of the study, only the radar signal was processed and used for detection of apnea events as shown in Fig. 7.

3.2.1 Training & Testing

The number of apnea epochs n_a were more than twice the number of epochs n_s corresponding to normal sleep in the data collected for the study. In the training phase, 10×5 cross-validation (CV) was used in training the classifier. Half the apnea epochs, i.e., $\frac{n_a}{2}$ were randomly selected from the complete set of apnea epochs in the first step. The randomly selected apnea epochs were divided into 5 folds in the next step. All the normal epochs n_s were also divided into 5 folds. Four folds from each class were used to train the classifier while the remaining fold from each class was used for validation. Once 5-fold CV was completed, the classifier was trained on complete data set which included $\frac{n_a}{2}$ and n_s normal epochs. The process of feature subset selection was also embedded in this 5-fold CV step. The wrapper method was used for feature subset selection [54]. The performance of the trained classifier was checked on the remaining $\frac{n_a}{2}$ apnea epochs from the first step. The whole process was repeated 10 times as shown in Fig. 7 and the results were averaged through all iterations.

3.2.2 Results & Discussion

The Linear Discriminant Analysis (LDA) classifier was used for the classification task. Data was collected from 4 subjects (3 male and 1 female, 48 ± 6.9 years, 210 ± 20.5 lbs and AHI 49 ± 29) who were previously diagnosed with sleep apnea. Full night recordings (6 - 7 hours) were obtained and after pre-processing, motion detection and removal, 476 OA, 392 OH and 361 normal epochs (NO) were extracted from the

Table 2: Classification results for apnea (OA & OH) and normal epochs

No. of f_k	Avg. results cross-validation (validation folds)			Test data
	Sensitivity (%)	Specificity (%)	Accuracy (%)	Sensitivity (%)
All	64.6	64	65.6	66
7	71.2	70.8	73.1	67

recordings. The data was partitioned according to Fig. 7. The results of classification between *Apnea* and *Normal* classes are summarized in Table 2. The classification results with all features is indicated by "All" in Table 2. The selected feature subsets have different numbers of features in each iteration. The average number of features rounded to nearest integer in the selected subsets is shown in Table 2. The values for sensitivity, specificity and accuracy in the table are for the data in validation folds of CV phase and averaged through the iterations of 10×5-fold CV. Similarly the sensitivity for the remaining $\frac{n_a}{2}$ apnea epochs in Step 4 of Fig. 7 (listed in the last column of Table 2) is averaged by the number of iterations in the outer loop.

The results indicate that the classifier when used with complete bag of features has an overall sensitivity of 64.6% and specificity of 64% during the CV steps and a sensitivity of 66% for the epochs in the test folds of *Step* 4 in Fig. 7 . There is an increase in overall sensitivity, specificity and accuracy when the LDA classifier is used after feature subset selection. The number of features selected is almost half the total number of features as the feature subset with lowest number of features is selected during feature selection.

3.3 Combined IR-UWB radar and Microphone based Sleep Apnea Detection

The results from the radar based sleep apnea detector did not show good accuracy in detection of both normal and apnea epochs. One reason for this low accuracy could be the presence of epochs containing OH events in the collected data set. OH is caused by partial obstruction of the upper air-way and is accompanied with a less decrease in respiratory signal amplitude as shown in Fig.8. It is evident from the diagram that 60-sec epoch containing an OH event is similar to 60-sec epoch corresponding to normal sleep.

In this part of the study, 7 features from the radar epochs were combined with the 7 snore-based features from the acoustic data for 3 subjects. One subject did not

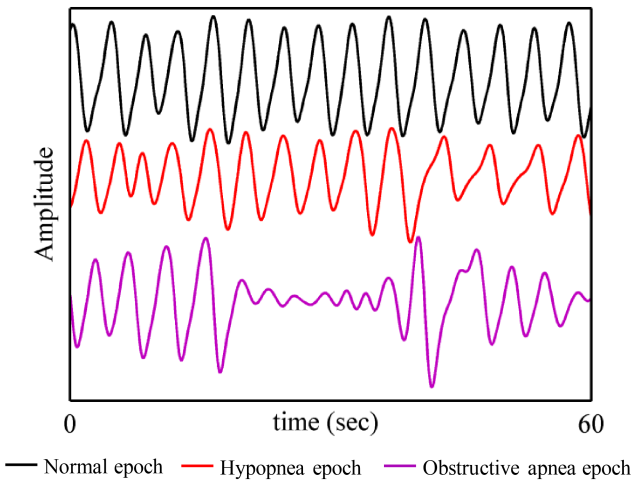

Figure 8: Three 60-sec epochs corresponding to normal sleep, containing a hypopnea event and an obstructive apnea event.

have audible snores and hence was not included in the study. The 7 features from the radar data included: $f_3, f_4, f_5, f_6, f_8, f_9$ and f_{11} from Table 1.

3.3.1 Training and Testing of the Combined Classifier

In order to check if the classifier worked with the combined feature set from radar and acoustic data, 5-fold CV was employed and two LDA classifiers were trained as shown in Fig. 9. In the first step, all the normal (NO), OA and OH epochs were divided into 5-folds. In 5-fold CV, 4 folds from each class were used to train the classifier while the remaining fold was used for testing. The process was repeated until each fold was used as a test fold. In the training phase, two classifiers LDA_1 and LDA_2 were trained. LDA_1 was trained using radar features only. LDA_2 was trained for those normal and apnea epochs which had a snore present in their corresponding microphone epochs. As the data were collected from patients with high AHI, the number of normal epochs were less than the total OA and OH epochs. Hence, before training, the number of normal epochs presented to LDA_1 were upsampled. Let the difference between the normal and apnea epochs be ΔN. Then ΔN normal epochs were randomly chosen and replicated to make number of instants equal for both

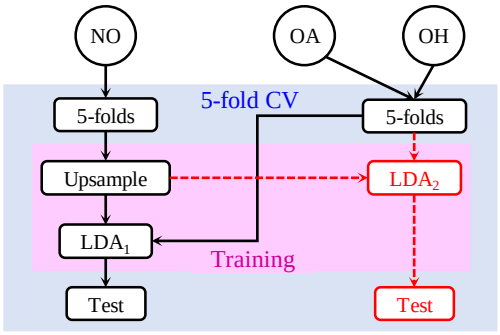

Figure 9: Flowchart for data division in training ans testing phases. The red boxes indicate that features from snores were also included in classification.

classes. It was observed that snores were absent in more normal epochs as compared to apnea epochs and hence in order to preserve this difference, the replication was not done for LDA_2 classifier that operated on radar and snore features. All features were standardized before training with both classifiers. In the testing phase, all the radar epochs in each test fold were analyzed with LDA_1 while only those epochs were analyzed with LDA_2 which included snores in the corresponding microphone epochs. The sensitivity, specificity and accuracy of both classifiers were calculated for the test folds and the results were averaged across the 5 iterations of 5-fold CV.

3.3.2 Results & Discussion

A total of 320 NO, 156 OA and 285 OH were extracted from the collected data. The radar alone classifier, LDA_1, showed a sensitivity of 77%, specificity of 64% and accuracy of 71%. There was an increase in the accuracy from 71% to 76% when the features from the microphone data were combined with the radar features in LDA_2. Similarly, the sensitivity of LDA_2 was found to be 80% for the radar epochs which had snores present in the corresponding microphone epochs. The specificity for combined classification was 70%.

It was observed that adding the snore features from the microphone epochs improved the classification performance. The gain in accuracy was on average 5% and might not indicate a significant increase. However, one contributing factor to it is the

sub-optimal location of the microphone sensors in this work. Usually, the microphone is placed on the neck or hung from a fixed support (such as ceiling) so that it stays few inches away from subject's face. The aim of this initial work was to come up with a overall system that does not put stringent constraints on subjects with regards to operation. Hence, future work should focus on adding multiple microphones placed or attached at different locations near the bed. The signal from multiple microphones can be combined, using beamforming techniques, to give better performance.

3.4 Limitations of the Work

One limitation of this preliminary work, was the small sample size involving only 3 subjects. Since it was a feasibility study, data should be collected more subjects which will lead to improvement in the classification results. Future work should also focus on using non-linear classifiers to assess the improvement in classification accuracy.

CHAPTER IV

HEMODYNAMIC ORIGINS OF BALLISTOCARDIOGRAM SIGNALS

4.1 Introduction

An important limitation in the field of BCG research is that while the BCG signal measures forces of the body, the information desired by clinicians and caregivers regarding mechanical health of the heart is typically expressed as blood pressure or in terms of parameters related to the flow of the blood. The understanding of the precise origin of the BCG signal and how the signal mathematically relates to blood pressure and aortic blood flow is limited and represents a fundamental scientific gap that must be addressed for the BCG to be adopted in clinical use.

The aim of this work was to explore the mathematical relationship between the BCG signal and the better-understood ICG and ABP waveforms, with a series of human subjects studies designed to modulate cardiac output (CO) and blood pressure asynchronously and with different magnitudes. One might consider directly measuring the ABP or blood flow parameters such as CO in the home rather than to measure the BCG in the first place and then attempt to relate it to these modalities. However, the current tools and devices for measuring the ABP and CO continuously are obtrusive, expensive and require a trained medical personnel to administer the measurement. The ABP is measured using volume-clamping finger-cuffs [10], while the CO (CO = stroke volume $\times$ heartrate), can be estimated from the ICG signals [3, 33], using eight electrodes placed precisely on the neck and thorax by a medical professional. Significant research efforts over the past several decades have led to a strong understanding of the physical origin of both finger-cuff based continuous

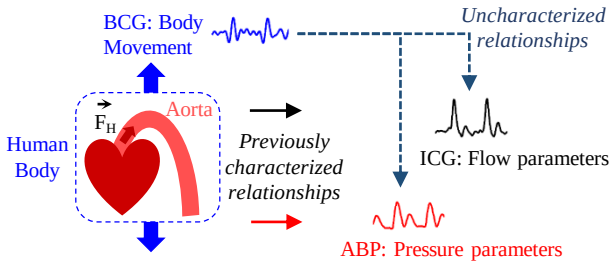

Figure 10: Physiological phenomena associated with the action of heart. The forced ejection of blood into the aorta (represented by the force vector $\vec{F}_H$) is characterized by blood pressure (derived from ABP, waveforms), blood flow (derived from ICG waveforms) and whole body movement (derived from BCG waveforms). Analyzing the relationship between BCG and ABP or ICG waveforms can provide insight into the hemodynamic origin of the BCG and thereby improve the ability to derive cardiovascular health parameters from this signal.

ABP and thoracic ICG waveforms. If the BCG waveform, which can be measured by unobtrusive, inexpensive, and simple hardware readily deployable in home settings, could be anchored to either of these well-understood measurement modalities, then ABP and CO can be readily measured at home.

The objective of this study was to analyze if the BCG signal was more in accord with the pressure of the blood or its flow, as shown in Fig. 10. It is important to mention here that while pulse pressure (PP)—which is the difference between systolic (S_P) and diastolic (D_P) blood pressure values—is closely related to CO, the relationship changes significantly throughout the day. For example, exercise, stress, or even simply fluctuations in ambient temperature can cause total peripheral resistance (TPR), the parameter that links PP to CO (specifically, PP = CO x PP), to change dramatically. In order to better understand the origin of the BCG, we first extracted features from the weighing scale BCG heartbeats and assessed correlations of these features with the corresponding features from the ABP and ICG heartbeats. Next, a method was designed to map the BCG heartbeats into corresponding ICG and ABP waveforms. The performance of the method was analyzed by using the BCG based ABP or ICG heartbeats to estimate changes in PP and stroke volume

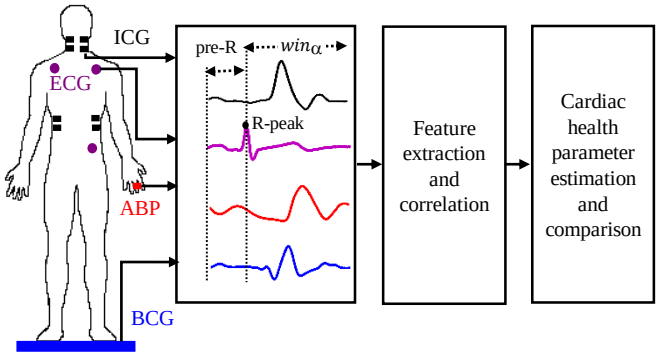

(a)

Rest (60s)	→ Valsalva (15s)	→ Recovery (60s)	→ Handgrip (30s)	→ Recovery (30s)
	ΔSV (ml):	4.8 ± 5.1	-1.1 ± 8	-1.9 ± 4.3
	ΔSystolic (mmHg):	-3.2 ± 6.8	12 ± 11	-0.8 ± 13

(b)

Figure 11: (a) Experimental setup and processing steps for the measured signals. (b) Different phases of the data protocol used for collection of data from each subject. The mean and standard deviation for change in PP and SV are shown for different phases in the protocol. The values shown are for post-Valsalva recovery, handgrip and post-handgrip recovery phases.

(SV). Finally, the performance of the proposed BCG-to-ICG mapping method was assessed in a single-subject multi-day trial that involved estiamtion of cardiac output using the modified-weighing scale sensor. This work could provide a tool, for example, for monitoring HF patients at home following discharge from the hospital, with the goal of potentially predicting exacerbations and thus reducing unnecessary re-hospitalizations.

4.2 Protocol

The data for the study were collected from nineteen healthy subjects under an IRB protocol approved by Georgia Institute of Technology (subject demographics: 5 females and 14 males, 24.4 ± 4.8 years old, 175 ± 8.8 cm tall and weighing 71 ± 12.5 kg). The aim of the protocol was to create changes in SV and blood pressure through perturbations as shown in Fig. 11. It consisted of five phases with two perturbations

separated by recovery time. Each subject stood on the BCG weighing scale in a resting state for 60 seconds. Then a Valsalva maneuver was performed for 15 seconds. During a Valsalva maneuver, a person forcefully expires against a closed airway, usually done by closing one's mouth and nose while 'bearing down' as blowing a balloon. This causes changes in intrathoracic pressure and dramatically affects venous return, arterial pressure, cardiac output and heart rate [76]. The Valsalva maneuver was followed by a recovery period of 60 seconds. Finally, each subject performed a handgrip exercise for 30 seconds that was also followed by 30 seconds of recovery. The handgrip exercise is an isometric (static) exercise that involves application of force without a change in muscle length. During an isometric exercise, the blood pressure rises due to increase in intramuscular pressure caused by stiffening of active muscle fibres [84]. The data in these phases was then used to analyze if the BCG captured more of the variability in SV or PP. The subjects stood in an upright posture on the weighing scale during the whole protocol. The ECG, ICG and ABP were all collected simultaneously with the BCG. A volume-clamping finger-cuff device was used to continuously measure the ABP.

4.3 Hardware & Data Processing

The ECG and ICG signals were measured using the BN-EL50 and BN-NICO wireless measurement modules (BIOPAC Systems, Inc., Goleta, CA) and then transmitted wirelessly to the data acquisition systems (MP150WSW, BIOPAC Systems, Inc., Goleta, CA). The ABP was measured non-invasively and on a continuous beat-by-beat basis with the A2SYS Nexfin Monitor (Edwards Lifesciences, Irvine, CA) that uses the volume-clamping technique on one finger [10]. The BCG signal was measured with a modified weighing scale using the strain gauge bridge and an analog amplifier [42]. All the signals were sampled at 1 kHz.

The signals from three measurement modalities, ICG, BCG and ECG, were filtered with finite impulse response (FIR) Kaiser window band-pass filters (cut-off frequencies: 0.8-35 Hz for the ICG, 0.8-15 Hz for the BCG and 2.5-40 Hz for the ECG). The ABP signals were only low-pass filtered (FIR, Kaiser window, cut-off: 20Hz) to preserve the DC value and to estimate the accurate values of systolic and diastolic blood pressure values. The R-peaks in the ECG signal, denoted by R_i (i represented the peak index), were detected using a simple peak detection algorithm and results were manually verified to make sure all peaks were detected correctly. Specifically, local maximas in the ECG signal above a pre-defined threshold (50% of the maximum signal amplitude) were detected as R-peaks. The R-peaks which were closer than 300ms were later discarded as false positives. The minimum R-R interval was calculated in each phase of the data collection protocol for each subject. Let the minimum R-R interval in each phase be denoted by win_α (α represents the phase, i.e., $\alpha \in [rest, Valsalva, recovery, handgrip, recovery]$). With the ECG R-peaks as reference, the BCG, ICG and ABP signals were segmented into individual heartbeats or frames [47]. Each frame contained samples from 300ms before the R-peak and win_α samples after the R-peak, i.e., one heartbeat = $R_i - 300$ms to $R_i + win_\alpha$, as shown in Fig. 11 (a). The first 300ms portion in the extracted heartbeats are refered to as pre-R samples in Fig. 11 (a). All the beats extracted in each of the phases were ensemble averaged [93] to reduce noise and features were extracted from the ensemble-averaged traces. The data from the 15-second Valsalva period were not analyzed as these included noise caused by subject-induced movement during the Valsalva maneuver. Hence for each subject, four ensemble-averaged traces corresponding to rest, post-Valsalva recovery period, handgrip and post-handgrip recovery period were obtained from the BCG, ICG and ABP signals.

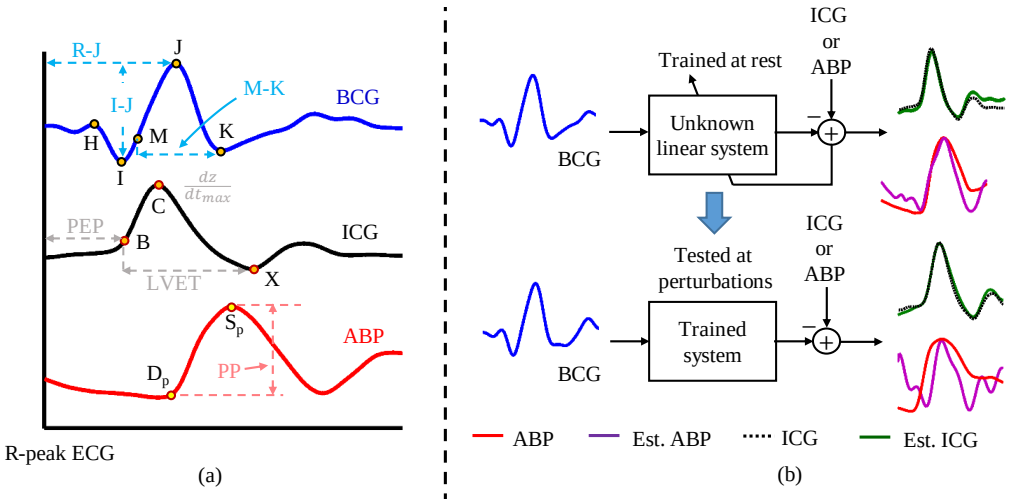

Figure 12: (a) Extraction of features from the heartbeats of three measurement modalities. (b) Block diagram from system identification based mapping of the BCG heartbeats to the ICG and ABP heartbeats. The system was trained for data in the resting phase of each subject and then tested on the data from the perturbation phases.

4.4 Extraction of Features from the BCG, ICG & ABP

In order to better understand the BCG-to-ICG and BCG-to-ABP relationships, we extracted a number of features from the BCG heartbeats and correlated (Pearsons correlation) these with the features obtained from the ICG and ABP. The annotated BCG, ICG and ABP heartbeats are shown in Fig. 12 (a). The features extracted from these three modalities are explained in the following sections:

4.4.1 Features derived from the BCG

The three features extracted from the BCG heartbeats included: (1) the I-J amplitude normalized by root mean square (RMS) energy in the heartbeat, i.e., I-J/E_{RMS}, where E_{RMS} represented the root mean square energy in the BCG heartbeat / frame and is given by $E_{RMS} = \sqrt{\frac{1}{n}\sum_{i=1}^{n} b_i^2}$ (n is the total number of samples in a BCG heartbeat b), (2) the R-J interval, i.e., the time interval between the ECG R-peak and the J-peak on the BCG heartbeat, and (3) the (M-K interval $\times$ I-J amplitude)/ E_{RMS}, where M corresponded to the point of maximum slope. The hypothesis behind multiplying the

BCG amplitude value and time interval feature was to design a feature that could capture the energy of the main BCG complex and to quantify the mechanical energy in each heartbeat, which could potentially increase with increased SV.

4.4.2 Features derived from the ICG

The three features extracted from the ICG heartbeats included: (1) the maximum peak value in the heartbeat, i.e., the $\frac{dz}{dt_{max}}$ value corresponding to the maximal speed of blood ejection, (2) the PEP, i.e., the time difference between the ECG R-peak and the B-point on the ICG called the R-B interval, and (3) the time difference between the X- and the B-point representing the LVET. These features characterized the blood flow in the vessels and were required for estimation of SV from the ICG [3].

4.4.3 Features derived from the ABP

The three features from the ABP heartbeats included: (1) the systolic blood pressure value obtained by detecting the maximum peak S_p in the heartbeat, (2) the foot value D_p before the maximum peak, denoting the diastolic blood pressure, and (3) the difference between S_p and D_p values called the PP [81].

4.5 Mapping the BCG to Other Modalities

In order to further analyze the relationship between the BCG and ICG / ABP, the BCG heartbeats were separately mapped to the corresponding ICG and ABP heartbeats using subject-specific FIR system identification methods. An impulse response was estimated for a subject-specific linear FIR filter that converted the BCG heartbeats to the ICG heartbeats and another impulse response for the BCG to ABP conversion.

In general, the output vector $\mathbf{y}$ of a linear filter of order Q operating on an input vector $\mathbf{x}$ is obtained by convolving the impulse response $\mathbf{w}$ of the filter with the input ($\mathbf{x}, \mathbf{y} \in \mathbb{R}^N$ and $\mathbf{w} \in \mathbb{R}^Q$). In the least squares terminology, the output is given by

the equation

$$\mathbf{y} = \mathbf{X}\mathbf{w}, \tag{1}$$

where $\mathbf{X}$ is the convolution matrix whose entries are made up of elements of $\mathbf{x}$. If the input vector is zero-padded to account for unavailable data during the convolution operation, then this method is called the *Auto-correlation method* [40]. If the elements of output $\mathbf{y}$, input $\mathbf{x}$ and impulse response $\mathbf{w}$ are represented by corresponding italic letters, then the matrices involved in equation (1) will be given by

$$\mathbf{y} = \begin{bmatrix} y_0 & y_1 & ... & y_{N-1} \end{bmatrix}^T, \tag{2}$$

$$\mathbf{w} = \begin{bmatrix} w_0 & w_1 & ... & w_{Q-1} \end{bmatrix}^T, \tag{3}$$

$$\mathbf{X} = \begin{bmatrix} x_0 & 0 & ... & 0 \\ x_1 & x_0 & ... & 0 \\ \vdots & \vdots & \ddots & \vdots \\ x_{N-1} & x_{N-2} & ... & x_{N-Q} \\ 0 & x_{N-1} & ... & x_{N-Q+1} \\ \vdots & \vdots & \ddots & \vdots \\ 0 & 0 & ... & x_{N-1} \end{bmatrix}. \tag{4}$$

Let the desired output signal be $\hat{\mathbf{y}}$, then the optimum solution (impulse response) $\hat{\mathbf{w}}$ can be obtained by minimizing the expression

$$\min_{\mathbf{w}} \|\mathbf{X}\hat{\mathbf{w}} - \hat{\mathbf{y}}\|^2. \tag{5}$$

The impulse response $\hat{\mathbf{w}}$ of the filter is then obtained as

$$\hat{\mathbf{w}} = (\mathbf{X}^T\mathbf{X})^{-1}\mathbf{X}^T\hat{\mathbf{y}}. \tag{6}$$

Since ordinary least squares is highly sensitive to noise, $\hat{\mathbf{w}}$ can be regularized by adding a term λ to the minimization expression in equation (5). This process is called *Tikhonov regularization* [35]. In other words, the solution approaches ordinary least squares solution as $\lambda \to 0$ and to 0 as $\lambda \to \infty$. The objective of λ, called regularization constant, is to avoid *over-fitting*. The modified minimization expression and the Tikhonov regularized solution are now given as

$$\min_{\mathbf{w}} \|\mathbf{X}\hat{\mathbf{w}} - \hat{\mathbf{y}}\|^2 + \lambda\|\hat{\mathbf{w}}\|^2, \tag{7}$$

$$\hat{\mathbf{w}} = (\mathbf{X}^T\mathbf{X} + \lambda\mathbf{I})^{-1}\mathbf{X}^T\hat{\mathbf{y}}. \tag{8}$$

In this study, the heartbeats from the 60-second resting portion of the BCG, ICG and ABP data for each subject were used to train the systems. We employed 5×2-fold CV [4] in the training phase and the performance of the trained systems was checked on the perturbation phases of the data protocol as shown in Fig. 12 (b). The objective was to find the optimum filter length (Q), number of samples before the R_i peak in each frame (pre-R samples) and the value of the regularization constant λ that provided the least error in mapping the BCG heartbeat (one frame) either to the ICG heartbeat or to the ABP heartbeat. This was accomplished by sweeping through filter lengths from 1 to 500 samples, 0 to 300 pre-R samples and values of $\lambda(10^{-6}$ to $10^{-1})$ in the training phase using 5×2 CV.

In subject-specific BCG to ICG mapping, for each combination of the above mentioned three parameters (Q, pre-R samples and λ), the BCG and ICG heartbeats in the resting phase data of each subject were randomly partitioned into 2-folds respectively. One fold from each modality was used in training while the other fold was used in validation phase. In the training phase, ensemble-averaged traces from one of the BCG and ICG folds were used as the input $\mathbf{x}$ and output $\mathbf{y}$. The filter impulse response $\hat{\mathbf{w}}$ was then estimated according to equation (8). Once the $\hat{\mathbf{w}}$ was

obtained, the ensemble-averaged trace from the other BCG fold was converted to an ICG trace (say $\hat{\mathbf{y}}$) and the error (Euclidean distance) was calculated between $\hat{\mathbf{y}}$ and the ensemble-averaged trace from the remaining ICG fold. The above process was repeated for the different combinations of Q, pre-R and λ values using 5×2-fold CV. The combination of the three parameters that gave the minimum error was then chosen to design a BCG-to-ICG filter (FIR) for that subject. A similar process was adopted to obtain subject-specific FIR filters to convert the BCG heartbeats to the corresponding ABP heartbeats.

Once subject-specific FIR filters were generated, they were used to convert the ensemble-averaged traces in the post-Valsalva recovery, handgrip and post-handgrip recovery phases into the corresponding ICG and ABP waveforms. For the ICG, the points of interest that include the B-, $\frac{dz}{dt_{max}}$ and the X-point as shown in Fig. 12 (a), were detected on the true ICG traces and also on the waveforms obtained from the FIR filters. The SV was then calculated using the Sramek's equation [18]

$$SV = \frac{(0.17H)^3}{4.25Z_o}.(\frac{dz}{dt_{max}}).LVET, \tag{9}$$

where H denotes the subjects height and Z_o represents the base impedance. The Z_o value was estimated as the foot of the ensemble averaged heartbeats of the raw impedance signal obtained from the ICG [3]. The value of Z_o, which could be considered as a constant, was estimated only in the resting phase for each subject and the same value was used during the perturbation phases. Let SV during the first 60-seconds of rest be represented by $\mathrm{SV_{rest}}$ and during the other phases be denoted by SV_α. The percentage change in SV during phase α was then calculated using the equation $\Delta\mathrm{SV} = (\mathrm{SV}_\alpha - \mathrm{SV_{rest}})/\mathrm{SV_{rest}}$. A linear regression / correlation analysis (Pearsons) was done between the values $\Delta\mathrm{SV_{ICG}}$ obtained from the ICG waveforms and $\Delta\mathrm{SV_{Sys}}$ values obtained from the trained filters from all subjects. The outliers in ΔSV estimates from both the ICG and the trained systems were detected using

the minimum-covariance distance (MCD) estimator [79] and were removed before correlation analysis.

Similarly, the points corresponding to S_p and D_p were detected in the true ABP waveforms and the ABP waveforms obtained from the FIR filters trained for mapping the BCG to ABP. The percentage change in PP for phases other than resting state was calculated as $\Delta PP = (PP_\alpha - PP_{rest})/PP_{rest}$ and correlation analysis was done for ΔPP data points obtained from the true and converted ABP waveforms for all subjects. The MCD method was again used to detect and remove outliers from the analysis.

4.6 Single-Subject Multi-Day Hemodynamic Assessment

In order to analyze the long-term performance of the above system identification based mapping method, we also collected data from one subject (24 years, 58kg, 162cm height) for five consecutive days. The objective was to assess the feasibility of training an FIR filter on the first day to convert BCG heartbeats to the ICG heartbeats and then assessing its performance on the remaining days for estimation of SV from the BCG. On all 5 days, the subject was asked to stand still for 2 minutes on the BCG weighing scale while BCG, ECG and ICG data was collected from him. An impulse response to map the BCG heartbeat to the ICG heartbeat was obtained from the first day using the method described earlier. The data on each of the remaining 4 days was ensemble averaged and used as input for the trained filter from the first day.

4.7 Results

4.7.1 Correlation Results from Waveform Features

The features extracted from the BCG heartbeats of 19 subjects in the post-Valsalva, handgrip and recovery phases showed good statistically significant correlation with the ICG-derived features while none of the BCG-derived features correlated well with the

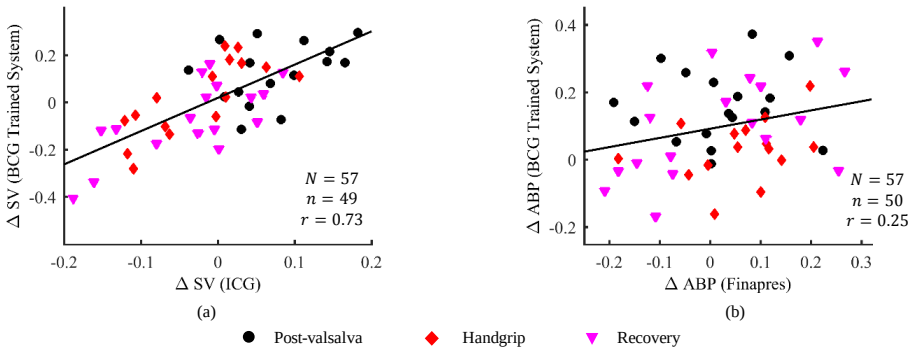

Figure 13: (a) Correlation results for SV values obtained from the BCG mapped waveforms and the ICG waveforms. The relationship is statistically significant ($p < 0.05$) (b) Correlation results for change in PP from the BCG mapped and original ABP waveforms. N represents the total number of data points while n denotes the number of data points considered in the analysis after outlier rejection.

features from the ABP heartbeats. The I-J amplitude normalized by the root mean square energy of the BCG heartbeat showed a correlation value of $r = 0.61$ ($p < 0.05$) with $\frac{dz}{dt_{max}}$ and also a value of $r = 0.58$ ($p < 0.05$) with the LVET from the ICG. The ICG maximum peak $\frac{dz}{dt_{max}}$ also showed a good correlation ($r = 0.71, p < 0.05$) with (M-K interval $\times$ I-J amplitude)/E_{RMS}. The R-J intervals obtained from the BCG heartbeats displayed a correlation of 0.75 ($p < 0.01$) with PEP (R-B interval) from the ICG, which is in agreement with a previous study [28].

All the amplitude and time based features from the BCG showed poor correlation with S_p, D_p and PP and hence are not explicitly reported here. The correlation values for all such comparisons were less than 0.05 and were also not statistically significant, i.e., $p > 0.05$.

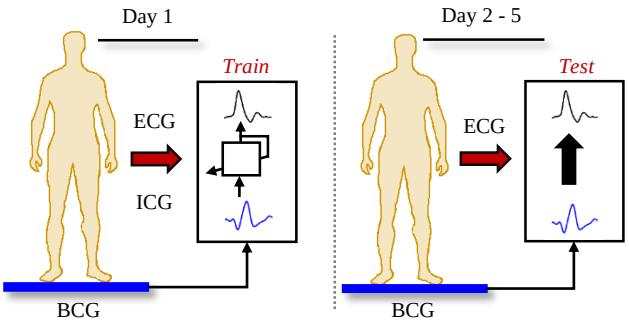

Error Results for Single Subject Stroke Volume Estimates from the BCG

Test Days	*2nd*	*3rd*	*4th*	*5th*
Error in SV (ml)	0.45	7	-1.6	1.7

Figure 14: Single subject multi-day trial results. The system was trained on the 1st day and tested on the remaining 4 days for estimation of SV from the BCG signals.

4.7.2 BCG Mapping Results

The subject-specific BCG-to-ICG mapping FIR filters, obtained from the resting phase heartbeats, were tested on the ensemble-averaged BCG traces from the post-Valsalva recovery period, handgrip and post-handgrip recovery phases for each subject. The ΔSV values were estimated from the filter generated and the true ensemble-averaged ICG traces in the three phases. Hence, three data points were obtained for each subject. The correlation results for percentage change in SV are summarized in Fig. 13 (a), which shows a correlation value of 0.73 ($p < 0.05$) for all subjects. Similarly, the BCG ensemble-averaged waveforms in the post-Valsalva, handgrip and recovery phases were also converted to the corresponding ABP waveforms using the subject specific BCG-to-ABP FIR filters. The percentage change in the PP estimated from the converted waveforms shows a correlation value of 0.25 with the corresponding values from true ABP waveforms in these phases.

4.7.3 Single-Subject Results

The results for single subject multi-day trial using the proposed system identification method are shown in Fig. 14. The ICG waveforms obtained from the BCG-to-ICG

FIR system were used to calculate SV on the test days. The results were compared with the corresponding SV values from the measured ICG. The trained system performed well on the testing days as the errors in SV from the ICG measurements and SV from the system estimated waveforms are very small on 3 of the 4 test days. There is a difference of 7 ml in the FIR based estimated and ICG based SV on the third day. The reason for this huge error on the third was found to be the low signal-to-noise ratio of the BCG signals due to the presence of motion artifacts.

4.8 Discussion

From the results derived in the previous sections, we conclude that leveraging the common features of BCG and ICG waveforms may provide a methodology by which hemodynamic parameters such as SV, pre-ejection period and left-ventricle ejection time can be extracted from BCG waveforms. The mapping technique presented in this study also shows that the BCG waveforms can accurately capture corresponding changes in ICG waveforms and, thus, changes in hemodynamic parameters. On the contrary, the features derived from the arterial blood pressure waveforms which include systolic blood pressure, diastolic blood pressure and PP associated with them do not show any significant relationship with the BCG-derived features and the BCG waveforms do not capture the change in blood pressure parameters. It has been shown in recent research that the BCG waveforms be used to provide a proximal timing reference for measurement of pulse transit time (PTT) to assist in ubiquitous monitoring for blood pressure [51, 65]. The pulse transit time, defined as the time interval required for a pressure wave to travel between two points on the arterial tree, has been shown to have a strong inverse relationship with blood pressure. To the best of our knowledge, this is the first time the BCG-to-ABP relationship has been explored on the basis of features derived from the two measurement modalities.

The results also suggest that the BCG phenomenon is more related with blood flow

curve as compared to the arterial pressure curve. The methods used for extraction of features from the ICG and ABP waveforms in this study are based on the existing literature regarding these two measurement modalities [3, 51]. On the other hand, the BCG based features, which are composed of different time intervals and amplitudes of different points on the BCG wave, are extracted to capture changes in the flow of blood.

The data for this study were collected from 19 healthy subjects which included 5 females and 14 males. However, no gender related differences were observed in the results. Another highlight of the work presented is that the proposed methods can be used with other BCG measuring sensors, such as wearable accelerometers, and also in settings other than the home for continuous assessment of hemodynamic parameters. However, correct estimation of these hemodynamic parameters require that the signal is free from all motion artifacts. The results from the single subject multi-day trial also corroborate this notion as an error of 7ml in the BCG- and ICG-estimated SV was observed on one of the test days. After further investigation into that days results, it was found that presence of motion artifacts in the measured signals, caused by even the slightest inadvertent subject motion, introduced errors in the mapping technique and thus rendered incorrect results. Hence, either the data should be free from all types of motion artifacts or algorithms should be designed to adaptively mitigate the effect of these artifacts and also improve the estimation accuracy.

4.9 Conclusion

In this study, we have systematically compared the BCG measurements obtained from a modified electronic weighing scale with the hemodynamic measurements from the ICG and ABP sensors. The results derived in this study not only provide insight into the physiological origin of the BCG but can also lead to design and implementation of algorithms and methods for using the BCG measurements for cardiac output

evaluation as well as cardiac contractility in unsupervised environments outside of the clinic.

An important limitation of this study was that data was collected from relatively young and healthy subjects. Hence, future work should include a more diverse group of participants and also subjects with cardiovascular disease. Moreover, work with additional subjects is also needed to validate the findings of the multi-day trial feasibility study presented in this work. The methods presented in this manuscript represent early translational work with the aim of providing a solution to monitoring HF patients at home and potentially predicting exacerbation using the BCG-derived cardiac output estimates. Predicting an HF exacerbation fundamentally requires the accurate measurement of cardiac output, and / or the components that it is derived from. Accordingly, the ability to accurately derive cardiac output changes from BCG recordings is a central element towards BCG-based scales being translated into use for monitoring HF patients at home.

CHAPTER V

POSTURE INDUCED DISTORTION IN BALLISTOCARDIOGRAM SIGNALS

5.1 Introduction

As the BCG is a measurement of the mechanical vibrations of the body in response to the heartbeat, the posture of the subject during the measurement can impact the quality of the signals. While intuitively this concept is sound, an in-depth, quantitative study of posture-induced distortion in BCG measurements has never been conducted. Understanding the nature of these distortions can greatly improve the ability to interpret BCG recordings in unsupervised settings—such as the home—by allowing the automatic identification of measurements taken from subjects with incorrect posture. These measurements can then be flagged and treated differently such that the distortion due to posture is not confused with changes in the BCG signal associated with changing cardiovascular health.

The requirement to stand in an upright posture poses limitations on the use of BCG in non-clinical environmens. In addition to a subject accidentally slouching forward for a measurement, it is possible that some subjects will have reduced physical strength, and thus the measurements must be taken in a seated position instead. It has been shown in different studies that the BCG signal can be affected by posture, using various measurement hardware such as fiber optic sensors [24, 55]. However, these postural effects have not been studied in depth.

In this study, we focused on the posture induced changes in the BCG signals from two sensors: (1) weighing scale, and (2) wearable accelerometer. The weighing scale form factor offers many benefits which include: (1) weighing scales are common in

almost every household in the US, (2) the sensors present in the weighing scale are already very sensitive and require slight addition and modifications for measuring the BCG, and (3) other sensors can be integrated into the weighing scale assembly for multi-modal patient monitoring at homes. The accelerometers, on the other hand, have emerged as a front-runner among sensors for wearable health monitoring. Their low-cost, miniature size and extreme sensitivity to vibrations make them ideal for wearable BCG measurements.

In the next section, we shall discuss the effect of different postures, standing and seated, on the weighing scale BCG. This will be followed by analysis of posture on wearable BCG from accelerometer signals in three different standing postures.

5.2 Effect of Posture on Weighing Scale BCG

The weighing scale BCG, as discussed earlier, provides many benefits which not only include benefits related to form factor and cost, but also that weighing scales are popular in millions of homes in the world. The objective of this work was to (1) investigate the changes in the BCG signal and derived parameters under different postures and positions, and (2) demonstrate novel methods based on our recent work [104, 103] to improve the system performance for seated postures. Specifically, we focus on improving the estimation of R-J intervals from the ECG and BCG, as a surrogate measure of contractility [44, 60], and evaluate our results based on standard measurements of the PEP from the ICG signals [3, 18]. The novel methods described in this work can improve the usability of the BCG scale in unsupervised settings (i.e. the home), by improving robustness to seated posture, as well as enabling high quality seated BCG measurements which would expand the available patient population.

5.2.1 Protocol for Data Collection

The data for the work were collected from 13 healthy subjects (12 male and one female, 24 $\pm$ 4 years, 75 $\pm$10 kg, 177 $\pm$ 7.7 cm height). The data collection protocol was

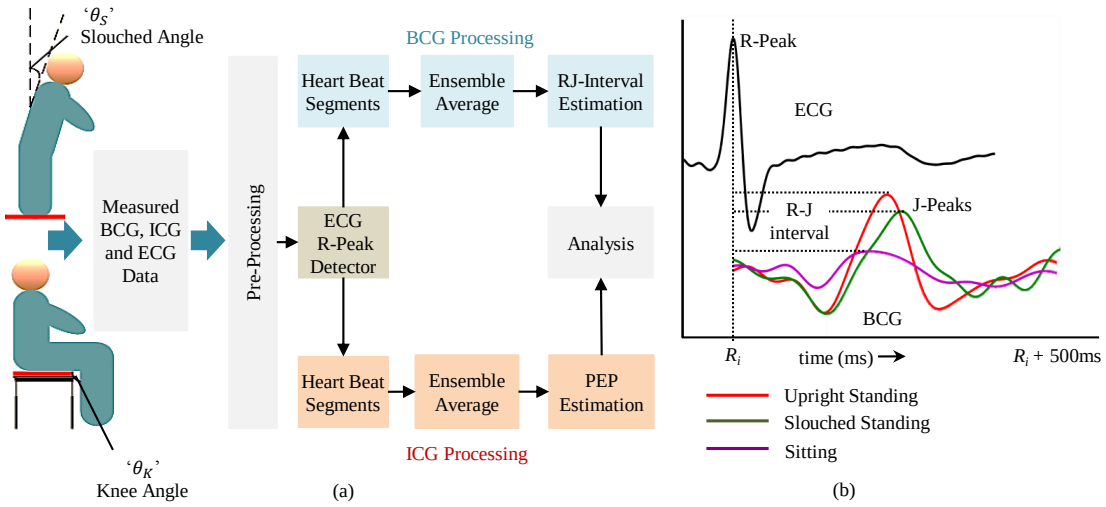

Figure 15: (a) Experimental setup. Three standing postures: upright ($\theta_S \approx 0°$), slightly slouched ($\theta_S = 20 - 40°$) and heavily slouched ($\theta_S = 40 - 60°$). Two seated postures: upright($\theta_k = 90°$) and bent knee upright($\theta_K = 60 - 80°$). (b) The BCG heartbeats in standing postures.

approved by Georgia Institute of Technology IRB and written consent was obtained from each subject before data collection. Each subject was asked to stand on the weighing scale in three different postures characterized by the angle θ_S made by upper back (more specifically the angle formed between the line joining the T2-T4 vertebrae) and sit on the weighing scale in two different postures defined by the knee angle θ_K as shown in Fig. 15. Each subject was asked to keep his or her back in an upright position for the two seated postures. Thus the five postures considered in the study are described below:

- Posture 1 (P_1): Upright standing position where $\theta_S \approx 0°$.
- Posture 2 (P_2): Slightly slouched standing position where $\theta_S = 20 \sim 40°$.
- Posture 3 (P_3): Heavily slouched standing position where $\theta_S = 40° \sim 60°$.
- Posture 4 (P_4): Seated position where knee angle $\theta_K \approx 90°$.
- Posture 5 (P_5): Seated position where knee angle is $\theta_K = 60° \sim 80°$.

The standing upright posture can be considered as a "gold-standard" posture and provides the best coupling of vertical (head-to-foot) cardiac forces to the scale as shown in previous studies [43, 44, 45, 36]. The two other standing postures, P_2 and P_3, were considered as these would simply represent the user accidentally taking measurements without standing completely upright or due to back problems. The upright sitting posture (P_4) was considered since some patients are not able to stand still on the scale. Such seated BCG measurements have also been considered in the literature [45, 75], but these do not consider the important comparison of signal quality and feature accuracy from the measured BCG signal. Finally, the last posture P_5 in this study was used to explore the increase in pressure wave reflections at the femoral bifurcation and how these reflections affect the BCG.

In the standing upright posture (P_1) and the upright sitting posture (P_4), each subject was asked to stand still for 30 seconds and then perform a Valsalva maneuver for 15 seconds. This was followed by a recovery period of 30-40 seconds in stationary state. In the remaining standing and sitting postures, each subject was asked to stand or sit in a stationary state for 30-40 seconds. The data from the 15s Valsalva period was not analyzed due to motion artifacts. The purpose of Valsalva was to modulate the hemodynamic parameters.

5.2.2 Hardware Design & Data Processing

The BCG was measured using a custom analog amplifier as described in the previous chapter. The ECG and ICG signals were measured using the BN-EL50 and BN-NICO wireless measurement modules (BIOPAC Systems, Inc., Goleta, CA) as in the study of Chapter IV and then transmitted wirelessly to the data acquisition system (MP150WSW, BIOPAC Systems, Inc., Goleta, CA). All the signals were sampled at a frequency of 1 kHz.

Once the data was recorded, the processing steps for the measured signals were

the same as in previous chapter. The ECG, ICG and BCG signal were band-pass filtered with FIR filters (Kaiser window with cut-off frequencies: 2.5 - 40 Hz for the ECG, 0.8 - 35 Hz for the ICG and 0.8 - 15 Hz for the weighing scale BCG. After the signals were filtered, the R-peaks, R_r (r was the peak index), in the ECG signal were automatically detected with a QRS complex detection algorithm and used as fiduciary points for segmenting the BCG data. Specifically, the signals in $R_r + 600$ms frames or "heartbeats" following each R-peak were extracted over the entire data period and aligned to form a collection or an ensemble. Let the individual frames or heartbeats from the BCG, ICG signals be represented by small letters $b_{k,m}$ and $i_{k,m}$, respectively ($b_{k,m} \in \mathbb{R}^{M \times d}$, where k denotes posture, $k \in [1, 2, ..., 5]$, m represents the number of heartbeats in one posture for a subject, $m \in \mathbb{R}$ and maximum number of heartbeats is M). Each sample in a BCG or ICG heartbeat be denoted by $b_{k,m}[l]$, where l is the sample number, $l \in \mathbb{R}^d$ and $d = 600$ due to frame size. Let the BCG trace obtained by averaging all the heartbeats $b_{k,m}$ in one posture be denoted by the bold letter $\mathbf{B}_k$. Similarly, $\mathbf{I}_k$ be the averaged ICG trace.

5.2.3 Time Domain Posture-Induced Differences

In order to analyze posture-induced differences in the time domain, we calculated for each subject and posture the RMS difference between each normalized BCG frame $b_{k,m}$ and its corresponding average $\mathbf{B}_k$. We termed this difference as an "error" in shape of individual BCG frames and the corresponding average trace. The normalization constant was calculated in the form of a scaling factor for each frame that minimized this RMS error. Because of this normalization, the RMS error quantified shape distortion that could not be corrected by a scaling factor. For the m-th unnormalized BCG frame $b^j_{k,m}$ for subject j in posture k and average $\mathbf{B}^j_k$, the amplitude scaling factor a_m was calculated for each individual beat [42] by the formula

$$a_m = \frac{R_{b_{k,m}\mathbf{B}_k}}{R_{\mathbf{B}_k\mathbf{B}_k}}. \tag{10}$$

where R denoted the cross-correlation operator. The RMS error e_k between individual beats weighted by a_m and the average for that posture was then calculated by

$$e_k = \sqrt{\frac{1}{Md}\sum_{m=1}^{M}\sum_{l=1}^{d}(\mathbf{B}_k[l] - a_m b_{k,m}[l])^2}. \tag{11}$$

The RMS errors thus calculated by (11) for postures P_2, P_3, P_4 and P_5 for each subject. These values were then normalized by division from the corresponding error in posture P_1 for that subject. Let $\tilde{e}_k$ represented this normalized error for a subject in posture k-th posture. The mean and standard deviation of $\tilde{e}_k$ was then calculated for all subjects in the k-th posture.

5.2.4 Frequency Domain Posture-Induced Differences

The PSD was estimated using the Discrete Fourier Transform (DFT) of BCG average $\mathbf{B}_k$ of each subject only in the three standing postures. The PSD estimates were interpolated to increase the resolution by a factor of four. Let $X_k[f]$ denoted the PSD estimate, where k again denoted the posture ($k \in [1, 2, 3]$) and f represented the frequency index. The mean and the standard deviation of PSD for $f = 0 \rightarrow 14$ Hz were calculated for each of the standing posture for all the subjects.

5.2.5 Parameter Extraction

The R-J intervals and PEP were calculated from the extracted heartbeats for each subject in all postures. However, instead of using the average trace for all the heartbeats for a subject, the heartbeats in 5-second periods were averaged to increase the number of data points. Since the 15 second post-Valsalva period was also included

in the data for P_1 and P_4 for all subjects, the heartbeats from the post-Valsalva 15 second period were also divided into sub-ensembles.

The J-peak in the BCG ensemble-averaged waveform was detected as the global peak in the first 400ms portion of the signal. Apart from the R-J interval, the R-K and the R-I intervals were also calculated. However, the R-J interval measurement was a more consistent feature in the BCG signal and the J-wave was larger in amplitude than either the I- or the K-wave. Thus the J-peak was more easily identifiable as it was less corrupted by noise and motion artifacts. Additionally, the R-J interval had been shown in previous papers [28, 36, 44] to be correlated to the PEP both for subjects at rest and with the use of physiological perturbations.

The PEP was extracted from an ICG waveform using the same method as in Chapter IV. The PEP was defined as the time elapsed from the R-point in the ECG to the B-point on the ICG signal.

5.2.6 Improved Feature Estimation from Seated BCG

It was observed from the data collected in the study that the J-wave amplitude and morphology for the seated BCG signals was significantly different from the standing measurements from the same subjects. In order to improve the noise reduction performance of the ensemble averaging, we employed weighted averaging techniques as described in [93]. It was also observed that the J-wave could split into two smaller peaks in some heartbeats leading to peak detection errors. In order to mitigate this problem, we devised a simple algorithm for consistently detecting J-wave peak based on low order polynomial fitting. First, the highest peak (p') was detected between 150 and 400ms portion of the weighted ensemble averaged BCG waveform. The zero-crossings before and after p' were then determined and a polynomial of order 2 was fitted across the waveform between these zero-crossings containing p' as shown in Fig. 16. Finally, the highest peak in the fitted waveform was detected as the new

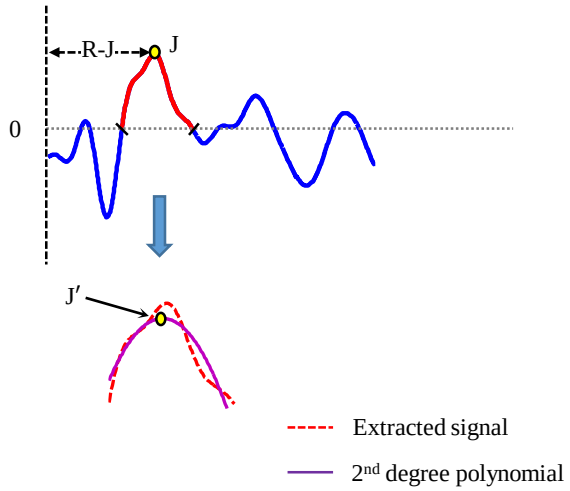

Figure 16: Modified R-J interval estimation method from the weighing scale BCG in sitting postures.

J-peak (say J′-peak) and the R-J interval was estimated as the time period between the newly detected J′-peak and the ECG R-peak.

Along with the improvement of R-J interval from seated postures, a system identification based method was designed for improved estimation of R-J intervals from the two slouched postures [47]. However, since it was collaboration work, the method along with the results will not be discussed here. The interested readers are referred to [47] for more details.

5.2.7 Statistical Analysis of Estimated Parameters

In order to analyze the improvement with the above modified method of J-peak detection in the seated postures, a paired t-test was conducted on absolute values of residuals of PEP from the regression line before and after the application of the polynomial fitting method. To remove the outliers in the linear regression model fitting the R-J interval to PEP, the mean (μ) and standard deviation (σ) of both PEP and R-J intervals was calculated for all subjects in each of the two sitting postures. The data points for which either PEP values or the R-J intervals were beyond their respective $\mu \pm 2\sigma$ values were then removed from the analysis for that

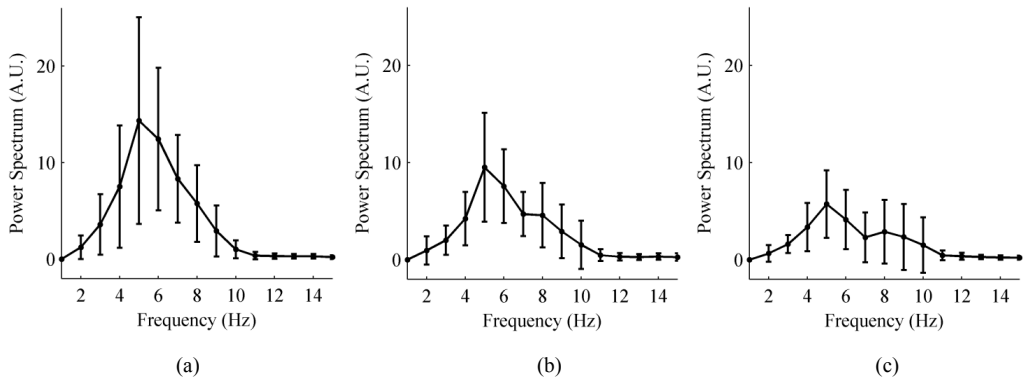

Figure 17: Average power spectra with standard deviations for all subjects. (a) Upright standing. (b) Slightly slouched standing. (c) Heavily slouched standing.

sitting posture. In order to remove additional outliers, the data points for which the squared Mahalanobis distance [22] was greater than $\chi^2_{0.95}$ were also removed from the analysis.

The objective for implementing this 2-tier outlier detection was that Mahalanobis distance, which finds outliers in multivariate regression, depended on the joint mean of the multivariate data and was affected by one or two erroneous points occurring at the extremes. Since the paired t-test required equal number of data points, the union set of outliers were removed from the R-J intervals and PEP data points before and after the application of improvement methods.

5.2.8 Results

It was observed that the mean and standard deviation of the normalized error $\tilde{e_k}$ exhibited an increasing trend across postures indicating more shape distortion in the measured BCG for bad postures. The values of normalized error calculated for slouched and seated postures were : 0.85 ± 0.25 (slightly slouched), 1.1 ± 0.5 (heavily slouched), 1.7 ± 1.1 (upright sitting) and 2.5 ± 1.8 (knees raised). The PSD results for the three standing postures are summarized in Fig. 17 which show the appearance of an additional peak, beyond 6 Hz, in the power spectra of slouched standing postures.

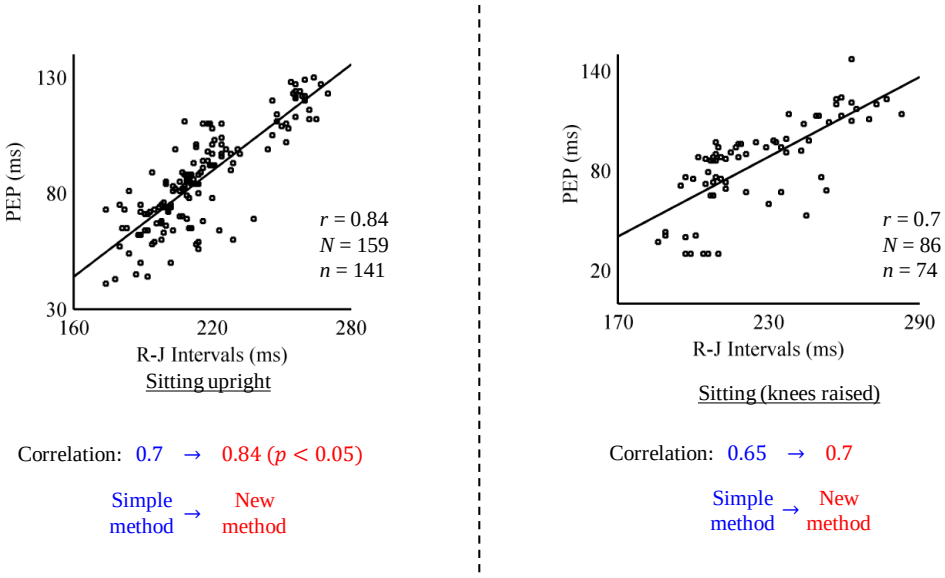

Figure 18: Correlation results. (a) Upright standing. (b) Slightly slouched standing. (c) Heavily slouched standing. (d) Upright sitting (e) Bent knees sitting. N is the total number of data points while n is the number of data points used in linear regression after removing the outliers.

The correlation between R-J interval and PEP for upright standing posture was $r = 0.85$, while the system identification based methods discussed in [47] resulted in correlation values of 0.65 and 0.54 for posture P_2 and P_3 respectively. The avid reader is referred to [47] for more details. The correlation results between the R-J interval from the BCG heartbeats and the PEP from the ICG in the seated postures are shown in Fig. 18. There was a statistically significant increase in correlation between the R-J interval and PEP for upright sitting posture when the modified R-J interval estimation is employed. The correlation increased from 0.7 to 0.84 for the upright sitting. There was a small increase from 0.65 to 0.7 in correlation between the R-J intervals and PEP for the knees raised sitting posture. However, this increase was not statistically significant.

5.3 Discussion & Limitations

The results derived in this work with weighing scale BCG indicated the presence of features in the measured signals that can be used to detect change in posture

as compared to a change in cardiovascular physiology. Specifically, the frequency domain analysis showed the appearance of second peak beyond 6Hz, in addition to the global spectral peak in the 0-6 Hz band, for the slouched standing postures. The peak became more prominent as the posture became more slouched indicating that more distortion was present in the weighing scale BCG signal. These additional peaks could also be contributed to other modes of vibration present in the slouched standing postures. A similar effect has been observed in the seated postures in previous studies [52, 61].

It can also be concluded from the results that with the help of suitable methods such as the polynomial fitting based R-J estimation method presented in this work, the J-peak can be detected more accurately for the sitting postures. This is evident from the increase in the correlation for the upright sitting posture. The improved correlation for the upright sitting posture approached the value of correlation between the R-J intervals and PEP for the "gold-standard" upright standing posture. Hence, similar methods can be employed with the weighing scale BCG signal to be used with the subjects who have difficulty in standing in an upright posture.

One important limitation of this work was the homogeneous nature of the pool of subjects selected for data collection. Future studies should focus on the inclusion of people with cardiovascular problems to better differentiate the posture related features from the physiological changes present in the BCG signal.

5.4 Effect of Posture on Wearable BCG

Wearable BCG, which includes local chest vibrations caused by the beating heart, can be easily measured with wearable accelerometers. Prior work [43] has shown that the cardiogenic vibrations measured from wearable sensors comprise multiple physiological origins. The SCG signals from a tri-axial accelerometer, placed at the sternum, contain components based on blood flow, but also from the heart sounds

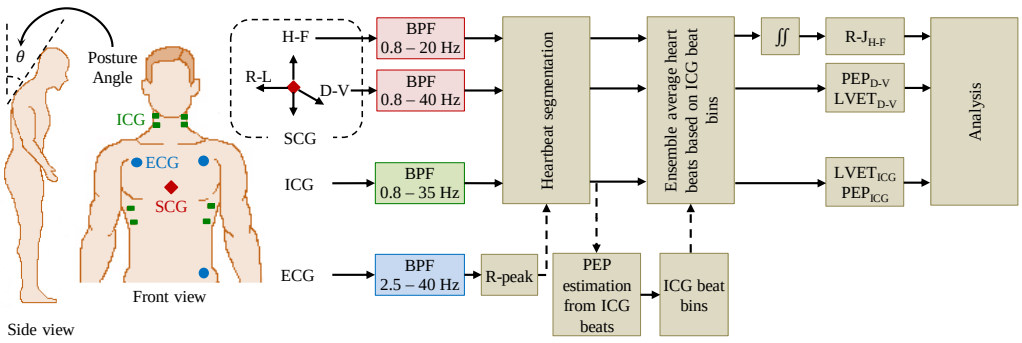

Figure 19: Experimental setup and processing steps.

produced by valve closure. Thus the signal from an accelerometer can be used to derive information about various mechanical events taking place in the heart—closing of mitral, tricuspid, aortic and pulmonary valves—and also regarding hemodynamics. When a tri-axial accelerometer is attached to various locations on the chest, the three components of acceleration from the accelerometer can contain a mixture of these vibrations.

Even though the wearable BCG signal is extremely sensitive to motion artifacts, change in posture can also affect the measured signal and parameters estimated from it. In this small study, we extend the work on posture induced distortion in the weighing scale BCG signal to wearable BCG and analyze the effect of three standing postures on the measured accelerometer signals.

5.4.1 Protocol & Experimental Setup

A small study was designed to examine the effects of postural and body position changes on SCG signals, with a particular focus on the ability to accurately extract STI features from the waveforms. The SCG signals were measured simultaneously for a set of 9 subjects with ICG and ECG reference measurements (see Fig. 19). The accelerometer for sensing SCG was placed on the sternum of each subject. Each subject was asked to stand in three different postures denoted by P_i: standing upright as in previous study with weighing scale BCG [36, 42], and slouching forward at two

different angles θ between the tangent to the thoracic spine (the tangent to the $T2-T4$ vertebrae) with the vertical axis. The three postures are summarized below:

- P_1: Upright standing posture i.e., $\theta \approx 0°$.
- P_2: Slightly slouched standing posture i.e., $\theta = 20 \sim 40°$.
- P_3: Heavily slouched standing posture i.e., $\theta = 40° \sim 60°$

Data were collected from 9 subjects (27 ± 4.2 years, 166 ± 20.8 lbs, 177 ± 7.7 cm height). In all postures, each subject was asked to breathe normally in a resting state for 40 - 60 seconds. The values of angle θ in the measured data for all subjects were $\theta = 35° \pm 3°$ for P_2 and $\theta = 52° \pm 4.5°$ for P_3.

5.4.2 Hardware Design & Data Processing

The ECG and ICG signals were measured using the BN-EL50 and BN-NICO wireless measurement modules (BIOPAC Systems, Inc., Goleta, CA), then transmitted wirelessly to the data acquisition system (MP150WSW, BIOPAC Systems, Inc., Goleta, CA) for subsequent digitization at 1 kHz. The SCG signal was measured using a small tri-axial accelerometer (356A32, PCB Piezotronics, Depew, NY) used in previous studies [44]. The acquired signals were sampled at frequency f_s of 1 kHz.

The ICG and ECG signals were filtered with FIR filters (Kaiser window, pass band cut-off frequencies: 0.8 - 35 Hz and 2.5 - 40 Hz). For the tri-axial accelerometer, the acceleration was measured along three axes as shown in Fig. 19. The three axes were: (1) the axis perpendicular to chest surface called dorso-ventral (D-V) direction, (2) the longitudinal axis along the surface of the body called head-to-foot (H-F) direction, and (3) the lateral axis called the right-to-left (R-L) direction. The D-V component was denoted by $\mathrm{SCG_{D\text{-}V}}$ and H-F component was denoted by $\mathrm{SCG_{H\text{-}F}}$. Both these components were band-pass filtered separately (FIR, Kaiser window, cut-off frequencies: 0.8 - 20 Hz for H-F and 0.8 - 40 Hz for D-V) as shown in Fig. 19.

The reason for choosing higher cut-off frequencies for the D-V signals as compared to H-F component was the presence of high-frequency vibrations in the former due to heart valves. The R-L signals were not analyzed in this study. Once the measured signals were filtered, the R-peaks in the ECG signal of each subject in every posture were detected with a simple QRS detection algorithm. These peaks were used as reference points for segmenting the ICG, and H-F and D-V components of SCG signals in the corresponding posture for that subject; i.e., the signal traces in ECG R-peaks+600ms, referred to as heartbeats or frames. Since the PEP period is different during the exhalation and inhalation phases of respiration, the PEP intervals were estimated for individual ICG beats. The mean μ and standard deviation σ of PEP values were calculated and the ICG beats were divided into three bins as shown in Fig. 20 (a): (1) ICG heartbeats with PEP values within $\mu \pm 0.25\sigma$ were assigned to Bin 1 (2) ICG heartbeats with PEP values greater than $\mu + 0.25\sigma$ were assigned to Bin 2, and (3) ICG heartbeats with PEP values less than $\mu - 0.25\sigma$ were assigned to Bin 3. The $SCG_{D\text{-}V}$ and $SCG_{H\text{-}F}$ heartbeats corresponding to the ICG heartbeats of Bin 1 were also labeled as Bin 1 beats while those corresponding to Bin 2 and Bin 3 ICG heartbeats were labeled accordingly. Thus, rather than obtaining one ensemble or collection of ICG, $SCG_{D\text{-}V}$ and $SCG_{H\text{-}F}$ heartbeats, three ensembles (bins) for each of these were obtained according to PEP values. The ICG, $SCG_{D\text{-}V}$ and $SCG_{H\text{-}F}$ heartbeats in each bin were then averaged to obtain the respective ensemble averaged traces. Hence, three ensemble averaged heartbeats for ICG, $SCG_{D\text{-}V}$ and $SCG_{H\text{-}F}$ were obtained for each subject in every posture as shown in Fig. 20 (b).

5.4.3 Feature Extraction from ICG & SCG

Features were extracted from the ensemble averaged traces of ICG, $SCG_{D\text{-}V}$ and $SCG_{H\text{-}F}$ signals for all subjects in each posture. The following subsections will explain these features in detail:

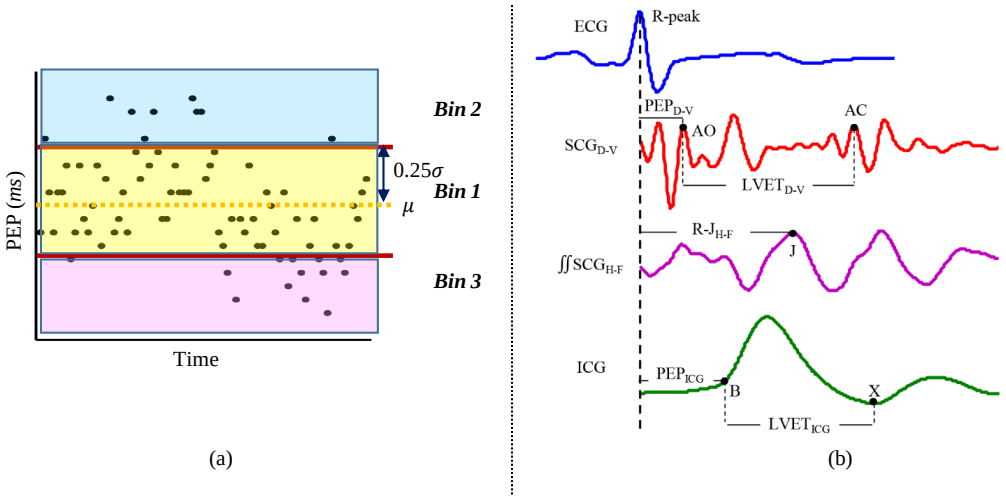

Figure 20: (a) The division of heartbeats into three bins based on mean and standard deviation of PEP values from individual ICG heartbeats. (b) Extraction of features from the ICG heartbeats and different components of sternal acceleration.

5.4.3.1 Features from ICG

The features extracted from the ICG signal included the PEP and LVET. The point of maximum acceleration before the global peak in the ICG frame was detected by filtering the ICG heartbeat twice with a Savitzky-Golay differentiator filter. The highest peak in the differentiated signal was selected as the B-point and PEP estimated was denoted by PEP_{ICG}. The X-point was detected as the mimima after the global peak in the heartbeat as shown in Fig. 20 (b). The difference between B and X points was estimated as LVET and denoted by LVET_{ICG}.

5.4.3.2 Feature from $SCG_{D\text{-}V}$

The most common methods for derivation of features from accelerometer data involve detection of peaks in the SCG traces [3]. These include the location of peaks corresponding to AO and AC events on the dorso-ventral SCG frames [43, 98] and the J-peak on the estimated BCG signal from H-F acceleration [13].

Accordingly, the features extracted from each ensemble averaged $\text{SCG}_{\text{D-V}}$ frame were the points corresponding to the AO and AC events. The AO-point was detected

as the positive peak that immediately followed the lowest negative peak in the first 200ms portion of the $SCG_{D\text{-}V}$ frame. The time between the R-peak of ECG and AO-point gave an estimate of the PEP interval and was denoted by $PEP_{D\text{-}V}$. In order to detect the location of the AC-point, the maximas and minimas in the $SCG_{D\text{-}V}$ heartbeat were detected. The upper and lower envelopes, E_u and E_l, of the $SCG_{D\text{-}V}$ frame were estimated by cubic interpolation of the maximas and minimas. The envelope difference signal was then obtained as $E_d = E_u - E_l$. The highest peak in E_d^2, located after the first 200ms portion, was detected and 150ms portion of $SCG_{D\text{-}V}$ frame on both sides of the peak was extracted. The maxima that preceded the lowest minima in the extracted portion of $SCG_{D\text{-}V}$ was chosen as the AC-point. The LVET was then estimated as $LVET_{D\text{-}V}$ = AC - AO (see Fig. 20 (b)).

5.4.3.3 Features from $SCG_{H\text{-}F}$

The H-F ensemble averaged acceleration traces were converted into displacement signals by integrating each trace twice using the trapezoidal rule [100]. Every trace was high-pass filtered before each integration step and also after the last integration step to remove the DC offset as in previous studies [103, 104]. The displacement trace thus obtained was the equivalent estimated BCG trace for the H-F acceleration signal. Let each estimated displacement trace be denoted by $\widehat{BCG}_{H\text{-}F}$ i.e. $\widehat{BCG}_{H\text{-}F} = \iint SCG_{H\text{-}F}$. The method of detecting the J-peak in the trace was similar to the method used in previous studies involving weighing scale BCG [28]. The J-peak was detected as the highest positive peak in the first 300ms portion. The time interval between ECG R-peak and the estimated J-peak formed the R-J interval denoted by $R\text{-}J_{H\text{-}F}$.

5.4.4 Results

5.4.4.1 Correlation Results between ICG and SCG Parameters

The heartbeats / frames were extracted for every subject in each of the three standing postures from the ICG and accelerometer signals and features were extracted

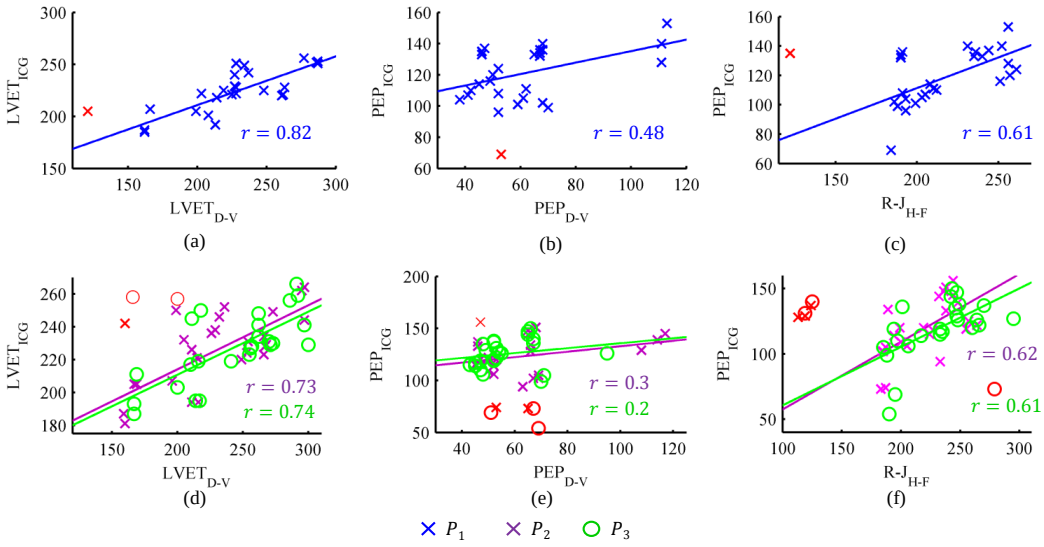

Figure 21: Correlation results: (a) $\text{LVET}_{\text{D-V}}$ vs LVET_{ICG} for P_1 (b) $\text{PEP}_{\text{D-V}}$ vs PEP_{ICG} for P_1 (c) $\text{R-J}_{\text{H-F}}$ vs PEP_{ICG} for P_1 (d) $\text{LVET}_{\text{D-V}}$ vs LVET_{ICG} for P_2 and P_3 (e) $\text{PEP}_{\text{D-V}}$ vs PEP_{ICG} for P_2 and P_3 (f) $\text{R-J}_{\text{H-F}}$ vs PEP_{ICG} for P_2 and P_3.

from the ensemble averaged traces of ICG, $\text{SCG}_{\text{D-V}}$ and $\widehat{\text{BCG}}_{\text{H-F}}$. The correlation coefficients were calculated using linear regression analysis between $\text{LVET}_{\text{D-V}}$ and LVET_{ICG}, $\text{PEP}_{\text{D-V}}$ and PEP_{ICG}, and $\text{R-J}_{\text{H-F}}$ and PEP_{ICG} in all three postures. The results for these are shown in Fig. 21. The results show no significant change in the correlation coefficient value for correlation between $\text{LVET}_{\text{D-V}}$ and LVET_{ICG} in slouched standing postures P_2 and P_3 (Fig. 21(d)) compared to correlation coefficient of good standing posture P_1 (Fig. 21(a)). The $\text{PEP}_{\text{D-V}}$, however show low correlation coefficient with PEP_{ICG} in all three postures (Fig. 21(b) for P_1 and Fig. 21(e) for P_2 and P_3). This is contrary to results obtained in previous studies [99, 96]. The correlation between R-J intervals from $\widehat{\text{BCG}}_{\text{H-F}}$ and PEP periods from ICG again show no change across all three postures in Fig. 21(c) & (f). The red data points in all the correlation plots of Fig. 21 indicate data outliers which were not included in the correlation analysis.

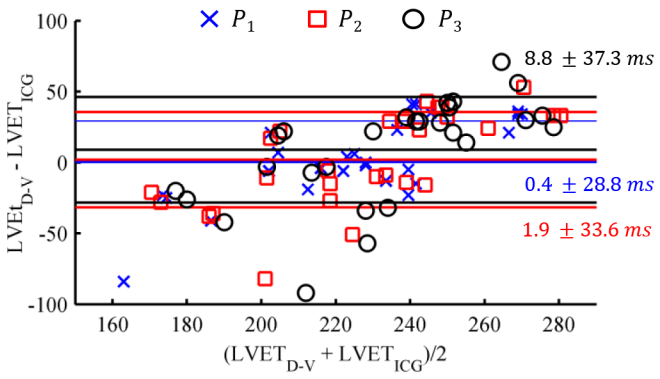

Figure 22: Bland-Altman plot for comparison of LVET estimated from SCG_{D-V} and ICG in different postures.

5.4.4.2 LVET Comparison

LVET was estimated from both ICG and SCG_{D-V} signals. Fig. 22 shows the Bland-Altman plot for LVET values estimated from SCG_{D-V} and ICG beats for all subjects in each of the three postures. The plot indicates that LVET from SCG_{D-V} shows similar level of agreement with LVET from ICG in all three postures. Thus based on features from SCG_{D-V} beats, there is not much difference in the accelerometer signals acquired in all three postures.

5.4.5 Discussion & Limitations

The results from this wearable BCG study suggest that for PEP estimation, the double-integrated H-F component, which approximates a BCG waveform, provides a better surrogate for PEP than the D-V component. Interestingly, the H-F component has largely been ignored for estimation of hemodynamic parameters from the wearable BCG in the existing literature. These results put an important emphasis on utilizing this component, which is simultaneously measured with the D-V signals, in estimation of hemodynamic parameters. On the other hand, the dorso-ventral component in the acceleration domain provides a robust estimate of LVET in the three different types of standing postures. Thus as suggested before, the combination of cardiogenic accelerations in both axes, with a physiology-driven treatment of the

components, is recommended for future studies aimed at comprehensive systolic time interval estimation from wearable accelerometers.

An important limitation of this study was the small sample size and the homogeneity of subject demographics. Future work should focus on expanding this work with larger data sets including patients with cardiovascular diseases.

CHAPTER VI

QUANTIFICATION AND REDUCTION OF MOTION ARTIFACTS FROM BALLISTOCARDIOGRAM SIGNALS MEASURED DURING WALKING

6.1 Introduction

A major challenge for wearable BCG, SCG and other mechanical measurements of cardiovascular function is that high fidelity signals can only be obtained typically when the user is stationary. Motion artifacts related to walking or other types of movements can reduce the SNR and even sometimes render the measured signals unreadable. Hence, most of the studies on wearable BCG using accelerometers report results only when the subject is at rest [23, 97] and in a good posture. Authors in [73] demonstrated a method to only extract heart rate from a chest-worn accelerometer. However, as we have discussed earlier, heart rate is not the only important parameter describing the cardiac function. It is also important to accurately estimate STIs during movement.

Analyzing BCG / SCG signals during movement is challenging, since the signals can be corrupted by motion artifacts associated with footsteps and other external vibrations coupling into the sensor. Nevertheless, such data during motion is of paramount importance for understanding how a person's cardiovascular system *responds* to exercise-induced stress; accordingly, the inability to analyze the BCG and SCG signals *during* motion is a technical obstacle that, if addressed, can greatly enhance the value of wearable BCG and SCG recordings. Rather than only measuring STIs at rest, the *changes* in STI associated with particular activities—even simple

activities such as walking—can potentially provide an earlier indication of cardiovascular disorders, and a more specific tool for monitoring patients outside of clinical settings. In particular, enabling the estimation of STIs during movement, when the cardiovascular system is stressed due to the increased demands of the skeletal muscles and skin for blood flow, can likely provide deeper insight into cardiovascular function for patients with CVD than measurements at rest alone.

In this chapter, we focus on estimation of STIs from wearable BCG using accelerometers. We first discuss the results of a pilot study that combined estimates from multiple accelerometers, placed at different locations on the body, during walking and employed a dynamic time warping (DTW) based algorithm to estimate STIs during walking at three different speeds. In the later sections, we present a data driven method for de-noising wearable BCG signals from a small patch that used a single accelerometer and ECG sensor. We also discuss a simple method for improving the time resolution of estimates from the wearable sensor during walking.

6.2 Motion Noise Reduction using Multiple Accelerometers

In this pilot study, we processed simultaneously acquired signals from more than one accelerometer under the condition of walking at slow to moderate speeds. The objective of this initial study was to find the best position for placement of accelerometer on the body and also analyze the recorded signals during walking for feasibility of designing more complicated algorithms (discussed later in section 6.3) for removal of motion artifacts. Hence, multiple accelerometers were placed at different locations on the body in this initial work. The features of interest in the accelerometer signals were detected in the resting phase and then these features were tracked during walking phases using a novel algorithm involving DTW pattern matching technique. We also demonstrated that fusion of data from more than one accelerometer could provide robust estimate of STIs and compared these against the corresponding reference

standard ICG estimates using correlation and linear regression analysis.

6.2.1 Protocol

The data for the pilot study were collected from 4 subjects (demographics: 27 ± 5.3 years, 171 ± 10.3 cm height, 170 ± 22.7 lbs). Each subject was asked to stand in a resting state for 1 minute and then walk on a treadmill for 3 minutes at three different speeds: 0.44 m/s during the first minute and then increased to 0.89 m/s and 1.34 m/s in the second and third minute as shown in Fig. 23 (a). Five accelerometers were placed on the body at various locations as shown in Fig. 23 (b). The specific body locations for placement of accelerometers in this study as shown in Fig. 23 (b) were chosen in consonance with the existing literature. Most of the prior work on wearable BCG using one of the five positions used in this study. The H-F data was analyzed for all 5 accelerometers since it contained the BCG component while the D-V data was analyzed only for the accelerometers placed on the chest area (sternum, neck and clavicle) due to presence of vibrations caused by closure of semi-lunar valves. The protocol was repeated twice on each subject to generate two sets of data due to only three accelerometers being available for the measurements. Data from the arm, neck and sternum positions were recorded in the first set while clavicle and ear data were collected in the next set. Each subject was given 10-15 minutes to relax between the two sets of data. The ECG and ICG data were also collected to assist in the processing of the BCG data and also for comparison of results.

6.2.2 Hardware Design & Data Processing

The ECG and ICG signals were measured using the BNEL50 and BN-NICO wireless measurement modules (BIOPAC Systems, Inc., Goleta, CA) while small tri-axial accelerometers (356A32, PCB Piezotronics, Depew, NY) were used to measure the body vibrations. The acquired signals were sampled at 2 kHz.

The ECG, ICG and accelerometer signals, like studies in the previous chapters,

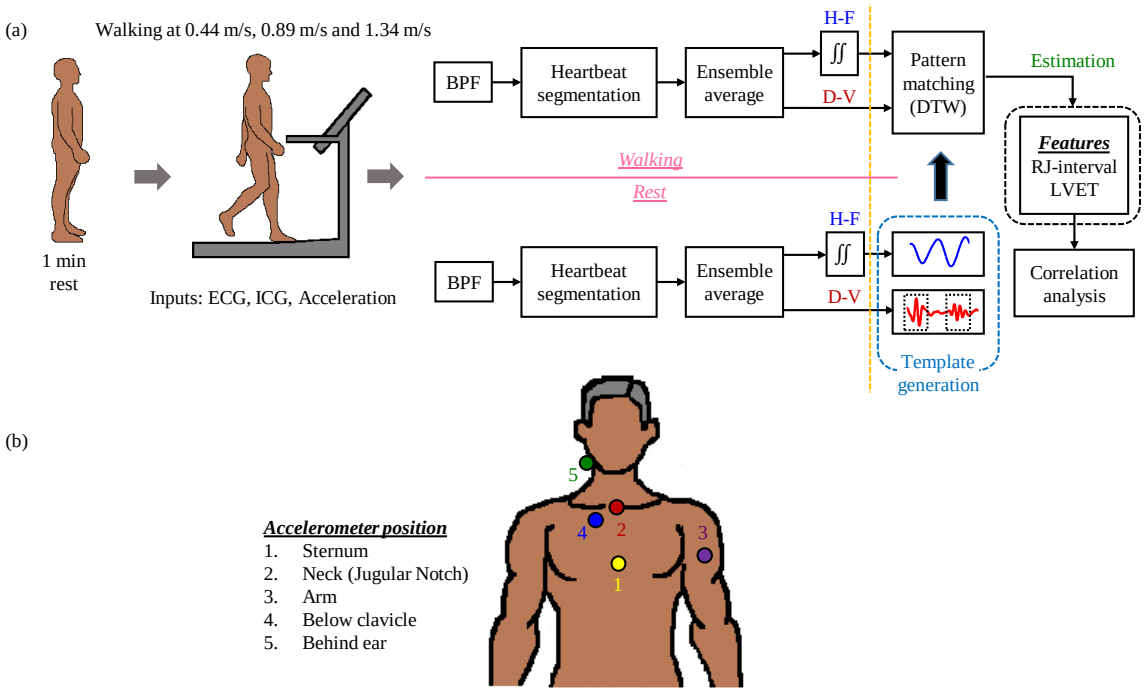

Figure 23: (a) Block diagram of the setup. Data were collected in resting and walking states. (b) Position of accelerometers on the body.

were band-pass filtered using FIR filters (Kaiser window, cut-off frequencies: 0.8 - 40 Hz for the ECG, 0.8 - 35 Hz for the ICG and D-V, and 0.8 - 20 Hz for the H-F). The R-peaks in the filtered ECG signal were detected and the minimum R-R interval was calculated for each subject. With R-peaks as reference markers and R-R interval as the frame length, the ICG and accelerometer data were segmented into individual frames called heartbeats and ensemble averaged to reduce noise [93], as shown in Fig. 23 (a). All the heartbeats in the resting state for each subject were ensemble averaged to give one trace while 15-second ensemble size was used for 0.44 m/s walking and a 30-second ensemble size for higher speeds. A larger ensemble size was chosen for 0.89 m/s and 1.34 m/s walking speeds to reduce noise. The H-F acceleration heartbeats were converted to the corresponding displacement traces by integration twice with high pass filtering (FIR, Kaiser window, cut-off: 6Hz) before and after each integration step to remove the constant terms [104]. The displacement traces will be referred to as the H-F heartbeats in the rest of the sections.

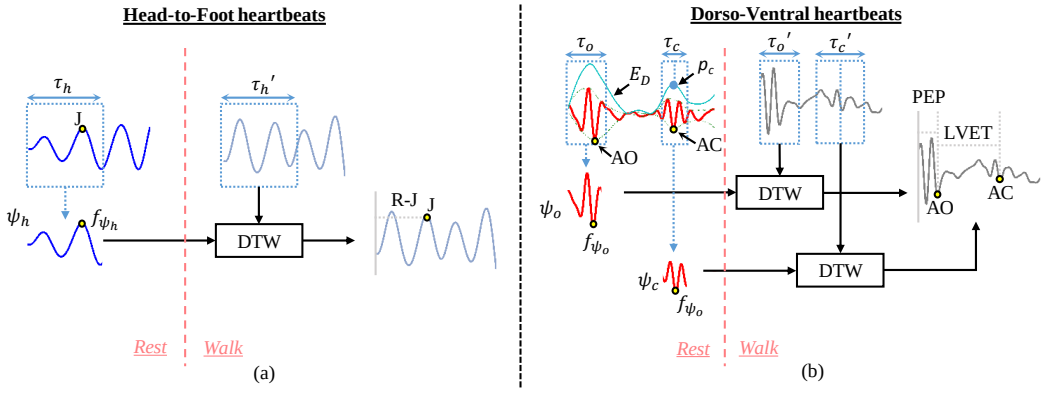

Figure 24: (a) Extraction of template ψ_h from the resting H-F heartbeat and detection of the feature f_{ψ_h} ($\tau_h = \tau_h' = 250ms$). ψ_h is matched to the H-F heartbeat during walking and the correct J-peak is detected. (b) Extraction of ψ_o and ψ_c from the D-V heartbeat in the resting state and detection of features f_{ψ_o} and f_{ψ_c}. ($\tau_o = \tau_o' = 125ms$, $\tau_c = 100ms, \tau_c' = 2\tau_c$)

6.2.3 BCG Feature Extraction & DTW based Algorithm

As discussed in Sec. 5.4.3, the most common features extracted from the wearable BCG signals are related to the positions of peaks in the heartbeat. Hence, in this study, the highest peak located in the first half of the H-F heartbeat was selected as the J-peak. Similarly, in the D-V component during the resting phase, the peaks that best corresponded to the opening and closing of aortic valves were chosen as the AO- and AC-points. However, during walking, the motion artifacts present in each heartbeat caused the selection of incorrect peaks and led to errors in estimation of systolic time intervals.

In order to overcome this problem, we employed DTW, which is a time series alignment algorithm [66, 82]. DTW finds similarities between two time series of equal or unequal lengths by warping the time axis and finding the optimal match under some restrictions. It was assumed that the BCG heartbeats did not change morphologically and were only translated along the time axis during walking. A portion of the BCG signal in the resting state of each subject was extracted and used as a known sequence or template ψ. The feature of interest f_ψ was then detected

in ψ. In order to detect the same feature from the BCG heartbeats during walking, DTW was performed between ψ and the motion corrupted heartbeat. The point on the motion corrupted heartbeat that mapped to f_ψ in ψ was detected as the feature. This process is described in Fig. 24 and explained in detail in the following subsections:

6.2.3.1 Feature Estimation & Tracking in H-F Heartbeats

The first τ_h ms portion ($\tau_h = 250$) of the resting H-F ensemble-averaged heartbeat was extracted as a template, denoted by ψ_h, as shown in Fig. 24 (a). The highest peak in ψ_h was detected as the J-peak. Let this peak be denoted by f_{ψ_h}. For an ensemble-averaged H-F heartbeat during walking, DTW was performed between its first τ_h' ms portion ($\tau_h' = \tau_h$) and ψ_h. The peak in the walking heartbeat that mapped to f_{ψ_h} in ψ_h after the application of DTW was then selected as the J-peak. The R-J interval was then estimated as the time difference between the detected J-peak and the ECG R-peak. If more than one point in the walking H-F heartbeat mapped to f_{ψ_h} due to DTW, then an average of all these points was estimated as the J-peak.

6.2.3.2 Feature Estimation & Tracking in D-V Heartbeats

The D-V heartbeats involved the detection and tracking of two features corresponding to AO- and AC-points. Hence, two templates needed to be generated from the D-V heartbeat in the resting state for each subject as shown in Fig. 24 (b).

In order to detect the AO-point, the first τ_o ms portion ($\tau_o = 125$) of the D-V beat was extracted from the D-V heartbeat of each subject in the resting phase. The portion was first de-trended and then standardized (set to zero mean and unity variance by subtracting the mean and dividing by standard deviation) to remove any low frequency noise that was not filtered out by the band-pass filter. The extracted portion was used as the first template ψ_o and the lowest minima in it was chosen as the AO-point denoted by f_{ψ_o}. For the walking phases, the first τ_o' ms portion ($\tau_o' = \tau_o$) of

each D-V heartbeat was de-trended and standardized. DTW was performed between the extracted portion and ψ_o and the minima in the extracted portion from the walking heartbeat that matched to f_{ϕ_o} in ϕ_o was chosen as the AO-point. Again, if more than one point mapped to f_{ψ_o}, then average of these was estimated as the AO-point.

For the detection of AC-point, the upper and lower envelopes of the whole D-V heartbeat were estimated by cubic interpolation of maximas and minimas. The envelope difference E_D was calculated and the second highest peak in the E_D signal was denoted by p_c as shown in Fig. 24 (b). A portion of τ_c ms ($\tau_c = 100$), denoted by ψ_c, was extracted from the original D-V signal around the position of p_c. This portion was again de-trended and standardized and the lowest minima in it was chosen as the AC-point, denoted by f_{ψ_c}. For the walking D-V heartbeats, a τ_c' ms ($\tau_c' = 2\tau_c$) portion around the p_c time instant (obtained from the resting state of each subject) was extracted. The portion was de-trended and standardized. The template ϕ_c was slid along the extracted portion and DTW was performed at each instant to find the best match. Once the instant of best match was found, the lowest minima in the part of the extracted portion that mapped to f_{ϕ_c} was chosen as the AC-point. LVET was the time difference between the AC- and AO-points.

6.2.4 Data Fusion from Multiple Accelerometers

The D-V axis data from the neck and sternum accelerometers were used for calculating the LVET estimates while the H-F data from all accelerometers were used to estimate the RJ-intervals. The ICG features, which included PEP and LVET, were estimated using the feature extraction methods described in chapter 4 and 5 (Sec. 4.4 and 5.4.3.1). In order to improve the correlation between the accelerometer and ICG estimated parameters during walking, data fusion was employed by averaging the estimates from two or more simultaneously collected accelerometers data.

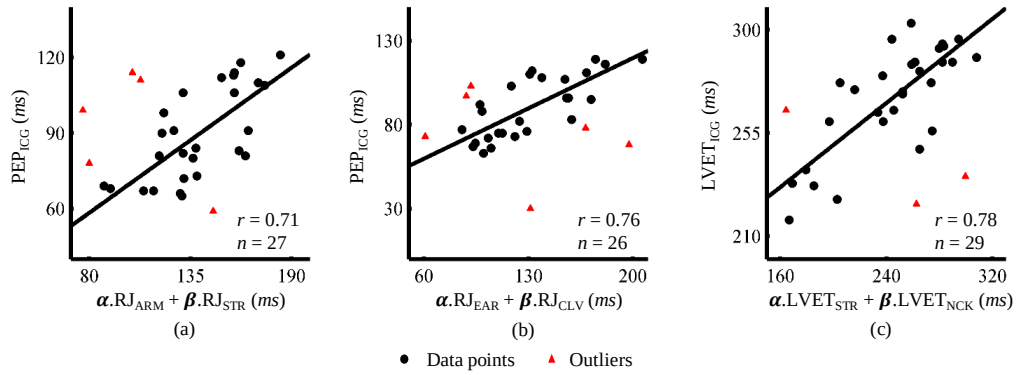

Figure 25: (a) Correlation plot between RJ-intervals from arm combined with sternum and the PEP from the ICG. (b) Correlation plot between RJ-intervals from ear combined with clavicle and the PEP from the ICG. (c) Correlation between LVET from sternum combined with neck and the LVET from the ICG. The red data points indicate the outliers and were not used in correlation analysis. n is the number of data points used in correlation. $\alpha = \beta = \frac{1}{2}$.

6.3 Results & Discussion

Linear regression based correlation analysis was performed between the R-J intervals from the H-F data for each accelerometer and the corresponding PEP values from the ICG and also between linear combinations of the RJ-intervals from two or more accelerometers and the PEP from the ICG. Similarly, LVET estimates from the D-V data of neck and sternum accelerometers and their combinations were also correlated with the LVET estimates from the ICG. The best correlation results are shown in Fig. 25. For linear combination, averaging ($\alpha = \beta = \frac{1}{2}$) provided the best results for two accelerometers. No significant increase in correlation was observed when estimates from more than two accelerometers were combined. The correlation plots indicate that DTW and linear combination of two accelerometer estimates achieve a correlation value greater than 0.7 ($p < 0.01$) for both types of systolic intervals.

6.3.1 Discussion & Limitations

The results suggest that combining estimates of the same axes from more than one accelerometer during physical activity provide a better surrogate for PEP and LVET

intervals. However, using more than one sensor has some disadvantages as well. It will lead to an increase in the cost of the overall system. Moreover, if one of the sensors is not attached properly to the body, the error due to motion artifacts in one sensor will propagate to the overall estimate. In order to reduce noise caused by walking, the time period during which the heartbeats were averaged was increased from 15-seconds to 30-seconds as the speed increased from 0.89 m/s to 1.34 m/s. However, such a larger ensemble size will not be able to track transient changes in the cardiovascular parameters. Hence, using better de-noising algorithms to remove motion noise becomes of paramount importance for wearable BCG to be used during movement periods. We shall discuss such an algorithm in the following sections.

6.4 Removal of Walking Noise

As discussed in previous section, the walking induced distortion in the wearable BCG signals can be reduced by using ensemble averaging. However, even for walking at a very slow speed of 0.44 m/s, an ensemble size of 15-seconds was considered for the averaging process. This is a large time interval considering the cardiovascular physiology undergoes transient changes during exercise. Hence, for robust and continuous cardiovascular monitoring, a smaller time duration or number of beats will be ideal to capture such small changes in the cardiovascular function corresponding to exercise stressors. This will only be possible if a signal or heartbeat de-noising algorithm processes the BCG heartbeats to remove movement related noise.

In this extension of the pilot study presented in the previous sections, we used a small wearable patch adhered on the sternum to simultaneously measure ECG and wearable BCG signals during walking at two different speeds. We focused initially on walking, since it is the most common form of motion that nearly all people perform during the day, and is the basis for the commonly-used clinical stress test named the 6-minute walk test [25, 39] for patients with cardiovascular problems. The 6-minute

walk test has emerged as a non-invasive and inexpensive method for assessment of submaximal exercise capacity of HF patients [39]. Previous studies have shown that different parameters obtained from the test, such as walking distance and left ventricle ejection fraction, can provide prognosis of the disease in HF patients [9, 12]. In addition to walking at a normal pace, data were also collected from each subject walking at 1.34 m/s on a treadmill for 5 minutes.

The objectives of this research were: (1) to provide a framework, using data driven methods such as EMD [41, 78, 105], to reduce motion-artifact corruption in the wearable BCG signals during walking, (2) to compare the performance of the wearable BCG with a state-of-the-art, commercially available ICG sensor for estimation of STIs during walking, and (3) to provide a method to objectively determine the minimum number of heartbeats before an accurate estimate of STIs can be generated using different techniques for feature detection. This work focused on methods that can be used with wearable BCG signals, but can also be extended to other sensing modalities such as ICG as well for de-noising signals during walking and, concordantly, assessing cardiovascular and respiratory health parameters during movement.

6.4.1 Protocol

Data were collected from 10 young, healthy subjects (Gender: 4 males and 6 females, Age: 24.9±4.3 years, Weight: 65.8±12.8 kg and Height: 1.68±0.10 m) under a protocol approved by the IRB at the Georgia Institute of Technology. Two sets of data were collected from each subject. In the first set, each subject was asked to stand in a resting state for 1 minute and then walk for 6 minutes at his / her normal pace followed by 2 minutes of rest (recovery period). In the second set, 1 minute of initial rest was followed by 5 minutes of walking at 1.34 m/s on a treadmill and subsequent recovery for 1-2 minutes. The objective of collecting two sets from each subject was to analyze acceleration signals under two scenarios: (1) normal subject-specific speed

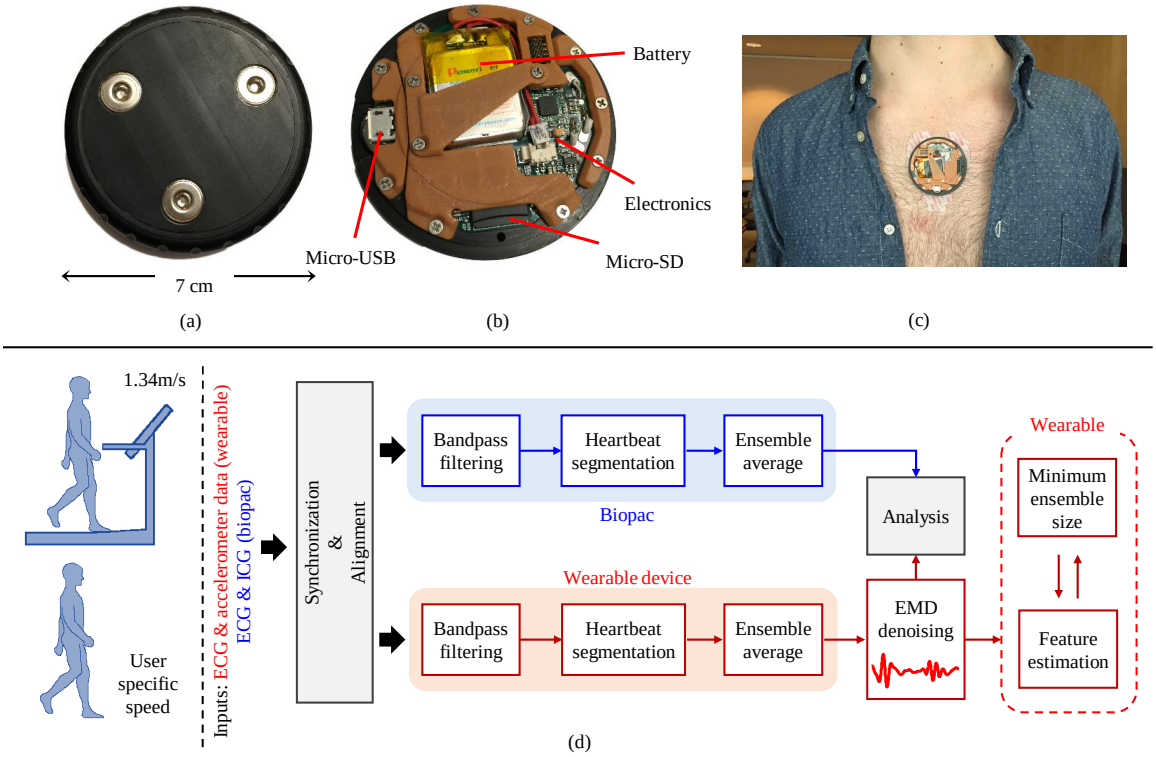

Figure 26: (a) The wearable patch that houses ECG and accelerometer sensors. Three adhesive electrodes are used with the device. (b) The inside assembly of the wearable patch houses a Micro-SD card on which the data is recorded. (c) The wearable patch attached to the sternum with three adhesive electrodes. (d) Block diagram of the setup. Two sets of data, which comprised of walking at normal speed (the speed at which each subject usually walked) and walking at 1.34 m/s on the treadmill, were collected from each subject.

of walking, and (2) controlled (treadmill) environment at a higher and uniform speed for all subjects. Each subject was given 10-15 minutes of relaxation time between the two sets of data.

6.4.2 Hardware & Data Processing

In both sets of data, the ECG and acceleration signals were collected with a novel wearable patch as shown in Fig. 26 (a - c) [27]. Along with the ECG and BCG signals from the wearable patch, ECG and ICG signals were also simultaneously measured using the BNEL50 and BN-NICO wireless measurement modules (BIOPAC Systems, Inc., Goleta, CA) to provide a reference gold-standard for the assessment of PEP

and LVET. The two ECG signals, from the wearable patch and Biopac, were used to synchronize data from Biopac and wearable sensor. This was done by tapping both the sensors before and after the start of measurements for both types of walking, and performing re-sampling in post-processing accordingly. All the signals from both the custom wearable patch and Biopac sensors were sampled at 1 kHz.

Once the signals from the sensors were aligned using the tapping artifacts introduced at the beginning and end of each data recording, the initial data processing steps included band-pass filtering of the ECG, ICG and accelerometer signals using FIR filters (Kaiser window, cut-off frequencies: 0.8 - 40 Hz for the ECG, and, 0.8 - 35 Hz for the ICG and D-V component of acceleration signals). The ECG R-peaks in the data from the custom patch and Biopac systems were detected using a simple thresholding algorithm and manually validated to correct for errors. With R-peaks as fiduciary points, R-peak+win ms frames, where win was the frame size, were extracted from the accelerometer and ICG sensors. The value of win was estimated as the minumum R-R interval in the portion of the ECG signal under consideration. Thus, the overall recording from each measurement modality was segmented into individual frames or heartbeats. Note that the accelerometer signals from the wearable device were segmented using the R-peaks of the ECG from the wearable patch while the ICG signals were segmented using the R-peaks from the Biopac wireless system as shown in Fig. 26 (d). The set or subset of heartbeats or frames thus obtained were then averaged to obtain ensemble-averaged traces, based on time intervals or the number of heartbeats to reduce noise in the individual heartbeats [93].

6.4.3 Signal De-Noising using EMD

EMD, an analytical and adaptive method, involves breaking down or decomposing a signal into components, and was developed by Huang et. al in 1998 for analysis of non-stationary signals [41]. The components which are obtained after EMD are

specific only to the signal from which they are generated. Specifically, EMD decomposes a non-stationary signal into a set of amplitude modulated (AM) and frequency modulated (FM) tones [78, 31], and these generated components are called intrinsic mode functions (*imfs*). The algorithm for obtaining the *imfs* from the given signal x is given below [78]:

1. Extract the local maximas and minimas in the signal x.
2. Form the upper e_u and lower e_l envelopes of the signal from interpolation of maximas and minimas, respectively.
3. Estimate the mean of the two envelopes, i.e., $e_m = (e_u + e_l)/2$.
4. Subtract e_m from x, i.e., $h = x - e_m$.
5. Repeat steps 1-4 on h, i.e., $x = h$.

The above steps (1–4) are called the *sifting process* and are repeated until h becomes a zero-mean signal or until some stopping criteria. Once the sifting process is completed, the signal h yields the first intrinsic mode function (*imf*). Let the first *imf* be denoted by I_1. This *imf* is subtracted from x to obtain the residue r_1 and the steps (1–5) are repeated on r_1 to obtain the second intrinsic mode function. The process of generating *imfs* can be stopped if the residue becomes a monotone from which no further *imfs* can be generated. Thus, the signal can be decomposed into finite number of components and can be reconstructed using the equation $x = \sum_i^n I_i + r_i$.

In this study, EMD was used to decompose the ensemble-averaged D-V heartbeat during the walking phase into *imfs* as shown in Fig. 27 (a). Each ensemble-averaged walking heartbeat produced 4 or 5 *imfs*. However, as shown in Fig. 27 (a), only the first *imf* closely resembled the resting state D-V heartbeat and thus was used for further analysis and feature extraction.

In order to assess the improvement in signal quality before and after the application of EMD, DTW was employed to find structural likeness between the walking heartbeats and resting heartbeat for each subject. DTW, as explained in the previous section, is a time series alignment method used to find similarities between two time series [82]. The D-V heartbeats in the resting portion of each subject's data were ensemble averaged to obtain an ensemble-averaged resting heartbeat. The walking heartbeats were divided into 15-second ensembles to obtain ensemble-averaged. The length of each ensemble-averaged walking heartbeat and resting heartbeat were made equal by clipping the later portion of the larger heartbeat. The warping distance between each walking heartbeat and resting heartbeat was calculated and normalized by the total number of samples present in both heartbeats. Let this normalized warping distance be denoted by d_α. The normalized warping distance was also calculated between walking heartbeat, after the application of EMD, and the resting heartbeat and was denoted by d_β. The process was repeated for all subjects and for both user-specific and 1.34 m/s data sets. The mean and standard deviation was calculated for d_α and d_β for all subjects and for both data sets.

6.4.4 Dorso-Ventral Feature Detection and Tracking

The typical method of feature detection from the D-V acceleration data involves detection of maximas or minimas in the D-V heartbeat [43]. Since the D-V heartbeats contain information about both the opening and closure of heart valves, the first half of the heartbeat was used to find the AO-point while the second half was used to find the AC-point. In this study, features or points corresponding to AO- and AC-points were detected from the heartbeats in the resting state for each subject and these features were tracked during the walking and recovery phases. The methods used for detecting the AO- and AC- points are described in the next subsections.

6.4.4.1 AO Feature

For the AO-point, the maximum or minimum with the highest absolute magnitude in the first 150ms of the heartbeat (as expected for aortic valve opening based on the physiology) was selected as a feature and denoted by f_a (see Fig. 27 (b). Note that we shall refer to the selected feature (maximum or minimum) as a peak in the rest of this chapter. The peak from this first segment was defined by two attributes that will be used as described below for identifying similar peaks in the motion-artifact corrupted signals acquired during walking: (1) its position in the frame denoted by p_a, i.e., the position of maximum or minimum which ever one was chosen on the basis of absolute magnitude, and (2) the sign of the maximum or minimum. A '+' sign was used if the selected peak was a maximum while a '−' sign was used if a minimum was selected as the peak. The time difference between f_a and the ECG R-peak was estimated as the PEP.

In the walking (after the application of EMD algorithm) and the exercise recovery heartbeats, the AO-point was detected by tracking the peak selected initially from the resting heartbeat. Specifically, we searched for a peak with same sign as f_a and in a window of w_a (ms) around the position p_a of f_a as shown in Fig. 27 (b). The peak which was closest to p_a was chosen as the desired AO-point, denoted by f'_a in the walking and recovery heartbeats. In case two peaks were found closer to f_a in w_a, the preference was given to the peak on the left, i.e., the peak whose position was less than p_a was chosen as the AO-point. The reason for this was that a *decrease* in contractility (or, in other words, an *increase* in PEP) is very unlikely during exercise, and thus setting the earlier peak as the preferred selection is more physiologically sound.

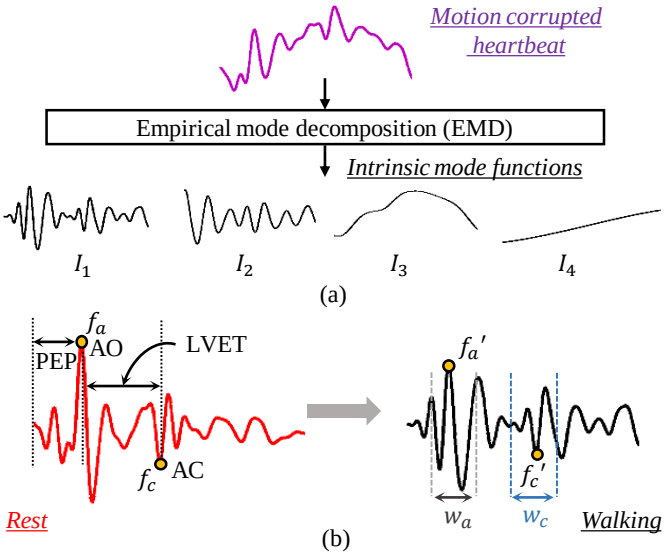

Figure 27: (a) De-noising of the D-V heartbeat during walking using EMD algorithm. Four intrinsic mode functions were generated after the application of EMD. The first intrinsic mode function (I_1) was chosen as the de-noised D-V heartbeat for feature extraction. (b) Extraction of features from the resting state D-V heartbeat. The features were tracked during the heartbeats measured while the subjects were walking. The values of w_a and w_c were chosen as 60ms and 100ms for user-specific walking and 100ms and 120ms for 1.34m/s walking.

6.4.4.2 AC Feature

An approach similar to the selection of the AO-point was implemented for the detection of the AC-point. The heartbeat was first divided into two parts according to the envelope based methods discussed in [46]. The AC-point was detected as the maximum or minimum with highest absolute magnitude in the second half of the heartbeat. Then, as for the AO-point, the AC-point, denoted by f_c, was characterized by a peak position and peak sign.

In the walking and recovery heartbeats, the peak with similar sign and closer to p_c was searched for in a window of w_c ms around the resting state AC-point. Again, preference was given to the peak which was less than f_c in terms of position, since systolic ejection is likely to shorten, not lengthen, with increased heart rates associated with exercise.

6.4.5 Comparison of ICG and Accelerometer Data

In order to compare the ICG and accelerometer data, the ICG heartbeats from the Biopac were partitioned into 15-second ensembles and averaged to obtain ensemble-averaged traces. Since, the data from the Biopac and the wearable patch sensor were time-synchronized, the D-V heartbeats from the accelerometer were also partitioned into 15-second portions and averaged to obtain ensemble-averaged acceleration traces. In order to detect the B-point on the ICG ensemble-averaged heartbeats, the heartbeats were twice differentiated with a Savitzky-Golay filter [28]. The position of the global peak in the double-differentiated signal was chosen as the B-point and the time difference between this peak and the ECG R-peak was estimated as the PEP from the ICG. The PEP from accelerometer was estimated as the time difference between the AO point and the ECG R-peak.

6.4.6 Quantitative Determination of Ensemble Size

Based on the ICG and accelerometer comparison, a method was devised to estimate the minimum ensemble size in terms of number of heartbeats required for the accelerometer data to yield accurate estimation of PEP and LVET intervals. In resting conditions, ensemble averaging is usually performed by using as many beats as are available, such that the extraction of features can be as accurate as possible. It is assumed that the cardiovascular state is relatively static, and thus a single ensemble average can capture all of the information required for assessing that state. However, during exercise, the cardiovascular state is changing dynamically, with heart rate, contractility, and stroke volume typically increasing to meet the increased demands of the skeletal muscles and skin for blood flow. This presents a major challenge from a feature extraction standpoint. On one hand, capturing the transient information associated with these changes—such as the time constant with which PEP decreases

at a given exercise intensity—can provide deep information regarding cardiovascular health, and the ability of the cardiovascular system to respond to the stress of exercise; thus, not using ensemble averaging at all would be ideal as one would obtain beat-by-beat information regarding these transients. On the other hand, motion artifacts are more significant during exercise and thus the noise and interference in the data is more substantial; thus, using ensemble averages with a high number of beats would be ideal as one would provide the maximal reduction of such noise and interference in the measured signals. We therefore aimed to provide a data-driven methodology for objectively determining the optimal number of beats that should be used in ensemble averaging during exercise for BCG signals.

Specifically, the optimum ensemble size for each subject was determined by first sweeping through overlapping window ensemble sizes composed of different number of heartbeats. Then, to determine the minimum ensemble size for PEP estimation, ensemble sizes of 64 to 4 heartbeats were traversed with 25% overlap, i.e., each ensemble contained 25% of heartbeats from the previous ensemble. The objective of using overlapping ensembles or moving average is to increase the number of estimates in the analysis. For each ensemble size, PEP was estimated by detecting the AO feature in the heartbeat obtained after the application of EMD algorithm. Once all the PEP estimates were obtained for a certain ensemble size during the walking phase, the mean (μ) and standard deviation (σ) of PEP estimates was calculated and the data points beyond $\mu \pm 1.75\sigma$ were removed from the estimated set. A third degree polynomial was then fitted to the remaining estimates to capture the trend in the estimated PEP values with respect to time, with an order low enough to avoid over-fitting. The time values were chosen as the mean of time index for the first and last heartbeat in the ensemble and were denoted by the variable t_m.

The distance of each point from the best fit line was estimated and root mean square error (RMSE) was calculated for the data points for that specific ensemble size.

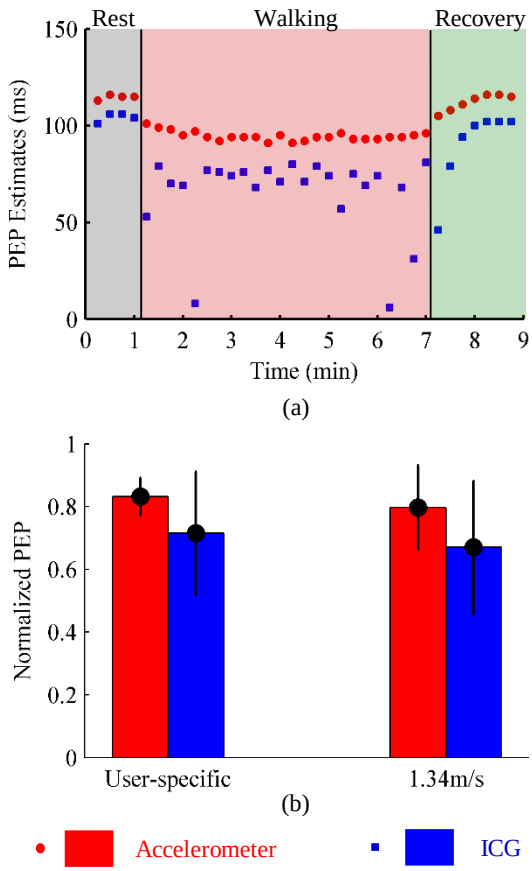

Figure 28: (a) The PEP estimates from the wearable patch and the Biopac ICG sensor for one subject during different phases of the 6 minute walk test. The data was divided into 15-s ensembles for both types of sensors. (b) The mean and standard deviation of PEP estimated from the accelerometer and ICG sensor for all subjects. The accelerometer estimates PEP with better accuracy for both types of walking tests and these are significantly different ($p << 0.05$) from the ICG estimates.

In order to further remove outliers and improve the polynomial fitting, one data point was iteratively removed from the estimated PEP estimates and RMSE was derived for the remaining data points. Hence, one data point for which the RMSE decreased considerably was excluded from the data set and final RMSE error was calculated for the remaining points. The process was repeated for different ensemble sizes and RMSE errors were derived for the PEP estimates for each subject.

A similar method was used to find the optimum ensemble size for LVET estimates by sweeping through ensemble sizes of 80 to 32 heartbeats (25% overlapping windows). After outlier rejection, a third order polynomial was fitted to the LVET estimates from

the wearable D-V heartbeats, and RMSE error was derived for each subject.

6.4.7 Results

6.4.7.1 EMD based De-noising

The normalized warping distance between the resting heartbeat and walking heartbeats, before and after the application of EMD, i.e., d_α and d_β, was calculated for all subjects. The warping distance decreased significantly after the walking heartbeats were de-noised using the EMD algorithm for all subjects. Since, warping distance indicates the cost of aligning two time series, a lower cost indicates greater similarity. The mean and standard deviation of normalized warping distance for walking at user-specific speed was 0.58 ± 0.27 and 0.32 ± 0.15 before and after the use of EMD based de-noising method outlined in this chapter. A paired t-test on d_α and d_β arrays for all subjects also showed statistical significance ($p << 0.01$). A similar analysis was done for walking at 1.34m/s and estimated mean and standard deviation of d_α and d_β were 0.48 ± 0.28 and 0.31 ± 0.17 ($p << 0.05$), respectively.

6.4.8 ICG vs Accelerometer

The PEP estimates from the ICG and accelerometer sensors are compared in Fig. 28. The PEP values for one subject during the 6-minute walk test, obtained from the accelerometer using methods discussed in this chapter, are shown in Fig. 28 (a). These accelerometer estimates show a strong correlation with the corresponding estimates from the ICG sensor in accordance with existing literature [97]. However, during the walking period, the ICG-based PEP estimates are not consistent with physiological expectations due to motion artifacts—for example, there are several data points where the PEP values fall below 10ms, and there are increasing and decreasing short-term spurts that are not consistent with what one would expect from the heart of a healthy person walking at a fixed rate. Indeed, for this reason, the ICG data could not be

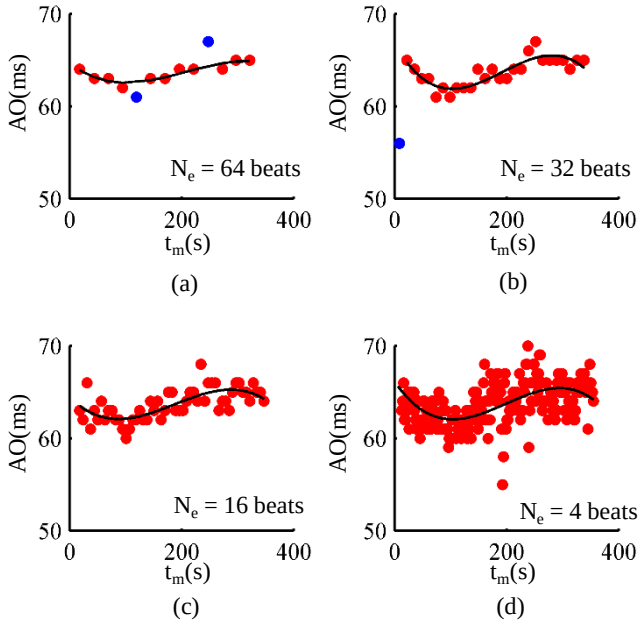

Figure 29: Determination of minimum ensemble size using the polynomial fitting approach for one subject. (a) 64 heartbeats. (b) 32 heartbeats. (c) 16 heartbeats. (d) 4 heartbeats. The data points in blue are outliers. In order to have same y-axis scale for each plot, the outliers for some plots are not shown in the above figures but are explained as follows: 2 data points were detected as outliers in (a), 1 data point as outlier in (b), 2 data points as outliers in (c) but are not shown, and, 5 data points as outliers in (d) which are not shown. An outlier was detected by removing the data point which was more than 1.75 standard deviation away from the mean of all data points.

used as a gold standard for assessing the BCG estimates during walking. The de-noised D-V heartbeats from the accelerometer, on the other hand, not only show a decreasing trend in the PEP as with the ICG during walking, but also provide precise and accurate estimates that are more in line with physiological expectations during the walking phase. This observation can be extended to the complete pool of subjects in this study as shown in Fig. 28 (b), where the standard deviation in relative changes in PEP at user-defined and 1.34 m/s walking speeds were significantly lower for the accelerometer as compared to the ICG based measurements.

Table 3: Results For Minimum Number of Heartbeats N_e in an Ensemble for PEP and LVET

Sub.	Age	Weight	Height	Min. N_e for PEP		Min. N_e for LVET	
(Gender)	(years)	(lbs.)	(inches)	User specific	1.34m/s	User specific	1.34m/s
M	31	200	70	12	36	32	68
F	24	115	63	12	8	32	64
M	24	150	69	8	8	32	32
M	22	172	70	8	12	32	32
M	33	171	73	8	4	36	36
F	19	160	66	20	32	48	72
F	22	115	60	8	48	56	44
F	27	165	64	32	52	36	80
F	24	120	63	12	12	32	44
F	23	140	65	8	24	32	36
μ	25	145.3	66.3	12.8	23.6	36.8	50.8
σ	4	28.3	4.1	7.7	17.5	8.4	18.3

6.4.8.1 Minimum Ensemble Size Analysis

The results for the minimum ensemble size methodology for one representative subject during the 6-minute walking phase are illustrated in Fig. 29. The minimum number of heartbeats N_e in an ensemble during walking were estimated for each subject by fitting a third order polynomial on the PEP values with respect to time. The value of N_e was decreased from 64 to 4 and the error was estimated at each value. However, Fig. 29 only shows the PEP estimates for 4 different values of N_e. As the number of heartbeat were decreased from 64 to 32 in Fig. 29 (b), the estimated values follow a similar trend as in Fig. 29 (a) without any considerable increase in error. Similar result is obtained as the number of heartbeats is decreased further in the Fig. 29 (c) and (d).

The results for all subjects are summarized in Table. 3. We chose an RMSE threshold of 2ms for PEP estimates for both the 6-minute and 5-minute walking tests, i.e., the lowest number of heartbeats were chosen for each subject as long as these

provided an RMSE of less than 2ms from the line of best fit (3rd degree polynomial). In order to determine the number of heartbeats for the LVET, a sweep of heartbeats from 80 - 32 was done as compared to 64 - 4 heartbeats and also the threshold for acceptable RMSE was taken as 10ms. The reason is that the LVET requires detection of AC-point which is prone to more errors than the detection of AO-point due to low SNR. The table shows that, if an RMSE of 2ms can be tolerated in PEP estimation, then on average 12 heartbeats are required while the person is walking at normal pace. Similarly, accurate LVET estimation within a tolerable 10ms RMSE can be achieved with an ensemble size of 28 heartbeats during normal walking speeds. As the speed increases, the number of heartbeats for accurate estimation of both the PEP and LVET also increase.

6.4.9 Discussion & Limitations

The results suggest that the wearable BCG signals processed using our de-noising and feature extraction techniques can provide improved estimation of systolic intervals during walking as compared to the commercially available Biopac ICG system. Recent research has shown that the D-V heartbeats can be used to extract features for calculating STIs during resting scenarios [97, 99]. However, the major hurdle in using wearable BCG for continuous monitoring has always been the exclusion of data during motion periods. The data during these movement periods can not only provide additional insight into cardiovascular health but also indicate how different stressors related to exercise affect cardiac function. In fact, to the best of our knowledge, recent efforts in this area have focused only on heart rate estimation during the movement periods. Though heart rate provides useful information about the electrical aspects of cardiovascular health, there is a strong need to also continuously estimate further parameters related to cardiac function. This chapter outlines a data driven signal decomposition method for non-stationary signals that can be used to reduce the

motion artifacts in wearable BCG measurements taken during walking.

The methods described in this chapter achieve a sufficiently fine time resolution for the PEP and LVET estimates from the acceleration signals to facilitate analyzing changes in cardiovascular function associated with walking. During stationary periods, the acquired signals have a high SNR and accurate estimates can be obtained on beat-by-beat basis. As the signal SNR decreases during walking or non-stationary periods, the need to perform ensemble averaging becomes unavoidable. The methods described in this work can readily be leveraged to obtain a minimum number of heartbeats that must be captured before an accurate and precise estimate, within some acceptable error thresholds, can be made for the STIs.

The results provided in the previous sections indicate that the number of heartbeats required for LVET during both self-paced and 1.34 m/s walking are more than the number of heartbeats for PEP. This is expected as estimation of LVET hinges on accurate detection of the point of closure of the aortic valve (the AC-point) in the heartbeat, which is associated with the relatively quiet second heart sound (i.e., quiet compared to the first heart sound).

The results in Table. 3 also show that the number of heartbeats required for accurate PEP estimates during 1.34 m/s walking are on average twice the number of heartbeats for self-paced walking (typically at a much slower pace than 1.34 m/s). One reason for this large difference can be attributed to the fact that treadmill represents an artificial controlled environment for walking. While walking on the treadmill, people actively adjust their gait and balance to overcome the mismatch in their natural pace and the treadmill speed. Such constraints are not present in the natural walking surfaces such as side-walks and jogging tracks. These inconsistent adjustments during walking on the treadmill add noise to the measured signals. To further investigate this hypothesis, we collected data for 1.34 m/s walking on a jogging track from a subject who had already provided data for the results in Table I. The same

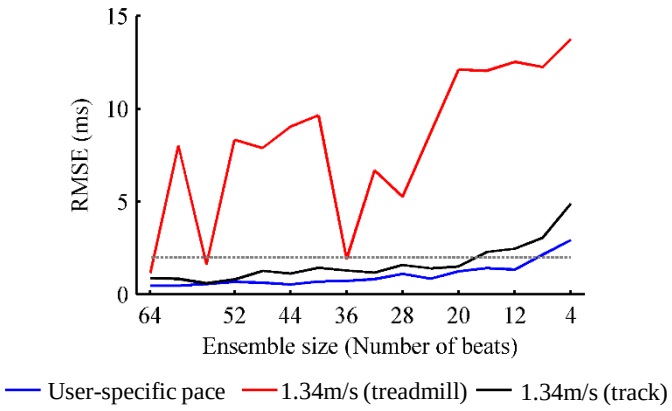

Figure 30: Comparison of minimum ensemble size for the PEP during walking at a self-determined pace and at 1.34 m/s on treadmill and track for one subject. The dotted grey line shows a threshold of 2ms RMSE for the PEP estimates. The minimum number of heartbeats required for the self-determined pace is greater than 8 while walking at 1.34 m/s in an uncontrolled environment such as a jogging track requires more than 16 heartbeats in the ensemble.

procedure for minimum ensemble size estimation was repeated and the results are summarized in Fig. 30. It can be observed that as the number of heartbeats are decreased in the ensemble, the error curves for self-paced walking and 1.34 m/s walking on a track are quite similar to each other while the treadmill walking curve shows abrupt changes in RMSE. The minimum ensemble size requirements for this subject, as observed from Fig. 30, are $N_e > 12$ (self-determined pace), $N_e > 16$ (1.34 m/s track) and $N_e > 36$ (1.34 m/s treadmill).

The perturbations such as walking or light exercises cause small changes to cardiovascular function of both healthy people and patients with CVDs. These brief changes can yield great insight into cardiovascular health. The common practice in existing research to overcome noise present in the signal involves ensemble-averaging heartbeat frames. The averaging operation, either performed on some specific number of frames or on frames present in some time interval, results in improved SNR, but fails to capture transients in the small changes in cardiovascular parameters from the measured signals. One of the results presented in this chapter shows that the number of heartbeats required in averaging operation to increase SNR is inversely

proportional to the speed of walking. Walking at higher speeds requires a greater number of heartbeats. Hence, it can be concluded that some measure of intensity of the activity (speed of walking in this instance) can be incorporated into algorithms for better estimation of parameters. Thus future work should build on the ideas presented in this chapter and focus on '*smart ensemble-averaging*' of heartbeats which is adaptive in nature and captures necessary changes in the cardiovascular physiology while maintaining a good SNR in the signal under analysis.

A limitation of this work is the homogeneous nature of the data set which includes only healthy and young subjects. The next chapter will include subjects with cardiovascular disorders and also investigate other feature tracking techniques based on subject specific parameters. Nevertheless, this work delineates novel methods for accelerometer signal recovery during motion which can form a foundation for these future studies and readily extended to other measurement modalities as well.

CHAPTER VII

WEARABLE MONITORING OF LEFT VENTRICULAR FUNCTION FOR HEART FAILURE SUBJECTS

7.1 Introduction

Heart failure is a progressive disorder in which heart cannot supply sufficient blood to meet the demands of the tissues and organs in the body [19]. As a result, fluid tends to accumulate at different locations in the body. In order to treat HF, diuretics are often used to get rid of excess fluid [6]. However, diuretics are accompanied with side-effects which include fatigue, dehydration and dizziness [71]. HF patients need to be monitored continuously and unobtrusively to assess their condition followed by modification in treatment and medications.

An important test for cardiovascular assessment is physical exercise, which produces a large burden on the cardiovascular system [14]. During exercise, the blood flow is directed towards working muscles. This increased blood flow makes the heart beat faster. It also causes an increase in the blood volume returning to the heart [80]. With the passage of time, the left ventricle adapt to higher blood volume and heart rate falls back towards normal value as more blood can be delivered in one beat. Hence, exercise is an excellent methodology to study the changes in circulatory system and how it interacts with respiratory and other systems of the body [62].

The 6-minute walk test, discussed in the previous chapter, is one of the most common exercise based tests to assess the cardiovascular health of people suffering from HF disease. The test provides parameters such as change in heart rate and percentage predicted values of the distance walked, which can be used to deduce important information about the condition of the HF patients.

The ultimate goal of this work is to develop a non-invasive wearable system for monitoring HF patients at home that can measure sufficiently rich information to enable titration of care. While several studies have attempted to use body weight, bio-impedance, heart rate variability, and other indirect methods for assessing left ventricular (LV) function at home for this purpose, none of these approaches has been successful in improving outcomes. The study uses a wearable patch that measures ECG and BCG signals, and can compute—from the time delay between the peaks of these signals —an index of myocardial contractility based on the PEP of the heart. We hypothesized that changes in PEP following an exercise stressor, specifically a 6-minute walk test, would be significantly muted for New York Heart Association Class IV HF patients as compared to Class I-II patients [16]. Our rationale was that in advanced HF (Class IV), the heart is less capable of increasing its performance to meet the increased demand for blood flow during exercise.

7.2 Protocol

A total number of 23 HF subjects (85±18.7 kg, 7 females) were recruited for this study. This pool was composed of both inpatients and outpatients. There were 9 patients in the Class I-II group, and 12 patients in the Class IV group. All patients were asked to stand in a resting state for 1 minute for the baseline readings. This was followed by 6 minutes of walking at normal pace. At the conclusion of the walking phase, each subject was asked to recover by standing stationary for 5 minutes. The distance walked by each subject was also recorded for the 6-minute walk test. Two of the subjects were morbidly obese, a factor which skews the percent predicted values for the 6-minute walk test; accordingly, these subjects were not included in the analysis.

7.3 Hardware & Data Processing

The wearable device used in the study was the same as shown in Fig. 26 (a) of chapter 6. The device measured ECG and wearable BCG signals. All the signals were sampled at 1 kHz. The ECG, H-F and D-V signals from the wearable BCG were band-pass filtered (Kaiser window, cut-offs: 0.8 - 40 Hz for ECG, 0.8 - 35 Hz for the D-V signals). This was followed by ECG R-peak detection and heartbeat segmentation. All the heartbeats in the resting 1-minute data were ensemble-averaged to obtain one trace while the post-walking data was averaged using an ensemble size of 16 beats. The data during the 6 minute walking period was not analyzed in this initial phase of this study. Also, only the D-V component of the accelerometer data was considered for this work. A simple algorithm was implemented to reject extremely distorted and noisy heartbeats from the ensemble averaging process.

7.4 Algorithm for Selective Heartbeat Ensemble Averaging

The objective of ensemble averaging which involves averaging a specific number of waveform traces or averaging all waveform traces present in a certain time interval is to reduce the noise present in each individual heartbeat. If the number of waveform traces / frames is increased, ensemble averaging gives a cleaner averaged trace as most of the noise is averaged out. However, this comes with a loss of time resolution as changes present in each waveform tend to average out during the process. Hence, there is a trade-off between the number of frames and time resolution required for each application. Increasing the time resolution implies a decrease in number of heartbeats for averaging operation and results in a noisy averaged signal. One reason for this noise is the presence of one or more extremely distorted heartbeats in the ensemble as shown in Fig. 31. In order to reject those heartbeats, following algorithm was implemented for ensemble averaging of n_e heartbeats present in the ensemble:

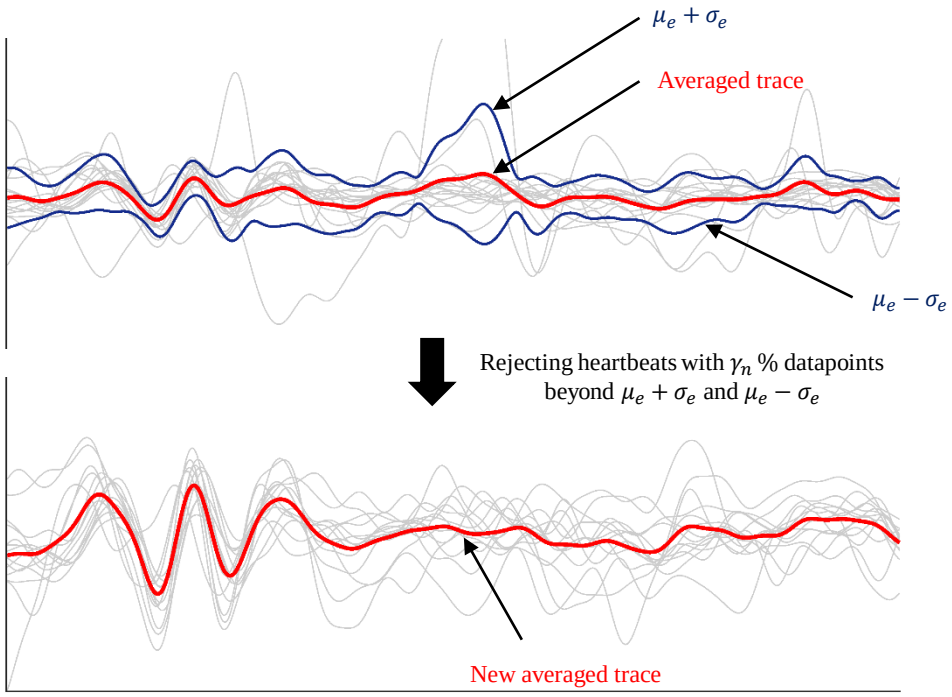

Figure 31: New method of ensemble averaging that involves rejection of extremely distorted or noisy heartbeats. The heartbeats which have more than γ_n % of total data points beyond one standard deviation above or below the mean trace are rejected. $\gamma_n = 40\%$ was chosen for the data set. The cleaner ensemble averaged trace is then calculated using the remaining heartbeats.

1. Calculate the averaged trace for the n_e heartbeats. The data point at a particular location in the averaged trace is the mean of all data points at that location from individual traces. Let this averaged trace be denoted by μ_e.

2. Calculate the standard deviation of each data point in n_e heartbeats. Let the trace formed by sum of mean and standard deviation of each data point be represented by $\mu_e + \sigma_e$. Similarly, the trace formed by difference between mean and standard deviation of each data point be represented by $\mu_e - \sigma_e$. These are shown in Fig. 31.

3. For each individual heartbeat, find the number of data points beyond the $\mu_e + \sigma_e$ and $\mu_e - \sigma_e$ regions.

4. If the percentage of data points for any individual heartbeat beyond the specified

regions is greater than a threshold γ_n, then reject the heartbeat.

5. Calculate the new ensemble-averaged trace using the remaining heartbeats in the ensemble.

7.5 Pre- and Post-Walk PEP Comparison

For each subject, we computed the percent changes in PEP following the 6-minute walk test (normalized to their baseline PEP value at rest), as well as the percent predicted value of the distance (based on age and subject demographics). The estimation of these two parameters is explained in the next sub-sections.

7.5.1 PEP Estimation

In order to estimate the PEP, the minima or maxima with the highest absolute value was detected as the AO-point from the ensemble averaged trace of the heartbeats in the first minute of baseline readings. The time difference between this feature and the ECG R-peak was estimated as the PEP in the resting state and denoted by PEP_{rest}. This AO-point detected from the resting state data for each subject was tracked using DTW based algorithm (used in Chapter VI) in the post-walk recovery period. For this study, the first 16 heartbeats immediately following the 6-minute walking period were considered for the post-walk PEP estimation. Let the PEP estimated from the ensemble-average of these 16 heartbeats be denoted by PEP_{post}. The change in PEP was then calculated as $\Delta PEP = (PEP_{post} - PEP_{rest})/PEP_{rest}$.

7.5.2 Percentage Predicted Walking Distance

The distance walked by each subject was measured during the 6-minute walk test. Let this distance be denoted by d_w. Also the distance supposed to be covered during the 6-minute walk test by each subject according to their respective gender, weight and height statistic was calculated as explained in [26]. The expected distance covered by each subject, denoted by d'_w, is given by the following equations [26]:

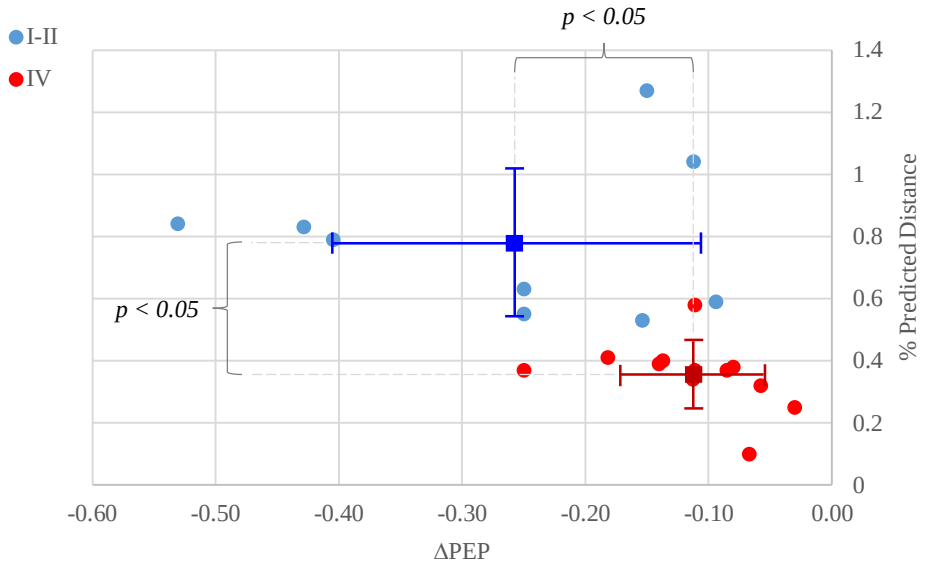

Figure 32: Δ PEP vs % Predicted Distance for HF subjects. The class IV subjects are concentrated in the lower right corner of the figure with mean and standard deviation of -0.11 ± 0.06 for Δ PEP and 0.35 ± 0.11 for the % Predicted Distance. Similarly, the class I-II subjects are concentrated in the upper left corner of the figure with mean and standard deviation of -0.26 ± 0.15 for Δ PEP and 0.78 ± 0.25 for the % Predicted Distance.

$$d'_{w_{(male)}} = (7.57 \times H) - (5.02 \times A) - (1.76 \times W) - 309 \tag{12}$$

$$d'_{w_{(female)}} = (2.11 \times H) - (2.29 \times A) - (5.78 \times W) + 667 \tag{13}$$

where H is the height in centimeters, A is the age in years and W is the weight in kilograms. The percentage predicted distance was then estimated as the ratio of the true and calculated distance, i.e., d_w/d'_w.

7.5.3 Analysis & Discussion

The results supported our hypothesis: the changes in PEP were significantly lower for the Class IV patients as compared to the Class I-II patients (Figure 1 (c), $p < 0.05$). As expected, we also found that the difference in percent predicted 6-minute walk test distance was significant between the two groups of patients, as was the average distance walked ($p < 0.05$). We did not find any significant difference in the heart rate

response in the two groups, supporting the importance of measuring a combination of electrical and mechanical signals from the heart (i.e., ECG and BCG).

While the 6-minute walk test requires the patients to perform a prescribed activity, changes in PEP can potentially be observed in response to any natural activity that patients are performing on their own while wearing the system; this may increase patient adherence as it will require less involvement, while still providing an indication of whether a patients condition may be worsening, and whether an exacerbation is imminent.

7.6 Future Work

The initial results obtained in this study indicate the potential of the wearable BCG methodology, used in tandem with sub-maximal exercise stressors, for monitoring heart failure patients at home following discharge. The next step involves a study with a larger pool of heart failure patients at different stages of the condition, and examining longitudinal changes in their PEP response to activity. The longitudinal trends in BCG based parameters can yield important insight into how these features can be used to track improvement or worsening of the condition in non-clinical settings. This will also lead to design of algorithms which can indicate the need for re-hospitalization or a clinical visit. Moreover, the daily report from the monitoring system can be sent to the patient's physician who can advise changes in medication or therapy with the changing state of the condition.

CHAPTER VIII

CONCLUSION & FUTURE DIRECTIONS

8.1 Conclusions

The work presented in this thesis lays the groundwork for augmenting the care of patients having respiratory disorders and heart failure. Specifically, algorithms were developed for extraction of features to detect sleep apnea with an under-the-mattress IR-UWB radar and a microphone placed on the side-table. Such a non-contact system can be used in home settings for whole night monitoring. However, in order to derive statistically significant results, future work would include a study of substantial size and duration. In cardiovascular disease monitoring, the BCG methodology was revisited with novel algorithms for improved estimation of STIs to compensate for posture and movement related artifacts.

The most important study, described in Chapter VI, deals with the removal of movement induced noise in the measured signals from a wearable accelerometer. Activity such as walking makes the wearable BCG signals completely unreadable. This work provides the basis for how data during the periods of simple exercise, such as walking, can be used to have a complete and thorough assessment of cardiovascular function. The device can be calibrated periodically during the stationary periods and this information can then be used with noise reduction algorithms, such as EMD, for accurate estimation of STIs during walking. The wearable accelerometer based BCG, when coupled with proper noise removal algorithm, worked better than the existing ICG methodology during the walking phases. Moreover, the results in Chapter VI also indicated that walking speed is inversely proportional to the accuracy and resolution of STI estimates from the wearable BCG. Thus, features related to speed of

walking can be incorporated in the estimation algorithms to adaptively change the resolution of obtained parameters with speed.

Another important contribution of this work involves the assessment of left ventricular function for HF patients in different stages of the disorder. Chapter VII briefly discusses the use of wearable BCG to assess the changes in PEP before and after a 6-minute walk test. The results from the study indicate that changes in PEP measured from the dorso-ventral axis of the wearable accelerometer are statistically significant for Class IV HF group as compared to Class I-II patients. This work, combined with algorithms for quantification and removal of noise from wearable BCG during walking, can herald the use of BCG methodology for continuous and robust cardiovascular assessment at home.

New methods for improved estimation of STIs in different standing postures were also conceived and developed. The BCG signals from weighing scale based sensors and wearable accelerometer were also analyzed during different postures to determine features which can be indicative of posture as compared to physiological changes. These features involve changes in power spectral density of measured signals in higher frequency bands during non-ideal postures which can potentially be used with posture detection algorithms.

The methods described in this dissertation, specifically for the BCG based measurements, can be readily extended to other measurement modalities. Moreover, parameters from different sensors can be combined with the BCG-derived features to further increase the range of physiological indicators for cardiovascular and respiratory assessment.

8.2 Future Directions

Future work in the sleep monitoring aspects of this thesis should focus on including more sensors to improve the quality of information obtained, increasing the number of

subjects studied and widening the subject demographics. In the cardiovascular monitoring application of this work, longitudinal data should be collected and analyzed from heart failure patients both in the hospital and at home; this data, combined with the intellectual contributions of this dissertation, can potentially lead to predicting and preventing exacerbations for patients at home, thus improving the quality of care.

Future work should also focus on ***intelligent algorithms*** that can change adaptively to stationary and activity periods and also incorporate the intensity of the exercise or activity for accurate estimation of parameters from the wearable sensors.

8.3 Final Remarks

The methods and algorithms developed and discussed in this work could significantly improve home monitoring of cardiovascular and respiratory diseases, and advance our understanding of basic physiology by providing a platform for easy and unobtrusive measurements of important mechanical parameters of physiological function. The rapidly growing need for inexpensive health care solutions in the developed world today, coupled with the exploding population and reducing health care resources is the main motivation behind this work. Many low-cost, miniature and easy-to-use sensors are available for unobtrusive monitoring at home. However, there are still gaps and limitations in using these for continuous monitoring and also during different phases of daily living. This dissertation addresses many of these limitations through the use of both novel algorithms and measurement modalities that can potentially improve the accuracy of health parameters measured outside of clinical settings.

REFERENCES

[1] Abeyratne, U. R., Wakwella, A. S., and Hukins, C., "Pitch jump probability measures for the analysis of snoring sounds in apnea," *Physiological measurement*, vol. 26, no. 5, p. 779, 2005.

[2] Abeyratne, U., De Silva, S., Hukins, C., and Duce, B., "Obstructive sleep apnea screening by integrating snore feature classes," *Physiological measurement*, vol. 34, no. 2, p. 99, 2013.

[3] Allen, M. T., Fahrenberg, J., Kelsey, R. M., Lovallo, W. R., Doornen, L. J., and others, "Methodological guidelines for impedance cardiography," *Psychophysiology*, vol. 27, no. 1, pp. 1–23, 1990.

[4] Arlot, S., Celisse, A., and others, "A survey of cross-validation procedures for model selection," *Statistics surveys*, vol. 4, pp. 40–79, 2010.

[5] Baek, H. J., Chung, G. S., Kim, K. K., and Park, K. S., "A smart health monitoring chair for nonintrusive measurement of biological signals," *Information Technology in Biomedicine, IEEE Transactions on*, vol. 16, no. 1, pp. 150–158, 2012.

[6] Bayliss, J., Norell, M., Canepa-Anson, R. e., Sutton, G., and Poole-Wilson, P., "Untreated heart failure: clinical and neuroendocrine effects of introducing diuretics.," *British heart journal*, vol. 57, no. 1, pp. 17–22, 1987.

[7] Ben-Israel, N., Tarasiuk, A., and Zigel, Y., "Nocturnal sound analysis for the diagnosis of obstructive sleep apnea," in *Engineering in Medicine and Biology Society (EMBC), 2010 Annual International Conference of the IEEE*, pp. 6146–6149, IEEE, 2010.

[8] Berry, R. B., Budhiraja, R., Gottlieb, D. J., Gozal, D., Iber, C., Kapur, V. K., Marcus, C. L., Mehra, R., Parthasarathy, S., Quan, S. F., and others, "Rules for scoring respiratory events in sleep: update of the 2007 aasm manual for the scoring of sleep and associated events," *J Clin Sleep Med*, vol. 8, no. 5, pp. 597–619, 2012.

[9] Bittner, V., Weiner, D. H., Yusuf, S., Rogers, W. J., McIntyre, K. M., Bangdiwala, S. I., Kronenberg, M. W., Kostis, J. B., Kohn, R. M., Guillotte, M., and others, "Prediction of mortality and morbidity with a 6-minute walk test in patients with left ventricular dysfunction," *Jama*, vol. 270, no. 14, pp. 1702–1707, 1993.

[10] Bos, W. J. W., van Goudoever, J., van Montfrans, G. A., van den Meiracker, A. H., and Wesseling, K. H., "Reconstruction of brachial artery pressure from noninvasive finger pressure measurements," *Circulation*, vol. 94, no. 8, pp. 1870–1875, 1996.

[11] Brüser, C., Stadlthanner, K., De Waele, S., and Leonhardt, S., "Adaptive beat-to-beat heart rate estimation in ballistocardiograms," *Information Technology in Biomedicine, IEEE Transactions on*, vol. 15, no. 5, pp. 778–786, 2011.

[12] Cahalin, L. P., Mathier, M. A., Semigran, M. J., Dec, G. W., and DiSalvo, T. G., "The six-minute walk test predicts peak oxygen uptake and survival in patients with advanced heart failure," *CHEST Journal*, vol. 110, no. 2, pp. 325–332, 1996.

[13] Castiglioni, P., Meriggi, P., Rizzo, F., Vaini, E., Faini, A., Parati, G., Merati, G., and Rienzo, M. D., "Cardiac sounds from a wearable device for sternal seismocardiography," in *Engineering in Medicine and Biology Society, EMBC, 2011 Annual International Conference of the IEEE*, pp. 4283–4286, IEEE, 2011.

[14] Coats, A., Adamopoulos, S., Meyer, T., Conway, J., and Sleight, P., "Effects of physical training in chronic heart failure," *The Lancet*, vol. 335, no. 8681, pp. 63–66, 1990.

[15] Commission, F. C. and others, "Revision of part 15 of the commission's rules regarding ultra-wideband transmission systems,"first report and order," fcc 02," *V48, April*, 2002.

[16] Committee, N. Y. H. A. C. and Association, N. Y. H., *Nomenclature and criteria for diagnosis of diseases of the heart and great vessels*. Little, Brown Medical Division, 1979.

[17] Cooper, R. A., Getzen, T. E., McKee, H. J., and Laud, P., "Economic and demographic trends signal an impending physician shortage," *Health Affairs*, vol. 21, no. 1, pp. 140–154, 2002.

[18] Cybulski, G., "Ambulatory impedance cardiography. the systems and their applications. series: Lecture notes in electrical engineering, vol. 76, isbn: 978-3-642-11986-6, 150 pp," *Springer-Verlag Berlin and Heidelberg GmbH & Co. KG, DOI*, vol. 10, pp. 978–3, 2011.

[19] Davis, J. O., "The physiology of congestive heart failure," *Handbook of physiology*, vol. 3, pp. 2071–122, 1965.

[20] De Chazal, P., Dwyer, M. O., and Reilly, R. B., "Automatic classification of heartbeats using ecg morphology and heartbeat interval features," *Biomedical Engineering, IEEE Transactions on*, vol. 51, no. 7, pp. 1196–1206, 2004.

[21] De Chazal, P., Hare, E. O., Fox, N., and Heneghan, C., "Assessment of sleep/wake patterns using a non-contact biomotion sensor," in *Engineering in Medicine and Biology Society, 2008. EMBS 2008. 30th Annual International Conference of the IEEE*, pp. 514–517, IEEE, 2008.

[22] De Maesschalck, R., Jouan-Rimbaud, D., and Massart, D. L., "The mahalanobis distance," *Chemometrics and intelligent laboratory systems*, vol. 50, no. 1, pp. 1–18, 2000.

[23] Di Rienzo, M., Meriggi, P., Vaini, E., Castiglioni, P., and Rizzo, F., "24h seismocardiogram monitoring in ambulant subjects," in *Engineering in Medicine and Biology Society (EMBC), 2012 Annual International Conference of the IEEE*, pp. 5050–5053, IEEE, 2012.

[24] Dziuda, L., Skibniewski, F. W., Krej, M., and Lewandowski, J., "Monitoring respiration and cardiac activity using fiber bragg grating-based sensor," *Biomedical Engineering, IEEE Transactions on*, vol. 59, no. 7, pp. 1934–1942, 2012.

[25] Enright, P. L., "The six-minute walk test," *Respiratory care*, vol. 48, no. 8, pp. 783–785, 2003.

[26] Enright, P. L. and Sherrill, D. L., "Reference equations for the six-minute walk in healthy adults," *American journal of respiratory and critical care medicine*, vol. 158, no. 5, pp. 1384–1387, 1998.

[27] Etemadi, M., Inan, O. T., Heller, J. A., Hersek, S., Klein, L., and Roy, S., "A wearable patch to enable long-term monitoring of environmental, activity and hemodynamics variables," *IEEE Transactions on Biomedical Circuits and Systems*, vol. 10, pp. 280–288, April 2016.

[28] Etemadi, M., Inan, O. T., Giovangrandi, L., and Kovacs, G. T., "Rapid assessment of cardiac contractility on a home bathroom scale," *Information Technology in Biomedicine, IEEE Transactions on*, vol. 15, no. 6, pp. 864–869, 2011.

[29] Etemadi, M., Inan, O. T., Wiard, R. M., Kovacs, G. T., and Giovangrandi, L., "Non-invasive assessment of cardiac contractility on a weighing scale," in *Engineering in Medicine and Biology Society, 2009. EMBC 2009. Annual International Conference of the IEEE*, pp. 6773–6776, IEEE, 2009.

[30] Fensli, R., Gunnarson, E., and Gundersen, T., "A wearable ecg-recording system for continuous arrhythmia monitoring in a wireless tele-home-care situation," in *Computer-Based Medical Systems, 2005. Proceedings. 18th IEEE Symposium on*, pp. 407–412, IEEE, 2005.

[31] Flandrin, P., Rilling, G., and Goncalves, P., "Empirical mode decomposition as a filter bank," *Signal Processing Letters, IEEE*, vol. 11, no. 2, pp. 112–114, 2004.

[32] Foo, S., "Ultra wideband monitoring systems and antennas," Apr. 23 2013. US Patent 8,428,696.

[33] Gallo, D., Anayiotos, A., and Morbiducci, U., "The evolution of computational hemodynamics as a clinical tool in decision making, patient specific treatment and clinical management," *Annals of biomedical engineering*, vol. 43, no. 1, pp. 1–2, 2015.

[34] Gerhard, D., *Pitch extraction and fundamental frequency: History and current techniques*. Regina: Department of Computer Science, University of Regina, 2003.

[35] Golub, G. H., Hansen, P. C., and O'Leary, D. P., "Tikhonov regularization and total least squares," *SIAM Journal on Matrix Analysis and Applications*, vol. 21, no. 1, pp. 185–194, 1999.

[36] Gonzalez-Landaeta, R., Casas, O., and Pallas-Areny, R., "Heart rate detection from an electronic weighing scale," *Physiological measurement*, vol. 29, no. 8, p. 979, 2008.

[37] Gordon, J., "Certain molar movements of the human body produced by the circulation of the blood," *Journal of Anatomy and Physiology*, vol. 11, no. Pt 3, p. 533, 1877.

[38] Gottlieb, D. J., Yenokyan, G., Newman, A. B., O'Connor, G. T., Punjabi, N. M., Quan, S. F., Redline, S., Resnick, H. E., Tong, E. K., Diener-West, M., and others, "Prospective study of obstructive sleep apnea and incident coronary heart disease and heart failure the sleep heart health study," *Circulation*, vol. 122, no. 4, pp. 352–360, 2010.

[39] Hamilton, D. M. and Haennel, R., "Validity and reliability of the 6-minute walk test in a cardiac rehabilitation population," *Journal of Cardiopulmonary Rehabilitation and Prevention*, vol. 20, no. 3, pp. 156–164, 2000.

[40] Haykin, S. S., *Adaptive filter theory*. Pearson Education India, 2008.

[41] Huang, N. E., Shen, Z., Long, S. R., Wu, M. C., Shih, H. H., Zheng, Q., Yen, N.-C., Tung, C. C., and Liu, H. H., "The empirical mode decomposition and the hilbert spectrum for nonlinear and non-stationary time series analysis," in *Proceedings of the Royal Society of London A: Mathematical, Physical and Engineering Sciences*, vol. 454, pp. 903–995, The Royal Society, 1998.

[42] Inan, O. T., Etemadi, M., Wiard, R. M., Kovacs, G. T., and Giovangrandi, L., "Novel methods for estimating the ballistocardiogram signal using a simultaneously acquired electrocardiogram," in *Engineering in Medicine and Biology Society, 2009. EMBC 2009. Annual International Conference of the IEEE*, pp. 5334–5347, IEEE, 2009.

[43] Inan, O. T., Migeotte, P.-F., Park, K.-S., Etemadi, M., Tavakolian, K., Casanella, R., Zanetti, J., Tank, J., Funtova, I., Prisk, G. K., and others, "Ballistocardiography and seismocardiography: A review of recent advances," *Biomedical and Health Informatics, IEEE Journal of*, vol. 19, no. 4, pp. 1414–1427, 2015.

[44] Inan, O., Etemadi, M., Paloma, A., Giovangrandi, L., and Kovacs, G., "Non-invasive cardiac output trending during exercise recovery on a bathroom-scale-based ballistocardiograph," *Physiological measurement*, vol. 30, no. 3, p. 261, 2009.

[45] Inan, O., Etemadi, M., Wiard, R., Giovangrandi, L., and Kovacs, G., "Robust ballistocardiogram acquisition for home monitoring," *Physiological measurement*, vol. 30, no. 2, p. 169, 2009.

[46] Javaid, A. Q., Fesmire, N. F., Weitnauer, M. A., and Inan, O. T., "Towards robust estimation of systolic time intervals using head-to-foot and dorso-ventral components of sternal acceleration signals," in *Wearable and Implantable Body Sensor Networks (BSN), 2015 IEEE 12th International Conference on*, pp. 1–5, IEEE, 2015.

[47] Javaid, A. Q., Wiens, A. D., Fesmire, N. F., Weitnauer, M. A., and Inan, O. T., "Quantifying and reducing posture-dependent distortion in ballistocardiogram measurements," *Biomedical and Health Informatics, IEEE Journal of*, vol. 19, no. 5, pp. 1549–1556, 2015.

[48] Jolliffe, I., *Principal component analysis*. Wiley Online Library, 2002.

[49] Kagawa, M., Ueki, K., Tojima, H., and Matsui, T., "Noncontact screening system with two microwave radars for the diagnosis of sleep apnea-hypopnea syndrome," in *Engineering in Medicine and Biology Society (EMBC), 2013 35th Annual International Conference of the IEEE*, pp. 2052–2055, IEEE, 2013.

[50] Khandoker, A. H., Palaniswami, M., and Karmakar, C. K., "Support vector machines for automated recognition of obstructive sleep apnea syndrome from ecg recordings," *Information Technology in Biomedicine, IEEE Transactions on*, vol. 13, no. 1, pp. 37–48, 2009.

[51] Kim, C.-S., Carek, A. M., Mukkamala, R., Inan, O. T., and Hahn, J.-O., "Ballistocardiogram as proximal timing reference for pulse transit time measurement: potential for cuffless blood pressure monitoring," *Biomedical Engineering, IEEE Transactions on*, vol. 62, no. 11, pp. 2657–2664, 2015.

[52] Kitazaki, S. and Griffin, M. J., "Resonance behaviour of the seated human body and effects of posture," *Journal of Biomechanics*, vol. 31, no. 2, pp. 143–149, 1997.

[53] Klabunde, R., *Cardiovascular physiology concepts*. Lippincott Williams & Wilkins, 2011.

[54] Kohavi, R. and John, G. H., "Wrappers for feature subset selection," *Artificial intelligence*, vol. 97, no. 1, pp. 273–324, 1997.

[55] Krej, M., Dziuda, L., and Skibniewski, F. W., "A method of detecting heartbeat locations in the ballistocardiographic signal from the fiber-optic vital signs sensor," *Biomedical and Health Informatics, IEEE Journal of*, vol. 19, no. 4, pp. 1443–1450, 2015.

[56] Lai, J. C. Y., Xu, Y., Gunawan, E., Chua, E. C.-P., Maskooki, A., Guan, Y. L., Low, K.-S., Soh, C. B., and Poh, C.-L., "Wireless sensing of human respiratory parameters by low-power ultrawideband impulse radio radar," *Instrumentation and Measurement, IEEE Transactions on*, vol. 60, no. 3, pp. 928–938, 2011.

[57] Lee, Y. S., Pathirana, P. N., Steinfort, C. L., and Caelli, T., "Monitoring and analysis of respiratory patterns using microwave doppler radar," *Translational Engineering in Health and Medicine, IEEE Journal of*, vol. 2, pp. 1–12, 2014.

[58] Lewis, R. P., Boudoulas, H., Welch, T. G., and Forester, W. F., "Usefulness of systolic time intervals in coronary artery disease," *The American journal of cardiology*, vol. 37, no. 5, pp. 787–796, 1976.

[59] Lewis, R. P., Rittogers, S., Froester, W., and Boudoulas, H., "A critical review of the systolic time intervals.," *Circulation*, vol. 56, no. 2, pp. 146–158, 1977.

[60] Lindqvist, A., Pihlajamäki, K., Jalonen, J., Laaksonen, V., and Alihanka, J., "Static-charge-sensitive bed ballistocardiography in cardiovascular monitoring," *Clinical Physiology*, vol. 16, no. 1, pp. 23–30, 1996.

[61] Matsumoto, Y. and Griffin, M., "Dynamic response of the standing human body exposed to vertical vibration: influence of posture and vibration magnitude," *Journal of Sound and Vibration*, vol. 212, no. 1, pp. 85–107, 1998.

[62] McArdle, W. D., Katch, F. I., and Katch, V. L., *Exercise physiology: nutrition, energy, and human performance*. Lippincott Williams & Wilkins, 2010.

[63] McNicholas, W. T., "Diagnosis of obstructive sleep apnea in adults," *Proceedings of the American thoracic society*, vol. 5, no. 2, pp. 154–160, 2008.

[64] Mozaffarian, D., Benjamin, E. J., Go, A. S., Arnett, D. K., Blaha, M. J., Cushman, M., de Ferranti, S., Despres, J.-P., Fullerton, H. J., Howard, V. J., and others, "Heart disease and stroke statistics-2015

update: a report from the american heart association.," *Circulation*, vol. 131, no. 4, p. e29, 2015.

[65] Mukkamala, R., Hahn, J.-O., Inan, O. T., Mestha, L. K., Kim, C.-S., Toreyin, H., and Kyal, S., "Toward ubiquitous blood pressure monitoring via pulse transit time: theory and practice," *Biomedical Engineering, IEEE Transactions on*, vol. 62, no. 8, pp. 1879–1901, 2015.

[66] Müller, M., "Dynamic time warping," *Information retrieval for music and motion*, pp. 69–84, 2007.

[67] Nepal, K., Biegeleisen, E., and Ning, T., "Apnea detection and respiration rate estimation through parametric modelling," in *Bioengineering Conference, 2002. Proceedings of the IEEE 28th Annual Northeast*, pp. 277–278, IEEE, 2002.

[68] Ng, A. K., San Koh, T., Baey, E., Lee, T. H., Abeyratne, U. R., and Puvanendran, K., "Could formant frequencies of snore signals be an alternative means for the diagnosis of obstructive sleep apnea?," *Sleep medicine*, vol. 9, no. 8, pp. 894–898, 2008.

[69] Ng, A. K., Wong, K. Y., Tan, C. H., and Koh, T. S., "Bispectral analysis of snore signals for obstructive sleep apnea detection," in *Engineering in Medicine and Biology Society, 2007. EMBS 2007. 29th Annual International Conference of the IEEE*, pp. 6195–6198, IEEE, 2007.

[70] Nguyen, V., Javaid, A. Q., and Weitnauer, M. A., "Harmonic path (hapa) algorithm for non-contact vital signs monitoring with ir-uwb radar," in *Biomedical Circuits and Systems Conference (BioCAS), 2013 IEEE*, pp. 146–149, IEEE, 2013.

[71] of America, H. F. S. and others, "Executive summary: Hfsa 2006 comprehensive heart failure practice guideline," *Journal of cardiac failure*, vol. 12, no. 1, pp. 10–38, 2006.

[72] Opie, L. H., *Heart physiology: from cell to circulation*. Lippincott Williams & Wilkins, 2004.

[73] Pandia, K., Ravindran, S., Cole, R., Kovacs, G. T., and Giovangrandi, L., "Motion artifact cancellation to obtain heart sounds from a single chest-worn accelerometer.," in *ICASSP*, pp. 590–593, 2010.

[74] Pevernagie, D., Aarts, R. M., and De Meyer, M., "The acoustics of snoring," *Sleep medicine reviews*, vol. 14, no. 2, pp. 131–144, 2010.

[75] Pinheiro, E., Postolache, O., and Girão, P., "Study on ballistocardiogram acquisition in a moving wheelchair with embedded sensors," *Metrology and Measurement Systems*, vol. 19, no. 4, pp. 739–750, 2012.

[76] Porth, C., Bamrah, V. S., Tristani, F., and Smith, J., "The valsalva maneuver: mechanisms and clinical implications.," *Heart & lung: the journal of critical care*, vol. 13, no. 5, pp. 507–518, 1984.

[77] Punjabi, N. M., "The epidemiology of adult obstructive sleep apnea," *Proceedings of the American Thoracic Society*, vol. 5, no. 2, pp. 136–143, 2008.

[78] Rilling, G., Flandrin, P., Goncalves, P., and others, "On empirical mode decomposition and its algorithms," in *IEEE-EURASIP workshop on nonlinear signal and image processing*, vol. 3, pp. 8–11, IEEER, 2003.

[79] Rousseeuw, P. J. and Driessen, K. V., "A fast algorithm for the minimum covariance determinant estimator," *Technometrics*, vol. 41, no. 3, pp. 212–223, 1999.

[80] Rowell, L. B., "Human cardiovascular adjustments to exercise and thermal stress.," *Physiological reviews*, vol. 54, no. 1, pp. 75–159, 1974.

[81] Safar, M. E., "Systolic blood pressure, pulse pressure and arterial stiffness as cardiovascular risk factors," *Current opinion in nephrology and hypertension*, vol. 10, no. 2, pp. 257–261, 2001.

[82] Sakoe, H. and Chiba, S., "Dynamic programming algorithm optimization for spoken word recognition," *Acoustics, Speech and Signal Processing, IEEE Transactions on*, vol. 26, no. 1, pp. 43–49, 1978.

[83] Shin, J. H., Chee, Y. J., Jeong, D.-U., and Park, K. S., "Nonconstrained sleep monitoring system and algorithms using air-mattress with balancing tube method," *Information Technology in Biomedicine, IEEE Transactions on*, vol. 14, no. 1, pp. 147–156, 2010.

[84] Smolander, J., Aminoff, T., Korhonen, I., Tervo, M., Shen, N., Korhonen, O., and Louhevaara, V., "Heart rate and blood pressure responses to isometric exercise in young and older men," *European journal of applied physiology and occupational physiology*, vol. 77, no. 5, pp. 439–444, 1998.

[85] Snell, R. C. and Milinazzo, F., "Formant location from lpc analysis data," *IEEE Transactions on Speech and Audio Processing*, vol. 1, no. 2, pp. 129–134, 1993.

[86] Sokolnikoff, I. S., Specht, R. D., and others, *Mathematical theory of elasticity*, vol. 83. McGraw-Hill New York, 1956.

[87] Sola-Soler, J., Jane, R., Fiz, J., and Morera, J., "Variability of snore parameters in time and frequency domains in snoring subjects with and without obstructive sleep apnea," in *Engineering in Medicine and Biology Society, 2005. IEEE-EMBS 2005. 27th Annual International Conference of the*, pp. 2583–2586, IEEE, 2006.

[88] Solà-Soler, J., Fiz, J. A., Morera, J., and Jané, R., "Multiclass classification of subjects with sleep apnoea–hypopnoea syndrome through snoring analysis," *Medical engineering & physics*, vol. 34, no. 9, pp. 1213–1220, 2012.

[89] Sola-Soler, J., Jane, R., Fiz, J., and Morera, J., "Spectral envelope analysis in snoring signals from simple snorers and patients with obstructive sleep apnea," in *Engineering in Medicine and Biology Society, 2003. Proceedings of the 25th Annual International Conference of the IEEE*, vol. 3, pp. 2527–2530, IEEE, 2003.

[90] Sola-Soler, J., Jané, R., Fiz, J. A., and Morera, J., "Formant frequencies of normal breath sounds of snorers may indicate the risk of obstructive sleep apnea syndrome," in *Engineering in Medicine and Biology Society, 2008. EMBS 2008. 30th Annual International Conference of the IEEE*, pp. 3500–3503, IEEE, 2008.

[91] Sola-Soler, J., Jane, R., Fiz, J., Morera, J., and others, "Automatic classification of subjects with and without sleep apnea through snoring analysis," in *Engineering in Medicine and Biology Society, 2007. EMBS 2007. 29th Annual International Conference of the IEEE*, pp. 6093–6096, IEEE, 2007.

[92] Somers, V. K., White, D. P., Amin, R., Abraham, W. T., Costa, F., Culebras, A., Daniels, S., Floras, J. S., Hunt, C. E., Olson, L. J., and others, "Sleep apnea and cardiovascular disease: An american heart association/american college of cardiology foundation scientific statement from the american heart association council for high blood pressure research professional education committee, council on clinical cardiology, stroke council, and council on cardiovascular nursing in collaboration with the national heart, lung, and blood institute national center on sleep disorders research (national institutes of health)," *Journal of the American College of Cardiology*, vol. 52, no. 8, pp. 686–717, 2008.

[93] Sörnmo, L. and Laguna, P., *Bioelectrical signal processing in cardiac and neurological applications*. Academic Press, 2005.

[94] Staderini, E. M., "Uwb radars in medicine," *Aerospace and Electronic Systems Magazine, IEEE*, vol. 17, no. 1, pp. 13–18, 2002.

[95] Starr, I. and Schroeder, H. A., "Ballistocardiogram. ii. normal standards, abnormalities commonly found in diseases of the heart and circulation, and their significance," *Journal of Clinical Investigation*, vol. 19, no. 3, p. 437, 1940.

[96] Tavakolian, K., *Characterization and analysis of seismocardiogram for estimation of hemodynamic parameters*. PhD thesis, Applied Science: School of Engineering Science, 2010.

[97] Tavakolian, K., Blaber, A. P., Ngai, B., and Kaminska, B., "Estimation of hemodynamic parameters from seismocardiogram," in *Computing in Cardiology, 2010*, pp. 1055–1058, IEEE, 2010.

[98] Tavakolian, K., Ngai, B., Blaber, A. P., and Kaminska, B., "Infrasonic cardiac signals: Complementary windows to cardiovascular dynamics," in *Engineering in Medicine and Biology Society, EMBC, 2011 Annual International Conference of the IEEE*, pp. 4275–4278, IEEE, 2011.

[99] Tavakolian, K., Portacio, G., Tamddondoust, N. R., Jahns, G., Ngai, B., Dumont, G. A., and Blaber, A., "Myocardial contractility: a seismocardiography approach," in *Engineering in Medicine and Biology Society (EMBC), 2012 Annual International Conference of the IEEE*, pp. 3801–3804, IEEE, 2012.

[100] Thong, Y., Woolfson, M., Crowe, J., Hayes-Gill, B., and Jones, D., "Numerical double integration of acceleration measurements in noise," *Measurement*, vol. 36, no. 1, pp. 73–92, 2004.

[101] Várady, P., Micsik, T., Benedek, S., and Benyó, Z., "A novel method for the detection of apnea and hypopnea events in respiration signals," *Biomedical Engineering, IEEE Transactions on*, vol. 49, no. 9, pp. 936–942, 2002.

[102] Wiens, A., Etemadi, M., Klein, L., Roy, S., and Inan, O. T., "Wearable ballistocardiography: Preliminary methods for mapping surface vibration measurements to whole body forces," in *Engineering in Medicine and Biology Society (EMBC), 2014 36th Annual International Conference of the IEEE*, pp. 5172–5175, IEEE, 2014.

[103] Wiens, A. D., Etemadi, M., Roy, S., Klein, L., and Inan, O. T., "Toward continuous, noninvasive assessment of ventricular function and hemodynamics: Wearable ballistocardiography," *Biomedical and Health Informatics, IEEE Journal of*, vol. 19, no. 4, pp. 1435–1442, 2015.

[104] Wiens, A. D. and Inan, O. T., "A novel system identification technique for improved wearable hemodynamics assessment," *Biomedical Engineering, IEEE Transactions on*, vol. 62, no. 5, pp. 1345–1354, 2015.

[105] Wu, Z. and Huang, N. E., "Ensemble empirical mode decomposition: a noise-assisted data analysis method," *Advances in adaptive data analysis*, vol. 1, no. 01, pp. 1–41, 2009.

[106] Yilmaz, B., Asyali, M. H., Arikan, E., Yetkin, S., and Özgen, F., "Sleep stage and obstructive apneaic epoch classification using single-lead ecg," *Biomedical engineering online*, vol. 9, no. 1, p. 39, 2010.

[107] Zaffaroni, A., De Chazal, P., Heneghan, C., Boyle, P., Mppm, P. R., and McNicholas, W. T., "Sleepminder: an innovative contact-free device

for the estimation of the apnoea-hypopnoea index," in *Engineering in Medicine and Biology Society, 2009. EMBC 2009. Annual International Conference of the IEEE*, pp. 7091–9094, IEEE, 2009.